DOT/FAA/AR-07/29

Air Traffic Organization
Operations Planning
Office of Aviation Research
and Development
Washington, DC 20591

Flammability Properties of Clay-Nylon Nanocomposites

June 2007

Final Report

U.S. Department of Transportation
Federal Aviation Administration

NOTICE

Technical Report Documentation Page

1. Report No.	2. Government Accession No.	3. Recipient's Catalog No.
DOT/FAA/AR-07/29		

4. Title and Subtitle	5. Report Date
FLAMMABILITY PROPERTIES OF CLAY-NYLON NANOCOMPOSITES	June 2007
	6. Performing Organization Code

7. Author(s)	8. Performing Organization Report No.
Xin Liu and J.G. Quintiere	

9. Performing Organization Name and Address	10. Work Unit No. (TRAIS)
Department of Fire Protection Engineering University of Maryland 0151 G. L. Martin Hall College Park, MD 20742	
	11. Contract or Grant No.

12. Sponsoring Agency Name and Address	13. Type of Report and Period Covered
U.S. Department of Transportation Federal Aviation Administration Air Traffic Organization Operations Planning Office of Aviation Research and Development Washington, DC 20591	Final Report
	14. Sponsoring Agency Code AJP-6320

15. Supplementary Notes

The Federal Aviation Administration Airport and Aircraft Safety R&D Division Technical Monitor was Richard E. Lyon, Ph.D.

16. Abstract

The flammability properties of nylon samples with different percentages of clay dispersed on the nanometer (molecular) scale were measured by a fire (cone) calorimeter. Specifically, chemical energy release rate, mass loss rate, and time to ignite (melt and char) were measured. This study consisted of samples of pure Nylon 6 and nylon that contained nanoclay additives at 2% and 5% by weight. In addition, the effect of sample thickness was considered for 1.6 to 24 mm. Data obtained over a range of radiant heat flux (17 to 55 kW/m^2) were analyzed to illustrate the effect of sample clay loading and thickness on heat of combustion, heat of gasification, and ignition temperature. The findings indicated that the heats of combustion based on mass loss did not change with clay loading, and were 28 ±1 kJ/g. The critical heat flux for ignition did not appear to be influenced by the clay additive; it decreased from 17.7 for pure nylon to 16.0 with 5% clay addition. These values correspond roughly to an ignition temperature of 430°C, compared to a decomposition temperature range from a thermogravimetric analyzer of 350° to 430°C. However, the addition of the clay could increase the ignition time by 30% to 100% over the pure nylon. This is believed to be due to the increased char residue and the decrease in the mass loss rate. The char-like residue yield was nearly identical to the clay loadings. The overall average mass loss rate was reduced by up to 50% with a 5% clay composition over pure nylon for a given heat flux and thickness. For the clay nanocomposites, the burning rate increased as the thickness decreased.

17. Key Words	18. Distribution Statement
Flammability, Heat release, Ignition, Temperature, Heat of combustion, Nanocomposite, Nylon, Clay, Ignitability	This document is available to the U.S. public through the National Technical Information Service (NTIS), Springfield, Virginia 22161.

19. Security Classif. (of this report)	20. Security Classif. (of this page)	21. No. of Pages	22. Price
Unclassified	Unclassified	154	

TABLE OF CONTENTS

APPENDICES

LIST OF FIGURES

LIST OF TABLES

LIST OF SYMBOLS AND ACRONYMS

a_p	Pre-exponential factor
c_p	Specific heat
d	Sample thickness
E_a	Activation energy
Δh_c	Heat of combustion
k	Thermal conductivity
$k\rho c$	Thermal inertia
L	Heat of gasification
m	Mass
M	Molecular weight
Q	Heat release
t	Time
T	Temperature
X	Mole fraction
X_c	Char fraction
α	Volumetric expansion factor
β	Constant heating rate
δ	Vaporizing front
δ_T	Thermal penetration depth
ε	Emissivity
ρ	Density
ϕ	Oxygen depletion factor
a	Air
ext	External
f	Final
fl	Flame
ig	Ignition
int	Initial
net	Net
O_2	Oxygen
p	Pyrolysis
v	Vaporization
peak	At the Peak Energy Release Rate
peak avg.	Average of the Peak Energy Release Rate
overall avg.	Average of the Overall Properties During Steady, Sustained Burning
$\dot{X}$	Per unit time
X''	Per unit area
X'''	Per unit volume
$\overline{X}$	Average value
MMT	Montmorillunite
NIST	National Institute of Standards and Technology
TGA	Thermogravimetric analysis
1-D	One-dimensional

EXECUTIVE SUMMARY

The flammability properties of nylon samples with different percentages of clay dispersion on the nanometer (molecular) scale were measured by a cone calorimeter device. Specifically, chemical energy release rate, mass loss rate, and time to ignite (melt and char) were measured. This study consisted of samples of pure Nylon 6 and nylon that contained nanoclay additives of 2% and 5%. In addition, the effect of sample thickness was considered for 1.6 to 24 mm. Data obtained over a range of radiant heat flux (17 to 55 kW/m^2) were analyzed to illustrate the effect of sample clay loading and thickness on heat of combustion, heat of gasification, and ignition temperature. The findings indicated that the heats of combustion based on mass loss did not change with clay loading, and were 28 ±1 kJ/g. The critical heat flux for ignition did not appear to be influenced by the clay additive; it decreased from 17.7 for pure nylon to 16.0 with 5% clay addition. These values correspond to roughly an inferred ignition temperature of 430^{o}C, compared to a decomposition temperature range from a thermogravimetric of 350° to 430^{o}C. However, the addition of the clay could increase the ignition time by 30% to 100% over the pure nylon. This is believed to be due to the increased char residue and the decrease in the mass loss rate. The char-like residue yield was nearly identical to the clay loadings. The overall average mass loss rate was reduced by up to 50% with a 5% clay composition over pure nylon for a given heat flux and thickness. For the clay nanocomposites, the burning rate increased as the thickness decreased.

1. INTRODUCTION.

Composites consisting of organic polymer and small additives of inorganic aluminum silicate have shown significant improvements in many mechanical and physical properties. This study examined the additive montmorillonite (MMT) clay with polycaprolactam, also called polyamide 6, or nylon 6 (PA-6), samples formed as a nanocomposite, in which there was a specific interaction between the clay platelet and the polymer. The objective of this study was to determine the effects of clay loading on flammability properties and to address the effect of the thickness, which was evident in previous work. For example, the study by Gilman, et al. [1] at the National Institute of Standards and Technology (NIST) found that peak heat release rates (firepower) were reduced by adding clay, at a heat flux of 50 kW/m^2, for this nanocomposite. The NIST group also found that the peak heat release rate dropped from about 2000 kW/m^2 to 1200, 600, and 400 kW/m^2 with the addition of 2%, 5%, and 10% clay to the nylon (figure 1).

However, these peaks were influenced by 8-mm thickness of the nanocomposite with an insulated back face. The insulated back face caused heat to be stored in the sample and led to an increase in the firepower at the late burning stage. Other measurements of pure nylon, at 25-mm thickness, showed a peak (steady) heat release rate of about 600 kW/m^2 compared to 2000 kW/m^2 at 8 mm [2]. However, the data for the 8-mm-thick specimens indicated a tendency to establish a plateau in their early burning at about 600 kW/m^2. Therefore, thickness effects are interfering with an independent assessment of the role of the clay agent. There is a need to sort out these effects and establish the direct influence of the clay.

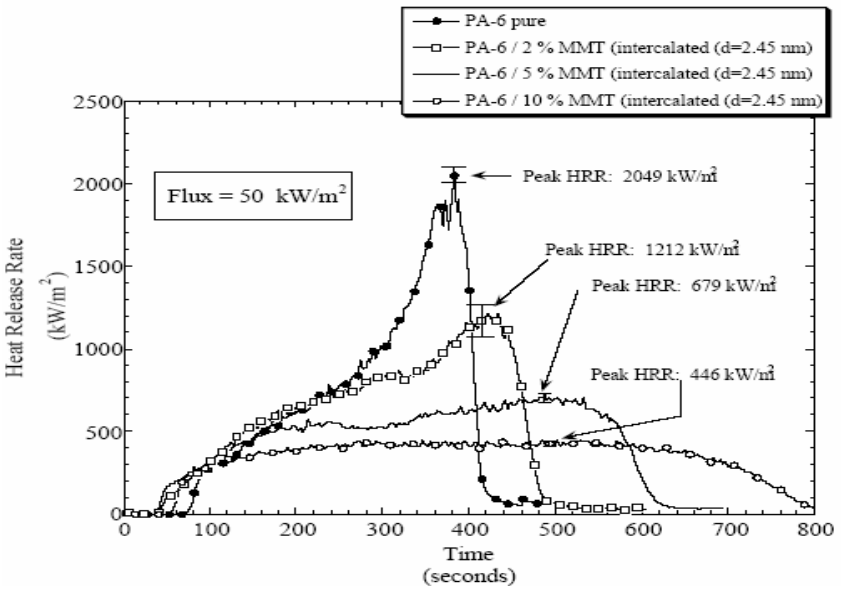

Figure 1. Effects of Clay Content on Heat Release Rate of 8-mm Nylon at 50 kW/m^2 [1]

It is clear that the clay affects the flammability characteristics of the nanocomposite. The measurements in this study will attempt to present these effects in terms of fire properties that are the physical and chemical properties representative of the bulk polymer. In some cases, they are approximate and are representative of idealized burning conditions. For example, they include the heat of combustion, Δh_c, measured for the flaming state; the heat of gasification, L,

representative of steady burning and ideally representing the enthalpies of phase change and the heat capacity effect based on its supply temperature; thermal properties, $k\rho c$, the char fraction, X_c, and the ignition temperature, T_{ig}. Gilman, et al. [1] found the energy release rate decreases while there is no change in the heat of combustion, remaining at about 27 kJ/g. Giannelis [3] reports that an increase in thermal stability and a decrease in permeability can also be achieved by the addition of clay. Both characteristics can affect flammability by increasing the time to ignite and reducing the production of volatile fuel gases, accordingly. Indeed, this indicates that the clay additive is reducing the flow rate of volatiles while not affecting the combustion of the nylon. A Transmission Electron Microscopy of a section of residue from the PA-6-MMT nanocomposite showed 1-nm-thick bands of carbonaceous-silicate char formed on the burning samples [1]. Charring materials yield a lower mass loss rate due to the char left behind. Subsequently, this char will oxidize in a fire environment and yield additional energy.

As a thin burning sample is depleted, its reduced thickness causes higher temperatures on its back surface. Thus, this reduced heat loss causes an increase in the burning rate. This increase is not an inherent characteristic of the polymer, but an effect of thickness. On the other hand, the nanocomposites show a reduction of this tendency to increase burning at the end of the test, and this reduction appears to correlate with the PA-6-MMT addition. The charring effects, induced by the MMT clay, are likely playing a role here. These are compensating actions between the tendency of the char to decrease burning and the back-face insulation to increase burning. The general characteristic of thick charring materials to decrease in burning rate, falling as $1/t^{1/2}$ after an initial rise to a peak following ignition, is not seen with the addition of the MMT [4]. Hence, the effects of char in the 8-mm-thick nylon tests appear more complicated or are affected by thickness.

Another factor observed in the Gilman, et al. study [1] is that as the MMT additive is increased, the overall total energy available to combustion appears invariant. Thus, the burning time is increased as the MMT is increased. For these same samples, the time to ignition is not necessarily changed. The ratio of the time to ignite (t_{ig}) and burn time (t_b) is significant in flame spread. Indeed, the burn time can be reduced in vertical spread by melting and dripping. This is a characteristic of nylon and other thermoplastics. These factors may be influential in small-scale tests such as the vertical application of UL-94, Flammability of Plastics Materials. It has been reported that PA-6 Nylon at 5% MMT receives a V-2 rating in UL-94 (meaning the cotton below was ignited from flaming drips), and PA-6 at 10% MMT failed the UL-94 (meaning that it burned for more than 30 seconds). The latter could be explained by char inhibiting the drips, holding more of the polymer in place and, hence, a longer burning time. The passing of the pure nylon test by might be due to its increased tendency to melt. Hence, the addition of the MMT can have various flammability outcomes depending on the fire process: ignition, spread, or static burning.

This study will examine the flammability in the cone calorimeter for nylon-MMT samples of 0%, 2%, and 5%. Thickness will range over 1.6, 3.2, 4, and 8 mm, but only the latter two sizes will be reported now. The burning data in the cone will range over heat fluxes from the minimum needed for ignition to about 60 kW/m^2. Properties will be reduced from these data by analysis, and will include:

- Heat of combustion, Δh_c: the energy released in combustion per unit mass lost
- Critical heat flux for ignition: the threshold of radiant heat flux for piloted ignition
- Ignition temperature, T_{ig}: the estimated surface temperature at ignition
- Thermal inertia, $k\rho c$: the effective thermal property for a thick material that indicates the ability to conduct heat into the material
- Heat of gasification, L: the energy required to gasify the material into fuel

The ratio $\Delta h_c/L$ is a measure of the energy release rate of the material given equal flame heat flux. The parameter $k\rho c(T_{ig} - T_{initial})^2$ is proportional to the ignition time for the same applied heat fluxes. The flame spread rate is inversely proportional to this quantity for the same flame heating conditions. These properties' terms relate to fire hazard potential, while the individual properties can give some indication of the mechanistic role of the MMT.

2. EXPERIMENTAL SETUP AND PROCEDURE.

2.1 EXPERIMENTAL SETUP.

The cone calorimeter is a commonly used device used to measure the mass loss rate per unit area (m'') and the heat release rate per unit area (Q'') for a given constant external radiative heat flux. Experiments for the nanocomposites materials were performed using a radiant cone heater assembly. The apparatus, shown in figure 2, consisted of a cone heater, a load cell, and an electric arc igniter. A computer program built by National Instruments LabVIEW (figure 3) was used as the data acquisition system.

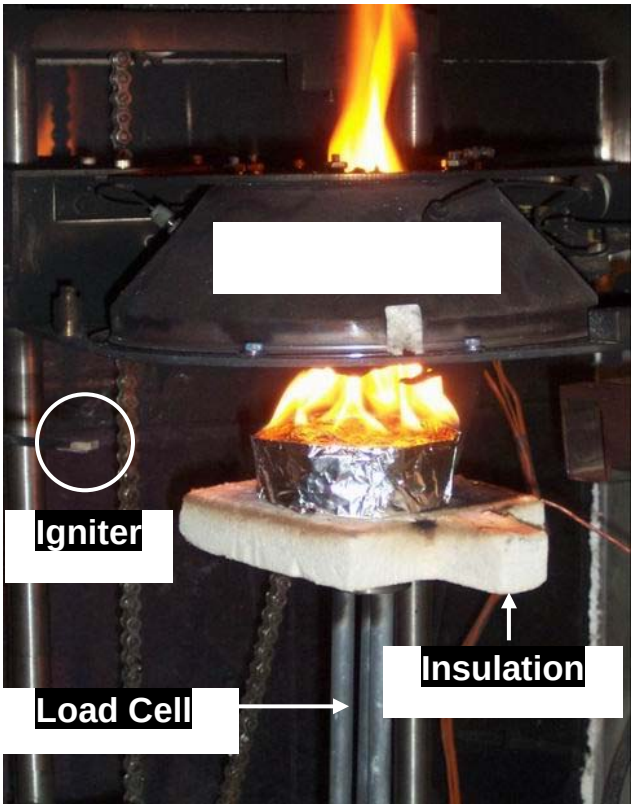

Figure 2. Experimental System

Figure 3. Data Acquisition System Built Using LabVIEW

2.2 MATERIALS AND SAMPLE PREPARATION.

Test samples consisting of pure Nylon 6 and nylon with 2% and 5% nanoclay additives were used in the study. Pure Nylon 6 is also called polyamide 6 (PA-6). The PA-6 homopolymers are

UBE 1015B with a molecular mass (M_W) ≈ 15,000 g/mol, UBE 1015C2 PA-6 with a M_W of ≈ 15,000 g/mol with an MMT of 2% by mass fraction, and UBE 1018C5 PA-6 with a M_W of ≈ 18,000 g/mol with MMT of 5% by mass fraction. All samples were dried for 2 hours at 75°C, and molded at 280°C. The disks were 75 mm in diameter and had a thickness of 1.6, 3.2, 4, and 8-mm [5].

The test samples were wrapped in aluminum foil to prevent melting. The back side of the sample was insulated with a 1-inch-thick Kaowool board (type M) to minimize heat loss.

2.3 EXPERIMENTAL PROCEDURE.

The experimental procedure consisted of exposing a test sample in the horizontal orientation to a constant external irradiance from the cone heater. A heat flux gauge was used to determine the initial incident heat flux. Each time before testing, the heat flux was checked in the same location above the center of the sample, and when a constant heat flux was recorded, the experiment was started.

The test procedure consisted of the following steps:

1. Start data acquisition system.

2. Cover the test sample surface with an aluminum sheet.

3. Place the sample onto the metal holder of the cone.

4. Quickly remove the aluminum sheet and start timing. The aluminum sheet prevents the radiation heat from reaching the sample before the timing starts.

In addition, an electric arc igniter was located approximately 1 cm above the sample surface and was used as a pilot ignition source of the fuel gas released by the sample surface.

The time to piloted ignition was measured by a stopwatch, and the ignition time is defined as the time at which a continuous flame is supported on the entire material surface. In some cases, flashing occurred on the surface before a sustained flame was observed, but it was not considered ignition time until the entire surface was covered by flame.

The mass loss readings were recorded every second by a load cell and the data acquisition program.

3. EXPERIMENT OBSERVATIONS.

3.1 BURNING BEHAVIOR.

The clay loading of a sample affects the burning process. The external heat flux from the heater of the cone ranged from 18 kW/m^2 to 56 kW/m^2 for testing the samples.

3.1.1 Nylon.

For high heat flux (above 30 kW/m^2), the pure nylon sample exhibited a melting-like behavior. When the heater was on, the sample surface began to bubble. Evaporative fuel gases were released from the sample when the concentration of fuel gas reached the lower flammable limit, the electric arc igniter ignited it. The whole sample swelled under the external heat flux from the cone heater and the flame heat flux. The center part can rise due to the swelling, shown in figure 4, and then recedes due to the sample melting. It kept melted until the whole piece turned to a liquid phase and burned until all of the fuel was consumed. Figures 4-6 show the burning process of 4-mm nylon under 56 kW/m^2 external heat flux. The order was from early stage burning with the center part rising (figure 4), to steady burning (figure 5), to finally, extinguished (figure 6).

Figure 4. A Burning 4-mm Nylon Center Rising Due to Swelling Under 56 kW/m^2 Heat Flux

Figure 5. Liquid-like Steady Burning of 4-mm Nylon Under 56 kW/m^2 Heat Flux

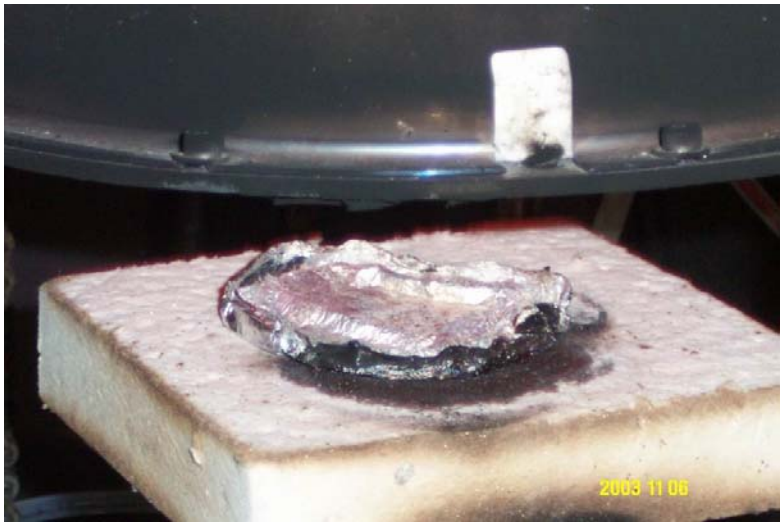

Figure 6. A 4-mm Nylon 6 Sample After Burning at 56 kW/m^2 Heat Flux

Under low-heat flux, the decomposition is relatively slow. The surface will oxidize first and form a thin carbonaceous skin. Figure 7 shows 3.2-mm nylon under 16 kW/m^2 external heat flux. No ignition occurred, but oxidation happened.

Figure 7. A 3.2-mm Nylon Sample at 16 kW/m^2 Heat Flux With no Ignition, but Oxidized and formed a Carbonaceous Skin

3.1.2 Nylon + Clay.

For test samples with clay, the time to ignite was increased as the clay loading was increased. The carbonaceous skin due to oxidation was always formed before ignition, and at a high heat flux of about 50 kW/m^2, the char skin was relatively thin and weak and evaporated fuel gases could still pass through the skin. When ignition occurred, the flame could cover the whole surface. Figure 8 shows the burning of a 24-mm nylon +2% clay under 50 kW/m^2 heat flux.

Figure 8. A Test Sample of 24-mm Nylon + 2% Clay Just After Ignition Burning Under 50 kW/m^2 Heat Flux

Lower heat fluxes (less than 30 kW/m^2) require a longer ignition time; the char skin forms before ignition, and it is thicker and stronger. Before ignition, fuel gas cannot go through the char skin; it accumulates underneath the skin and a big bubble is formed. The whole sample looks like a muffin. As the bubble keeps increasing, the char skin cannot cover the whole sample any more and there are leaks at the edge of skin. Due to its accumulation, the dense fuel gas is released and it is sufficient for ignition. Flames at these gas leaks consume fuel and the gas bubble shrinks causing the char skin to fall back. Sometimes, it can seal the leaks. The same process will happen again until the gas evaporating rate is high enough to support a flame at the edge. Flame heat flux also offers extra heating to the sample, which speeds up the melting and evaporating. The spreading flame will extend the leak along the edge or maybe to some part of the skin and the whole piece can be completely covered by flame. The carbonaceous skin is not flammable and it remains until all the fuel shielded under it is consumed. Figure 9 shows the bubble formed before ignition, and figure 10 shows the flame burning at edge. Both figures 9 and 10 show 8-mm nylon +2% clay samples heated under a 34 kW/m^2 heat flux.

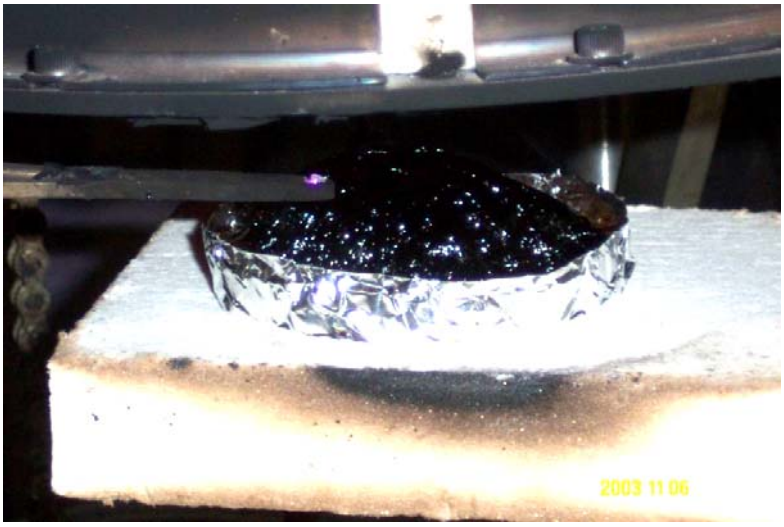

Figure 9. An 8-mm Nylon +2% Clay Test Sample Under a 34 kW/m^2 Heat Flux Before Ignition

Figure 10. An 8-mm Nylon +2% Clay Test Sample Under a 34 kW/m^2 Heat Flux Burning at Leaks at the Edge

3.2 RESIDUE.

Samples consisting of different clay additives have different amounts of residue remaining after burning. For pure nylon, the flame consumes the skin and no residue is left after burning. A char skin may be formed under low heat fluxes, but it is very thin.

For nylon with 2% clay, the char skin remains under the skin at the end of burning. On the bottom of the aluminum cup containing the sample piece, only small pieces of char remain. It is nearly hollow between the top char skin and the bottom of the aluminum cup. In figure 11, a cut of the side of the aluminum cup clearly shows the residue inside.

Figure 11. A 24-mm Nylon +2% Clay Test Sample Under 50 kW/m^2 Residue After Burning

For nylon with 5% clay, char skin formed before ignition and remained on the top. However, as the test clay percentage was increased, more char was left. It filled the space between the top skin and the bottom of the cup, as shown in figure 12.

Figure 12. A 24-mm Nylon +5% Clay Under 50 kW/m^2 Residue After Burning

4. RESULTS AND ANALYSIS.

4.1 EXPERIMENTAL RESULTS.

4.1.1 Specimen Mass (g).

The mass was measured by the load cell of the cone and was recorded by a LabVIEW data acquisition program. Figure 13 shows the sample mass changing with time.

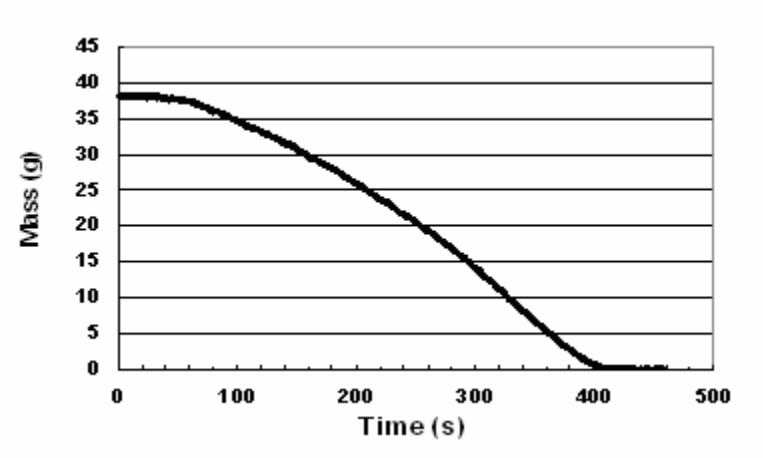

Figure 13. Mass Curve of 8-mm Nylon +2% Clay Under 55 kW/m^2

4.1.2 Mass Loss Rate (g/s).

In order to get mass loss rate $\dot{m} = \frac{dm}{dt}$, which is the numerical derivative of mass-time data, a 3-point interpolation formula (equation 1a) was used [6], which follows from

$$\frac{dy}{dx} = \frac{1}{h}(\Delta y_n - \frac{1}{2}\Delta^2 y_n + \frac{1}{3}\Delta^3 y_n - \frac{1}{4}\Delta^4 y_n + \cdots)$$

$$\Delta^2 y_n = \Delta y_{n+1} - \Delta y_n = y_{n+2} - 2y_{n+1} + y_n$$

$$\Delta^3 y_n = \Delta^2 y_{n+1} - \Delta^2 y_n = y_{n+3} - 3y_{n+2} + 3y_{n+1} - y_n$$

3-point interpolation

$$\dot{m}_i = \frac{dm_i}{dt} = \frac{1}{t}(-0.5m_{i+2} + 2m_{i+1} - 1.5m_i) \tag{1a}$$

t: time interval

Also, 4- and 5-point interpolation formulas were tried. Figure 14 shows that the 3-point formula is smoother than the other two, and therefore, the 3-point formula was used in this analysis.

4-point interpolation

$$\dot{m}_i = \frac{dm_i}{dt} = \frac{1}{t}(\frac{1}{3}m_{i+3} - \frac{3}{2}m_{i+2} + 3m_{i+1} - \frac{11}{6}m_i) \tag{1b}$$

5-point interpolation

$$\dot{m}_i = \frac{dm_i}{dt} = \frac{1}{t}\left(-\frac{1}{4}m_{i+4} + \frac{4}{3}m_{i+3} - 3m_{i+2} + 4m_{i+1} - \frac{25}{12}m_i\right) \tag{1c}$$

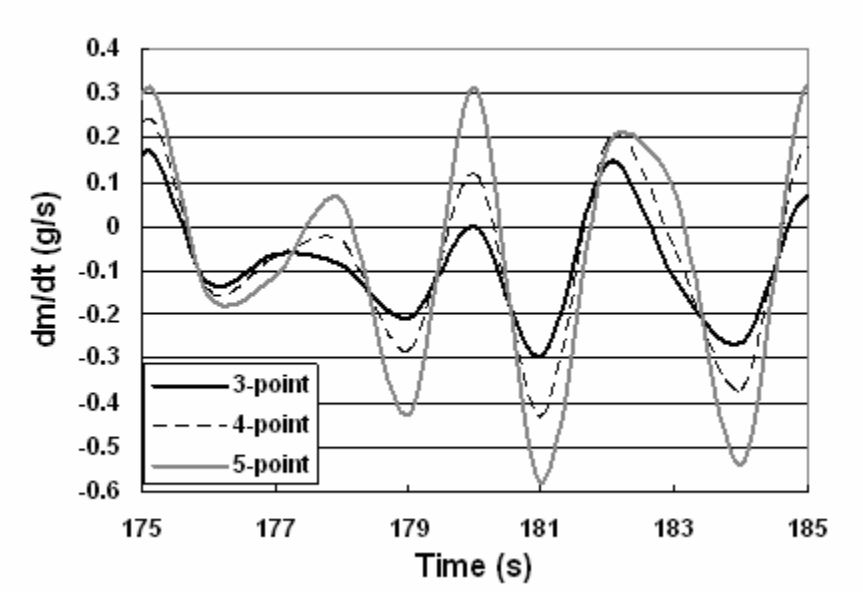

Figure 14. Comparison of the Mass Loss Rate of 8-mm Nylon +2% Clay Under 55 kW/m^2 Using the Three Different Interpolation Formulas

4.1.3 Mass Loss Rate per Unit Area (g/m^{2}s).

$$\dot{m}'' = \frac{\dot{m}}{Area} \tag{2}$$

Even though the 3-point interpolation formula was chosen to find the derivative, the $\dot{m}''$ versus time curve shown in figure 15 was still noisy. Therefore, a moving average value was needed to show the trend more clearly.

The comparison of 5-, 9-, and 19-point averages is shown in figure 16. The 19-point moving average clearly showed the trend and was used in the tests.

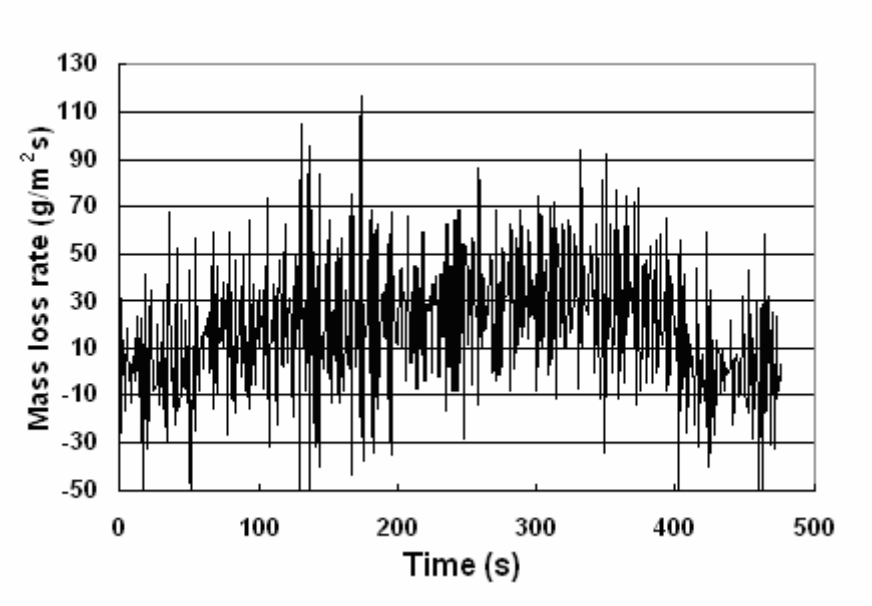

Figure 15. Mass Loss Rate of 8-mm Nylon +2% Clay Under 55 kW/m^2 Before Using the Moving Average

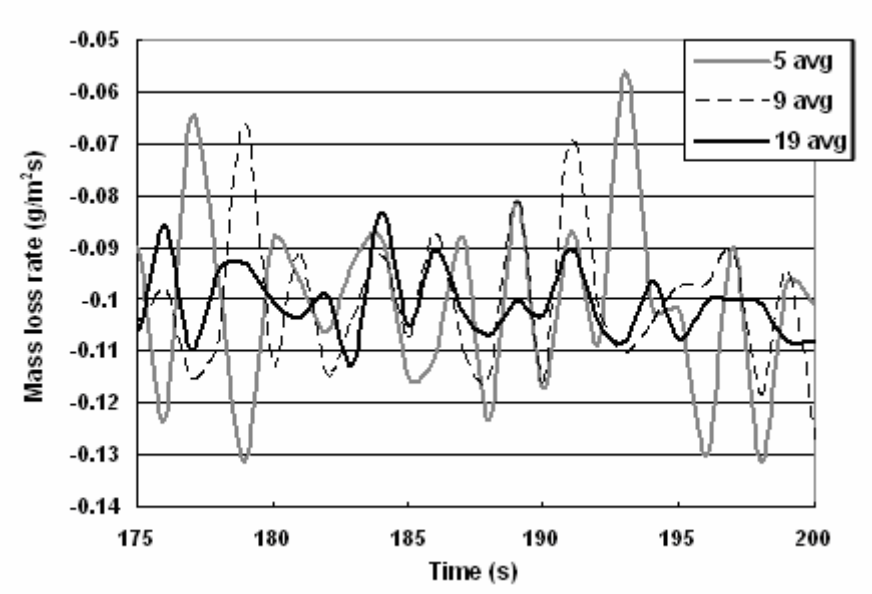

Figure 16. Mass Loss Rate of 8-mm Nylon +2% Clay Under 55 kW/m^2 Using the Moving Average Comparison

After using the 19-point moving average, the trend of the mass loss rate per unit area was relatively smooth (figure 17).

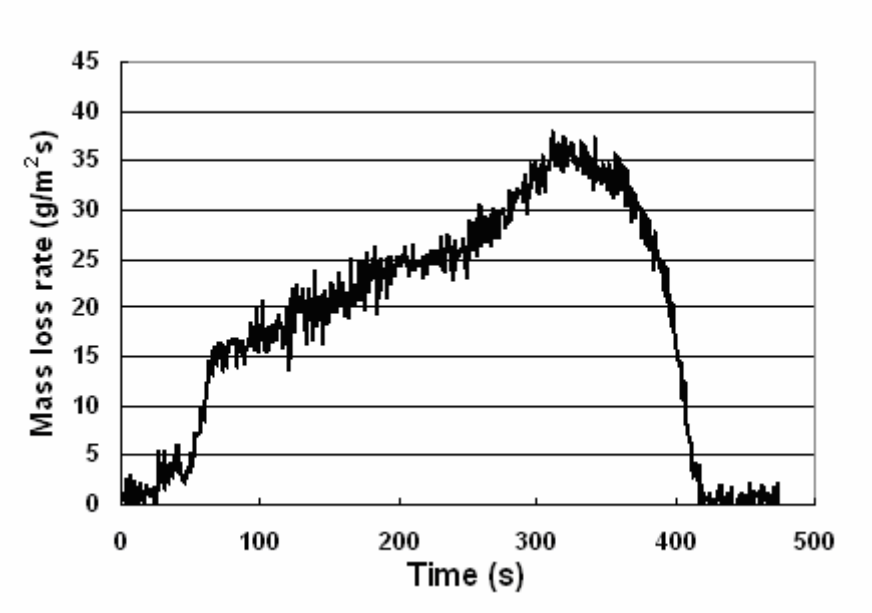

Figure 17. Mass Loss Rate of 8-mm Nylon +2% Clay Under 55 kW/m^2

Figure 18 shows the mass loss rate per unit area of the nylon +5% clay for different thickness under 53 ±3 kW/m^2, and how the mass loss rate peak value decreased with increased thickness.

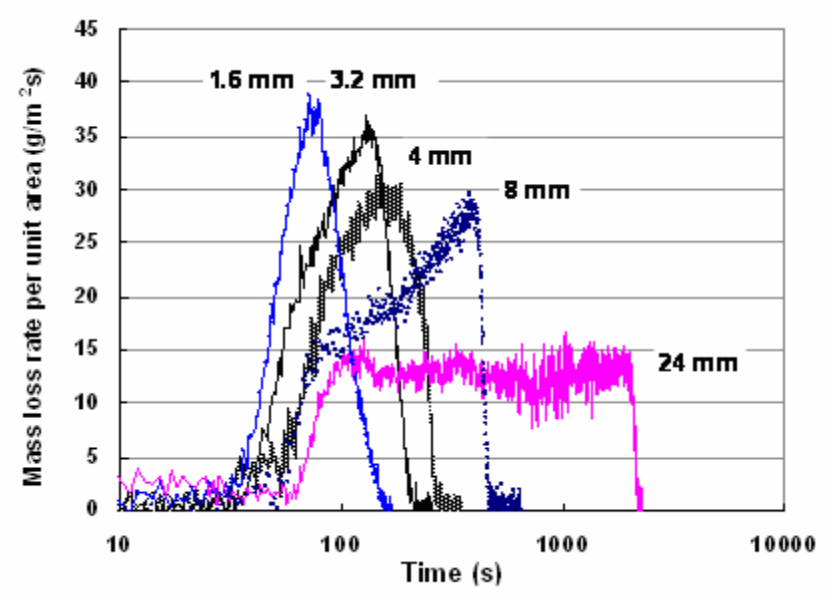

Figure 18. Mass Loss Rate Curves of Nylon +5% Clay With Different Thickness Under 53 ±3 kW/m^2

4.1.4 Oxygen Concentration (%).

The oxygen concentration was measured by a Combi-Analyzer oxygen sensor ULTRAMAT/OXYMAT 6 from Siemens.

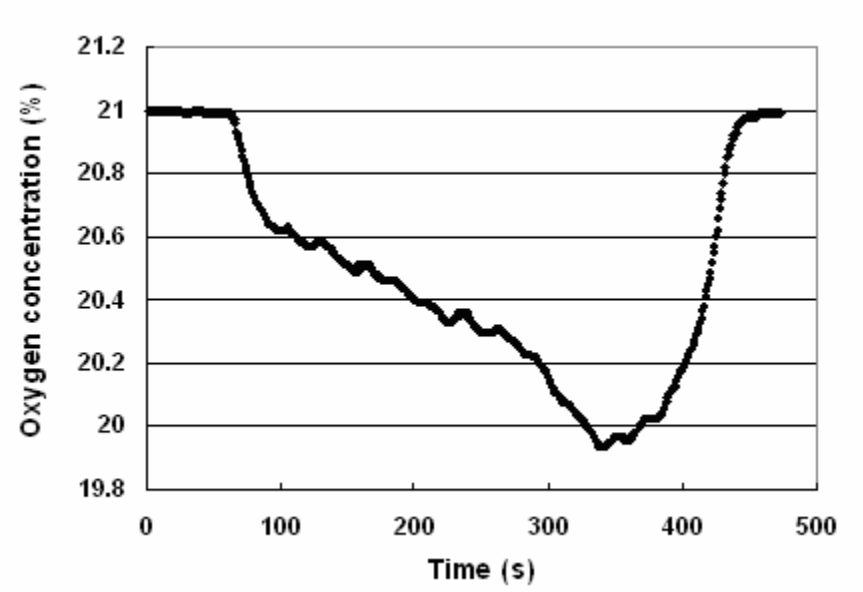

Figure 19. Oxygen Concentration Curve of 8-mm Nylon +2% Clay Under 55 kW/m^2

4.1.5 Heat Release Rate per Unit Area (kW/m^2).

The rate of heat release was determined by the measurement of the oxygen consumption as determined by the oxygen concentration and the flow rate in the exhaust product stream.

In the test, water vapor (removed by a cooling unit and a moisture sorbent) and the CO_2 (removed by a chemical sorbent) had to be removed from the exhaust gas sample stream prior to O_2 measurement at the Combi-Analyzer ULTRAMAT/OXYMAT 6 from Siemens oxygen sensor. As shown in figure 20, all of the combustion products are collected and removed through an exhaust duct. Both the flow rate and composition of the gases were measured.

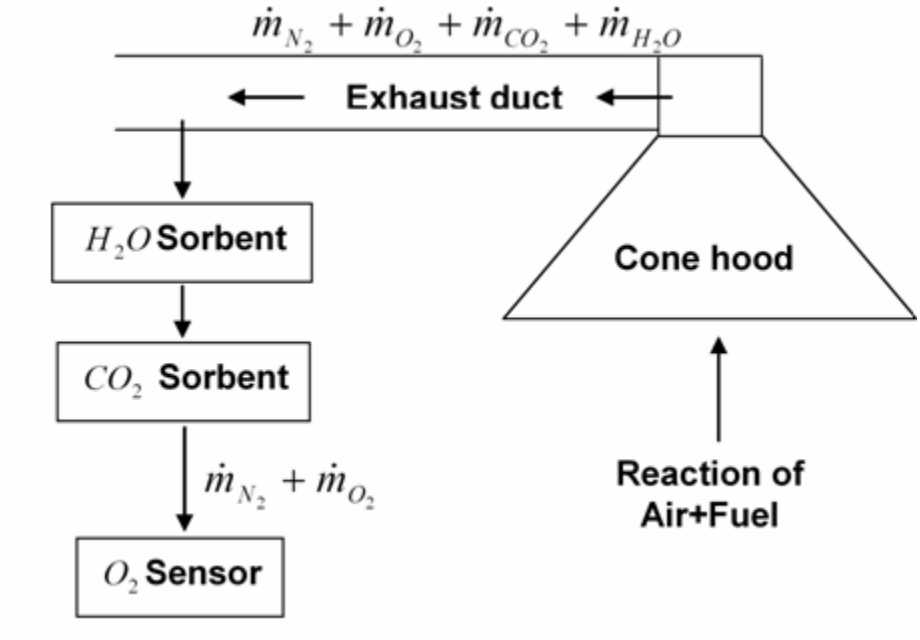

Figure 20. Equipment Arrangement for the O_2 Measurement

Since the sample gas only consists of O_2 and N_2, the standard [7 and 8] gives the heat release rate (firepower) as:

$$\dot{Q} = \Delta h_{O_2} \left[\frac{\phi}{1 + \phi(\alpha - 1)} \right] \dot{m}_e \frac{M_{O_2}}{M_a} X_{O_2}^0 (1 - X_{H_2O}^0 - X_{CO_2}^0) \tag{3}$$

$$\text{with } \phi = \frac{X_{O_2}^0 - X_{O_2}}{(1 - X_{O_2}) X_{O_2}^0} \tag{4}$$

where:

ϕ = oxygen depletion factor
α = volumetric expansion factor
M_{O_2} = molecular weight of oxygen (28 g/mol)
M_a = molecular weight of the combustion air (29 g/mol for dry air)
$X_{O_2}^0$ = initial reading from the oxygen analyzer
X_{O_2} = final reading from the oxygen analyzer
$X_{H_2O}^0$ = mole fraction of H_2O in the incoming air
$X_{CO_2}^0$ = mole fraction of CO_2 in the incoming air
$X_{H_2O}^0$ and $X_{CO_2}^0$ were small and negligible

After simplification:

$$Q = \frac{\Delta h_c}{r_{O_2}} m_e \left(\frac{M_{O_2}}{M_a}\right) \frac{X_{O_2}^0 - X_{O_2}}{\alpha - \left(1 + \frac{\alpha - 1}{X_{O_2}^0}\right) X_{O_2}} \tag{5}$$

Generally $\frac{\Delta h_c}{r_{O_2}} = 13.1$ kJ/g, $\frac{M_{O_2}}{M_a} = 1.10$, $X_{O_2}^0 = 0.21$

In the literature, ASTM E1354-99, the particular value for the expansion factor α is not specified, but the heat release equation is presented with an average value for the expansion factor (α = 1.105).

In a more detailed analysis (appendix A), the same oxygen consumption measurement method was used to determine the heat release rate equation with consideration of stoichiometric chemical reactions for many materials. Comparing the following heat release equation (6) with equation 5 shows how the expansion factor, α , and how it varies for materials. The derivation is explained in the appendix A, and the result was:

$$\dot{Q} = \frac{\Delta h_c}{r_{O_2}} \dot{m}_e \left(\frac{M_{O_2}}{M_a}\right) \frac{X_{O_2}^0 - X_{O_2}}{1 + \frac{Y_{O_2,\infty}}{r_{O_2}} - \frac{r_{CO_2} + r_{H_2O}}{r_{O_2}} \left(\frac{M_{O_2}}{M_a}\right) X_{O_2}} \tag{6}$$

Comparing equations 5 and 6 shows that the only difference is the denominator. In the ASTM literature, α =1.105 and $\left(1 + \frac{\alpha - 1}{X_{O_2}^0}\right) = 1.5$. The test analysis of the different fuels produced an average value of the corresponding terms $\alpha \equiv 1 + \frac{Y_{O_2,\infty}}{r_{O_2}}$ and $1 + \frac{\alpha - 1}{X_{O_2}^0} \equiv \frac{r_{CO_2} + r_{H_2O}}{r_{O_2}} \left(\frac{M_{O_2}}{M_a}\right)$ for a range of materials is 1.08 and 1.44, respectively. Therefore, there is not much difference. However, for a specific fuel, it is easy to get the chemical properties, and equation 6 gives a more accurate result. For the current test, the samples are nylon with different clay distributions, and, to be consistent with previous literature results for the nylon nanocomposites, the standard heat release equation was used.

The heat release rate per unit area curve of 8-mm nylon +2% clay under 55 kW/m^2 is shown in figure 21.

Under the same external heat, the curves for different thickness of nylon +5% clay are shown in figure 22.

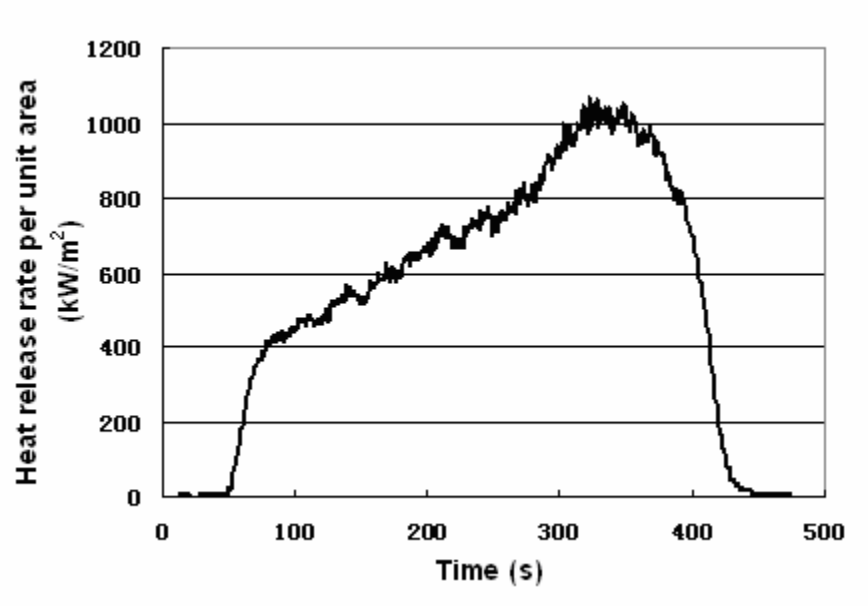

Figure 21. Heat Release Rate per Unit Area of 8-mm Nylon +2% Clay Under 55 kW/m^2

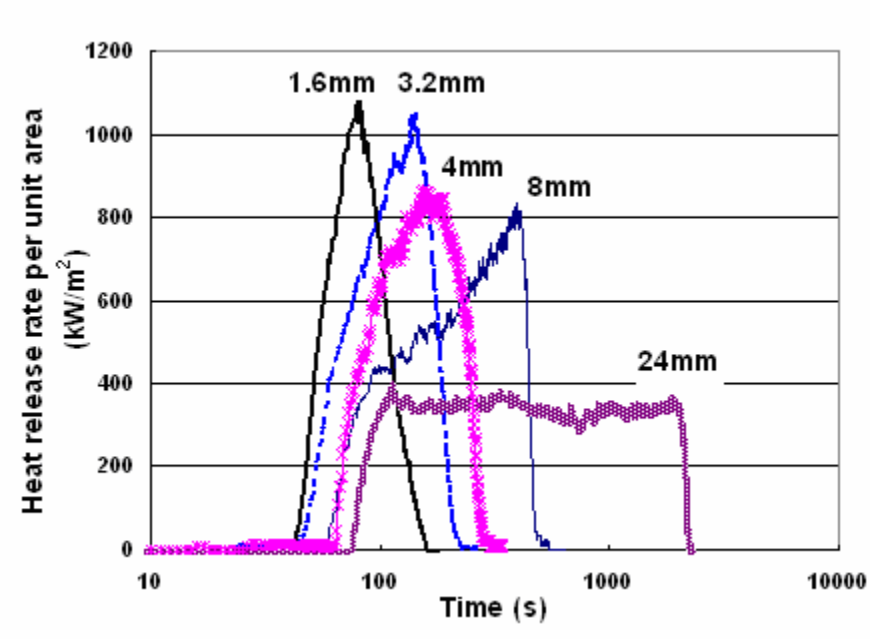

Figure 22. Heat Release Rate per Unit Area of Nylon +5% Clay With Different Thickness Under 53 ±3 kW/m^2

4.1.6 Total Energy Release (MJ/m^2).

The total energy release is the amount of energy released over the duration of the test. It can be calculated by integrating the heat release rate over that period, equation 7.

$$Q''_{total} = \int \dot{Q}'' dt \tag{7}$$

Figure 23 shows the total energy release for each time of an 8-mm nylon +2% clay sample under 55 kW/m^2. Each time on the timeline is the integration of heat release rate from the beginning to that point.

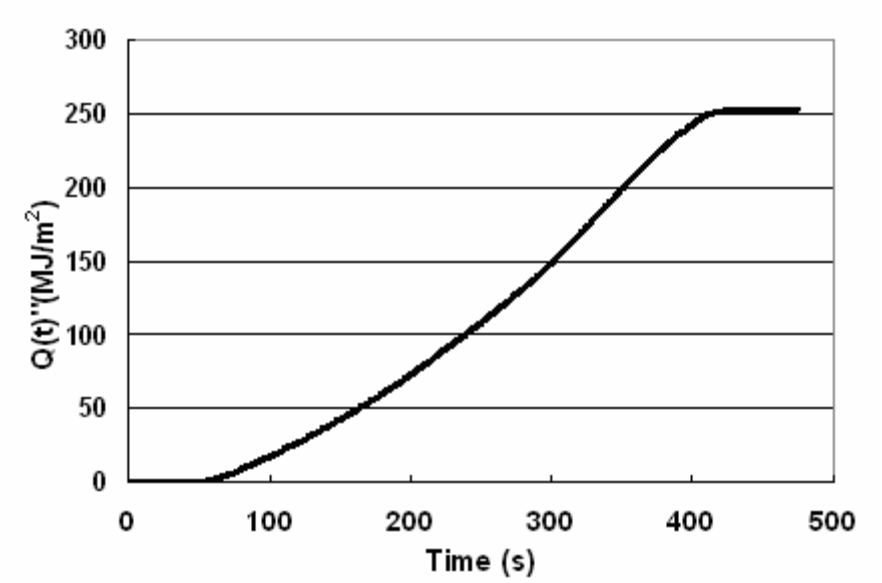

Figure 23. Total Energy Release of 8-mm Nylon +2% Clay Under 55 kW/m^2

The samples have the same surface area, but a different thickness. A thicker sample means that more fuel can be burned and more energy can be released. In order to eliminate the thickness factor, it can be expressed in terms of a unit volume (Q''_{total}). The total energy per unit volume is calculated by:

$$Q'''_{total} = \frac{Q''_{total}}{d} \tag{8}$$

where d is the sample thickness.

As shown in figure 24, the total energy release per unit volume is independent of the incident heat flux. The addition of clay had little affect on the total energy release and was nearly invariant.

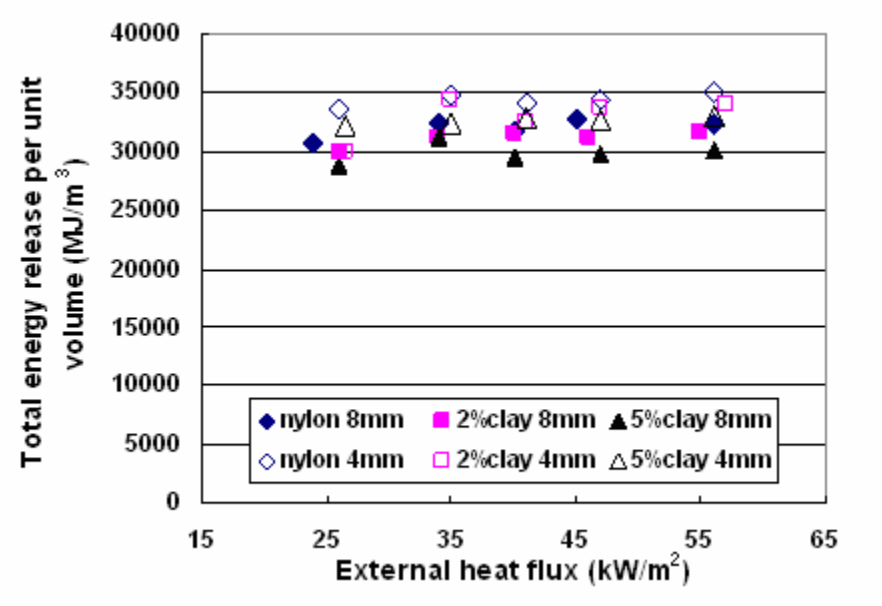

Figure 24. Total Energy Release per Unit Volume of Different Samples Under Different External Heat Flux

4.2 THERMAL PROPERTIES.

4.2.1 Heat of Combustion Δh_c.

The heat of combustion is the amount of energy released as one mole of a given substance is burned in the presence of oxygen. It is defined as the positive value of enthalpy change per unit mass or mole of fuel reacted at 1 atm and in which the temperature of the system before and after the reaction is 25°C [9].

The cone calorimeter standard [10] specifies the time-varying heat of combustion value to be calculated by $\Delta h_c = \frac{\dot{Q}''(t)}{\dot{m}''(t)}$ which is defined as the rate of energy produced divided by the sample mass loss rate.

- $\dot{Q}''(t)$ Heat release rate per unit area (kW/m^2)
- $\dot{m}''(t)$ Mass loss rate per unit area (g/m^{2}s)

Figure 25 shows the heat of combustion, mass loss rate per unit area, heat release rate per unit area of 8-mm nylon +2% clay under 55 kW/m^2.

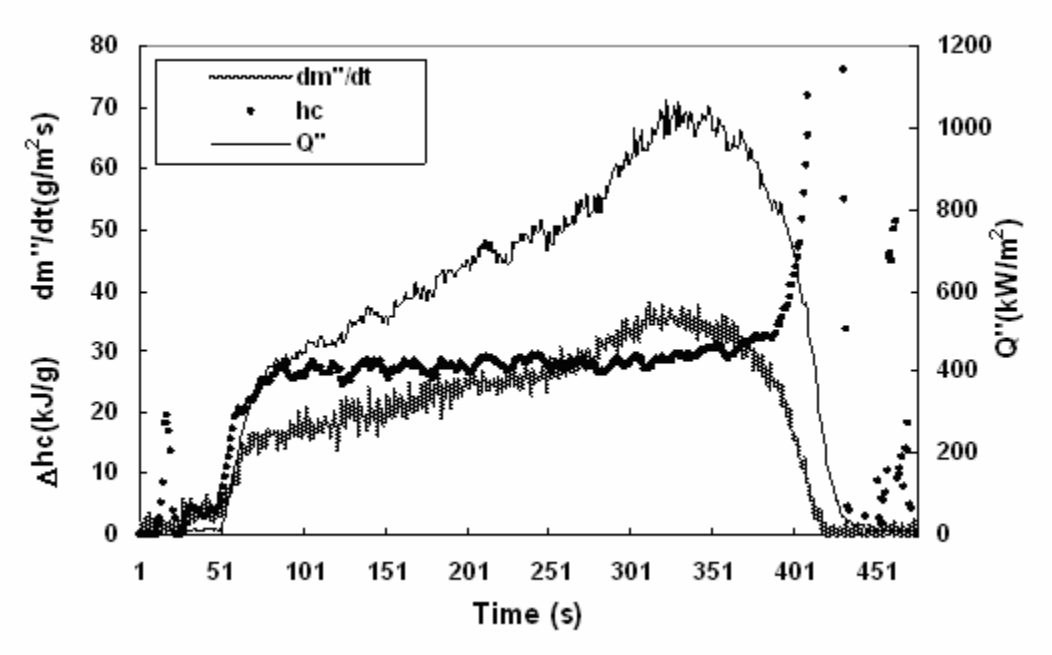

Figure 25. Mass Loss Rate, Heat of Combustion, and Heat Release Rate of 8-mm Nylon +2% Clay Under 55 kW/m^2

4.2.2 Peak-Average Heat of Combustion.

The peak-average value is intended to represent an energy release rate that is more consistent with steady burning as opposed to an instantaneous maximum value or the average of the entire burning process. In this study, two peaks were considered. The heat of combustion curve appeared to reach a plateau (first peak), but may continue to increase due to the thickness effect (second peak). In some cases, two peaks are clearly seen. In other cases, the first peak was not as clear. For this analysis, the first peak-average value is the average over the perceived peak period. The second peak-average value is estimated from an average peak energy release rate that occurred over a time period that continuously included values 20% below the peak value of $\dot{Q}''$ [4]. The peak-average was taken to be an integrated average of the measured values over a time period. This is illustrated, for the heat of combustion, by equation 9 and figure 26.

$$\Delta\bar{h}_{c,peakavg} = \frac{1}{t_2 - t_1}\int_{t_1}^{t_2} \Delta h_c \, dt \tag{9}$$

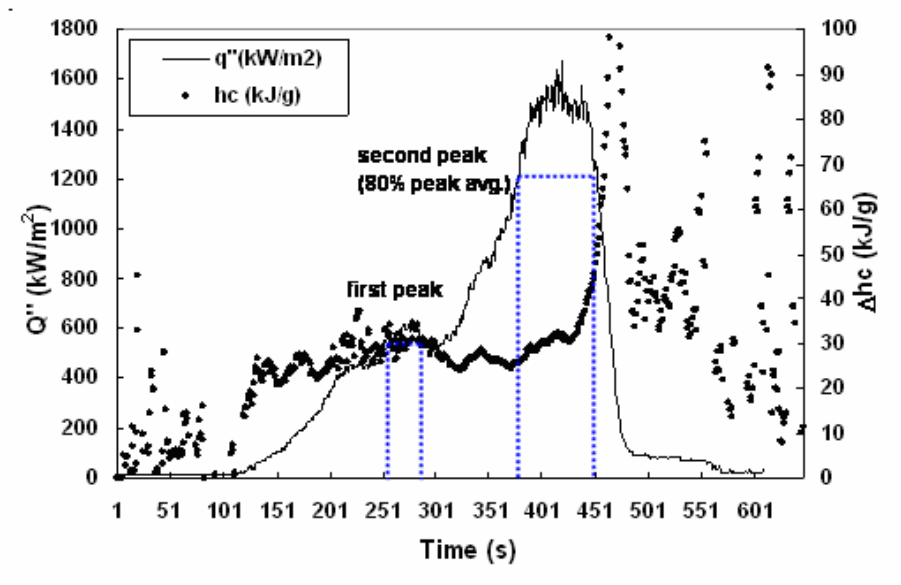

Figure 26. Two Peak Averages of 8-mm Nylon Under 34 kW/m^2

Figure 27 gives the heat of combustion values as a function of heat flux, clay loading, and thickness based on the second peak average. Table 1 shows the invariance of the heat of combustion with respect to the peaks and samples, essentially 30 ±2 kJ/g.

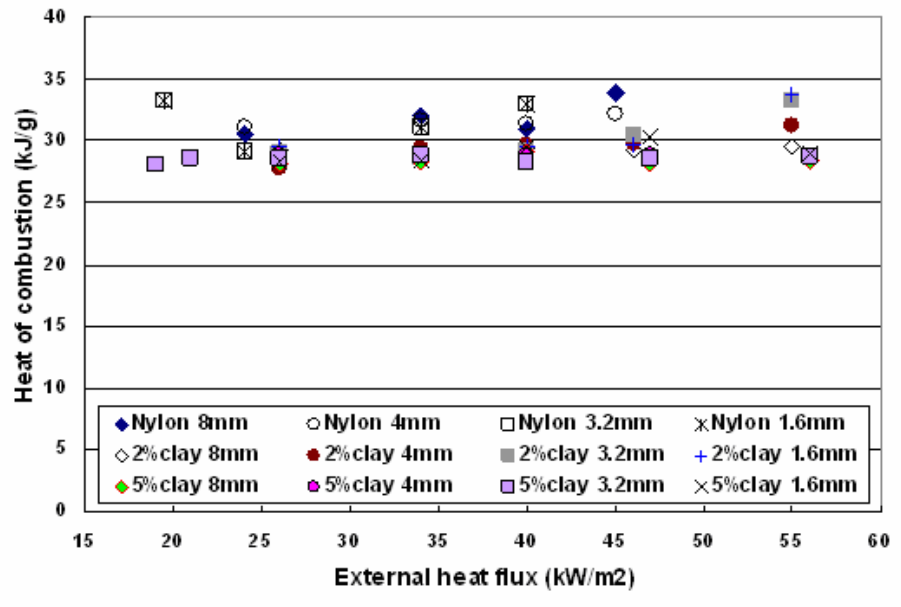

Figure 27. Heats of Combustion for Different Samples Based on the Second Peak

Table 1. Summary for the Heat of Combustion (kJ/g)

Additive	Thickness (mm)	First Peak	Second Peak	Overall
0	24	29.2	29.8	28.6
	8	30.1	32.5	28.8
	4	26.8	33	28.6
	3.2	24.8	33.7	27.0
	1.6	--	30.1	27.7
2% Clay	24	27.3	27.4	26.4
	8	29.0	29.3	28.5
	4	26.2	29.6	28.2
	3.2	--	29.7	27.3
	1.6	--	30.2	27.3
5% Clay	24	27.2	27.0	26.4
	8	27.5	28.4	28.0
	4	26.2	28.8	28.1
	3.2	--	29.3	29.8
	1.6	--	29.0	27.5

4.2.3 Overall Heat of Combustion $\Delta h_{c,\ overall\ avg}$.

The overall heat of combustion is calculated by dividing the total heat release from each sample by the total specimen mass loss. This overall value represents an average of the burning characteristics over the entire test duration. The average values shown in figure 28 are determined by taking the numerical average of the values calculated from each cone test. There was very little reduction due to the addition of clay.

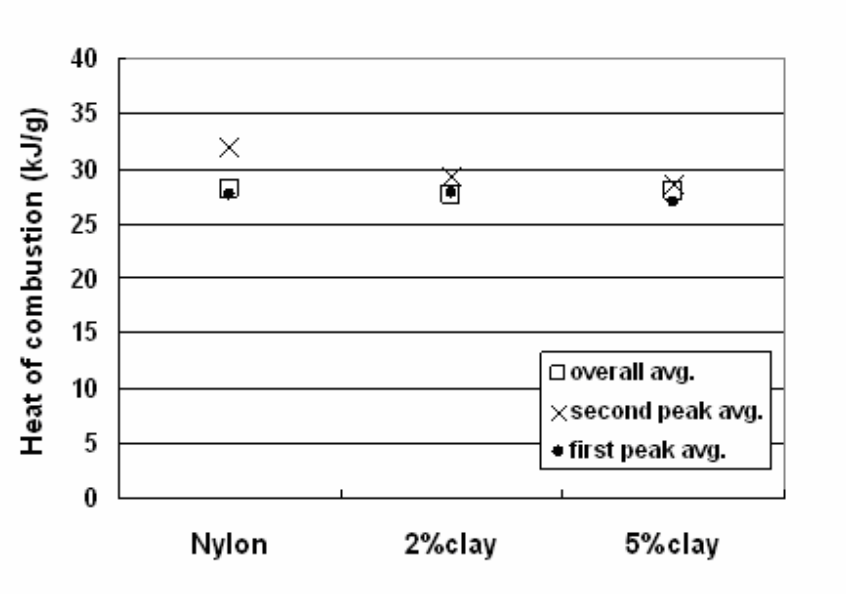

Figure 28. Overall Average Heats of Combustion for Different Samples

4.2.4 Heat of Gasification, *L*.

When exposed to a given heat flux, the test material will vaporize at a certain rate. This rate can be expressed by the mass loss rate per unit area of material $\dot{m}''$ at a given net heat flux to the material $\dot{q}''_{net}$. The heat of gasification is the energy required to produce the fuel volatiles per unit mass of the material.

Materials may be approximated as vaporizing solids in order to represent, on average, their ability to vaporize under heating. An exact solution for a thermally thick, steadily vaporizing solid indicates a mass flux proportional to the net heat flux:

$$\dot{m}'' = \frac{\dot{q}''_{net}}{L} \tag{10}$$

The heat of gasification represents the total energy needed to vaporize from its initial state. The net surface heat flux for the gasification period is:

$$\dot{q}''_{net} = \varepsilon \dot{q}''_{ext} + \dot{q}''_{fl} - \varepsilon \sigma T_v^4 \tag{11}$$

For the following analysis, the surface emissivity ε of the burning material was approximated as being equal to 1, as to simplify the analysis. The formation of an oxidized skin or char justifies this approximation. If the flame heat flux in equation 11 was assumed to be constant, which has been shown to be the case for thermoplastic-like materials burning in the cone calorimeter, then the equation 10 can be written as:

$$\dot{m}'' = (\frac{1}{L})\dot{q}''_{ext} + \frac{(\dot{q}''_{fl} - \varepsilon \sigma T_v^4)}{L} \tag{12}$$

where:

$\dot{q}''_{fl}$ is the incident flame heat flux

$\dot{q}''_{ext}$ is the external heat flux provided by the cone heater (kW/m^2)

T_v is the vaporization surface temperature

Using the mass loss rate data from the cone calorimeter, estimations of the heat of gasification were made. In order to use equation 12, the flame heat flux and re-radiant heat loss for each material in the cone calorimeter was considered to be constant. Therefore it was assumed that the $\dot{q}''_{net}$ was only linearly dependent on q''_{ext}.

Plotting the peak-average mass loss rate data against the applied external flux yields an average value for L as the slope represents the inverse of the heat of gasification, $1/L$. Figure 29 indicates this theoretical interpretation for second peak regions. It should be noted that when the second peak occurs due to the insulated back, the material begins to act thermally thin with an internal temperature distribution approaching the vaporization temperature. This makes the effective L value smaller.

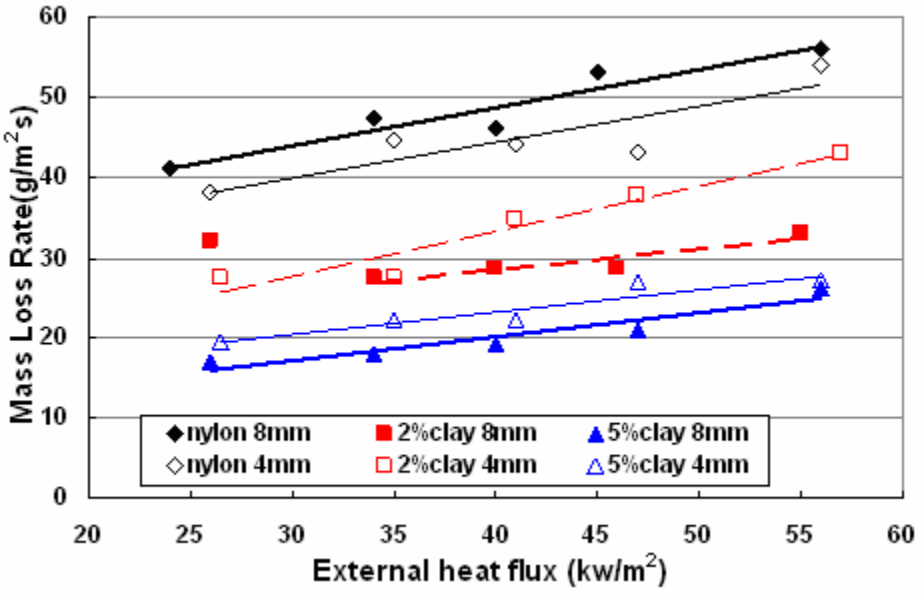

Figure 29. Peak-Average Mass Loss Rate per Unit Area at the Second Peak for L Calculation

The negative intercept of the straight lines on the $m''= 0$ line gives the net flame heat flux $q''- \sigma T_v^4$. It is seen in figure 30 that it decreases with the addition of clay.

The heat of gasification also allows the heat release rate of a material to be predicted [4]. $Q'' = m''\Delta h_c$, where Q'' is the heat release rate per unit area (kW/m^2). Thus, from equation 10 and 12

$$\dot{Q}'' = \dot{q}''_{net}\frac{\Delta h_c}{L}$$

$$\dot{Q}'' = (\frac{\Delta h_c}{L})\dot{q}''_{ext} + (\frac{\Delta h_c}{L})(q''_{fl} - \varepsilon\sigma T_v^4) \tag{13}$$

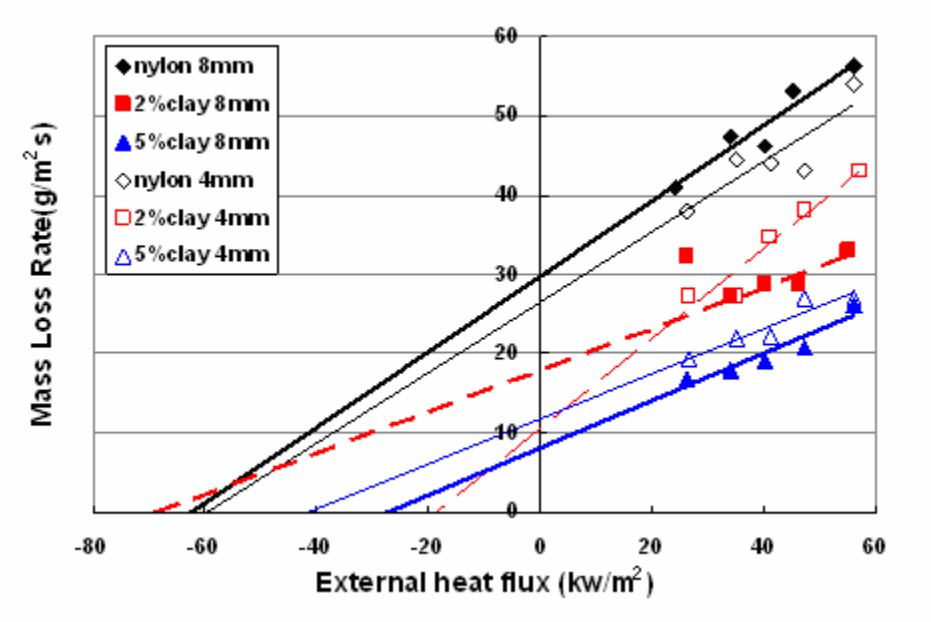

Figure 30. Peak-Average Mass Loss Rate per Unit Area at the Second Peak for Net Flame Heat Flux

Plotting the peak-average heat release rate data against the applied external flux will yield an average value for L as the slope represents $\frac{\Delta h_c}{L}$. These results are shown in figure 31, and are summarized in table 2 for the first and second peaks. The first peak L should not contain the effects of thickness. There was a tendency for the heat of gasification to increase with clay loading, but this was inconclusive. It would be expected that the first peak, if it was truly representative of a thermally thick steady-state burning rate, to have a lower L than the second peak. However, this is not evident and a deeper analysis is needed.

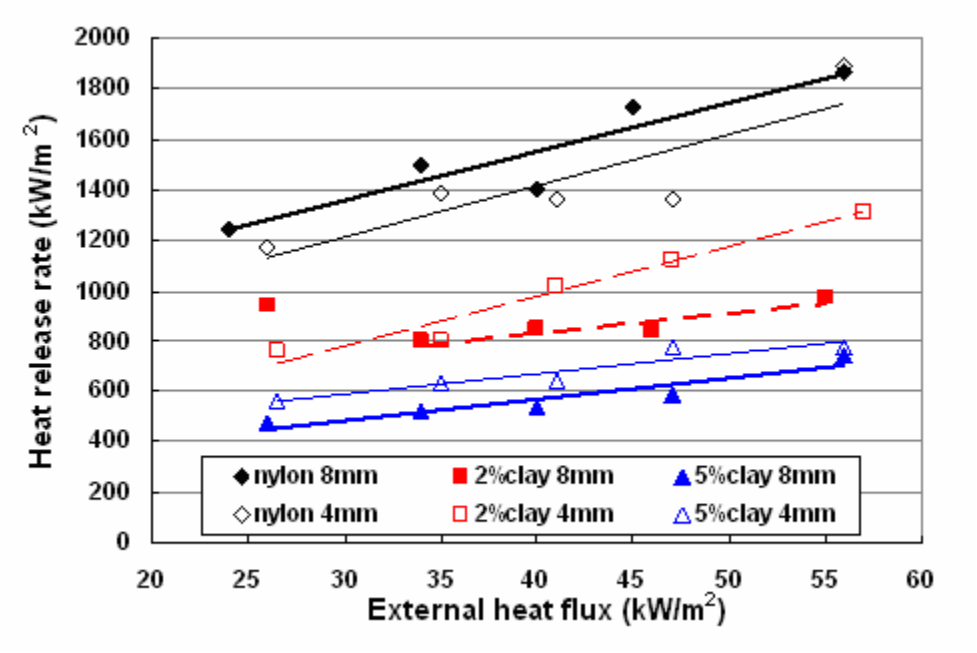

Figure 31. Peak-Average Heat Release Rate for the Second Peak for *L* Calculation

Table 2. Summary for Heat of Gasification for the First and Second Peaks

Additive	Thickness (mm)	L From $\dot{m}'' = \frac{\dot{q}''_{net}}{L}$		L From $\dot{q}'' = \dot{q}''_{net}\frac{\Delta h_c}{L}$	
		First	Second	First	Second
0 %	8	3.47	2.08	4.18	1.68
	4	3.60	1.96	5.31	1.62
	3.2	2.63	1.43	3.7	1.23
	1.6	--	2.27	--	1.34
2% Clay	8	3.18	3.85	3.33	3.80
	4	1.34	1.79	1.51	1.52
	3.2	--	1.92	--	1.56
	1.6	--	1.69	--	1.46
5% Clay	8	--	2.33	--	3.40
	4	--	3.57	--	3.60
	3.2	--	1.85	--	2.0
	1.6	--	1.67	--	1.70

To see a general trend for each thickness, all of the *L* values are averaged. As shown in figure 32, there are two factors affect *L* value:

- Effect of char—A trend was not very clear.
- Effect of thickness—*L* will increase with a thickness increase.

For steady burning:

- a thin sample $L = \Delta h_V$, the temperature distribution becomes nearly uniform
- a thick sample $L = \Delta h_V + c_p \Delta T$

where Δh_V is the heat of vaporization, and $c_p \Delta T$ is the energy needed to bring the material from its original temperature to its evaporation temperature.

So a thicker sample has a higher heat of gasification. This trend is shown in figure 32.

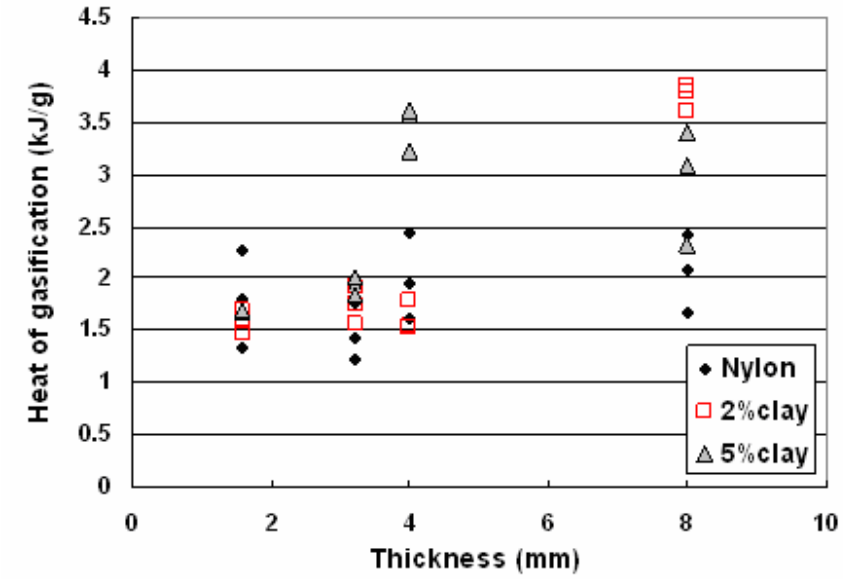

Figure 32. Heat of Gasification Versus Thickness for Different Samples

4.2.5 Residue Fraction.

The nominal residue fraction can be estimated from the initial and final mass of the sample $\frac{m_{final}}{m_{initial}}$.

The samples were weighed before the tests to identify the initial mass. The weight of the aluminum cup was also measured before testing. After burning, the residue and the cup are weighed together, and then the weight of the aluminum cup is subtracted. The pure residue mass is the m_{final}.

The residue fraction results are shown in figure 33. The results show the residue fraction is primarily a function of clay loading and varies from about 0.02% to 0.045% for 2% to 5% clay.

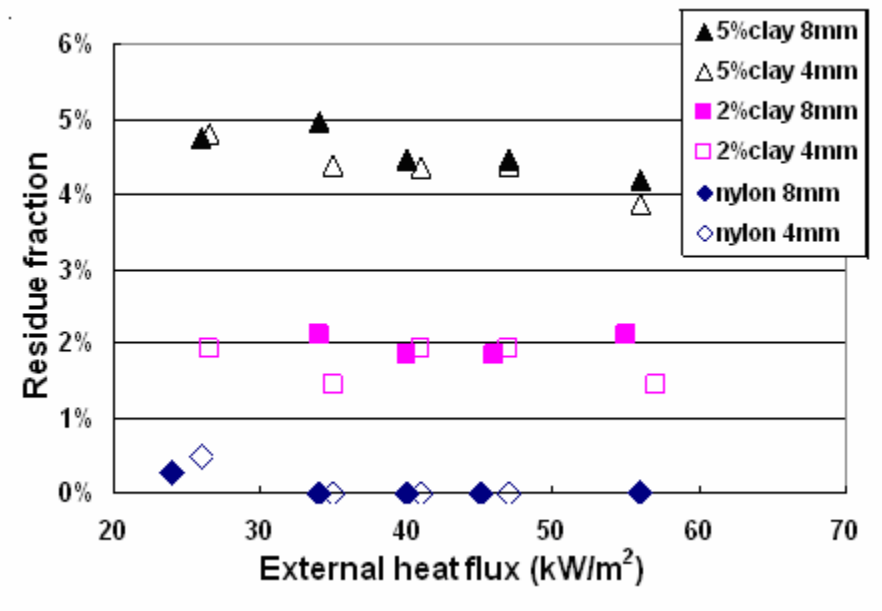

Figure 33. Residue Fraction Versus External Heat Flux

4.3 IGNITION CHARACTERISTICS AND PROPERTIES.

4.3.1 Time to Ignite.

The time to ignite can be computed by:

$$t_{ig} = Ck\rho c \frac{(T_{ig} - T_{\infty})^2}{(\dot{q}''_{ext} - \dot{q}''_{cr})^2} \tag{14}$$

where the value C depends on q''_{ext}, approaching $\pi/4$ for large q''_{ext} [11].

By using this theoretical expression, the data can be processed to derive ignition properties. Figure 34 shows the general trends of the time to ignite as a function of thickness. Thick samples need more time to be ignited. Figure 35 shows the effect of clay loading, and the addition of clay also tends to increase the time to ignition.

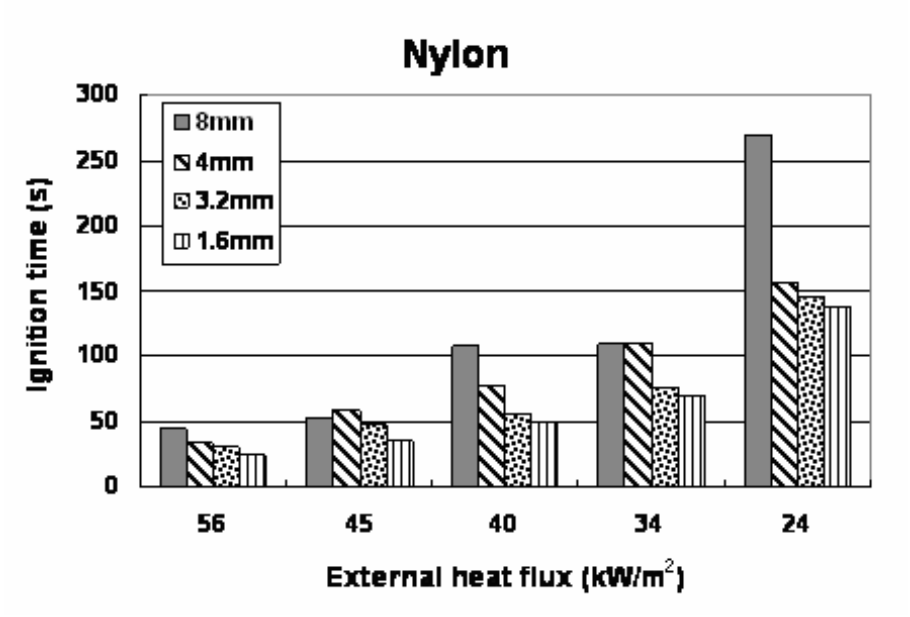

Figure 34. Ignition Time of Nylon With Different Thickness

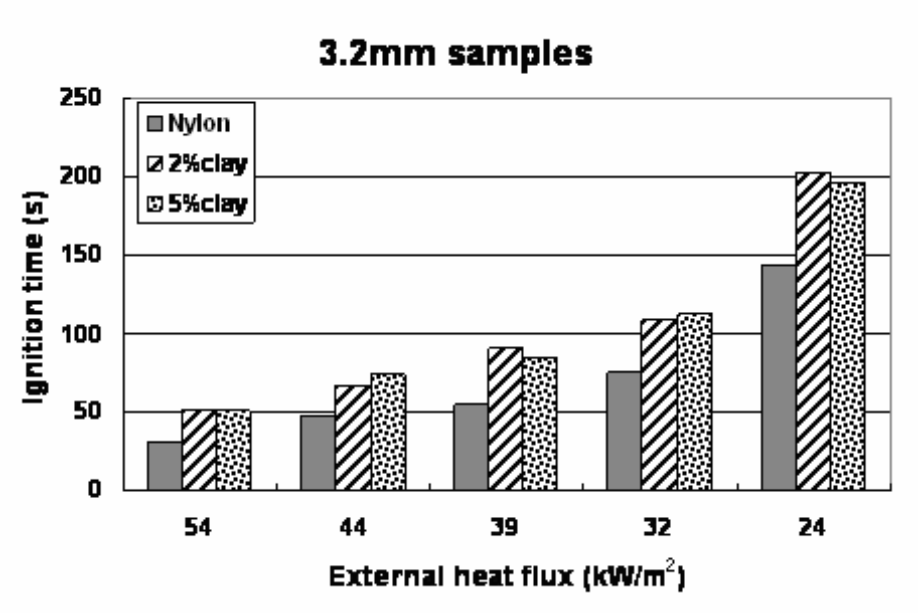

Figure 35. Ignition Time of 3.2-mm Samples With Different Clay Loading

4.3.2 Critical Heat Flux.

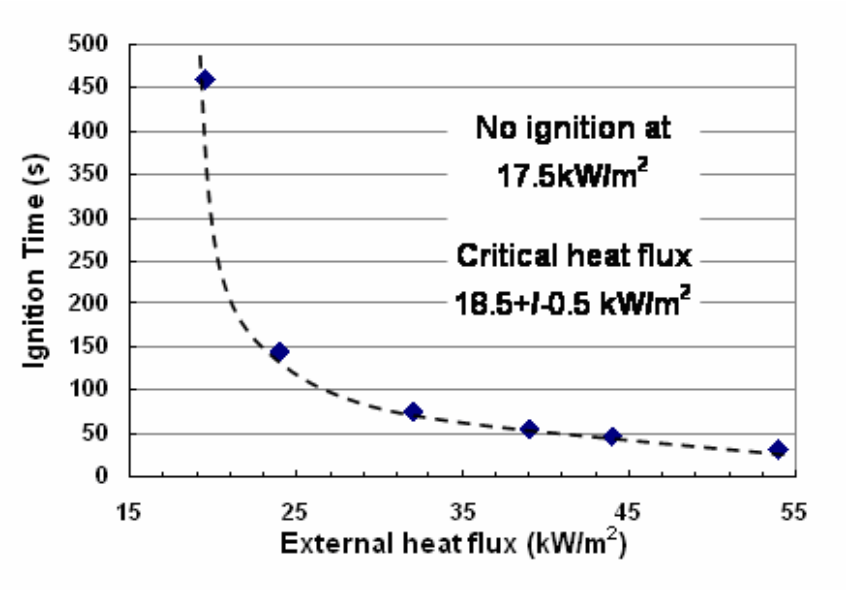

Figure 36. A 3.2-mm Nylon Critical Heat Flux by $t_{ig} \rightarrow \infty$

In order to predict the ignition temperature and thermal inertia, the critical flux for ignition must be determined. The critical heat flux for ignition occurs where $t_{ig} \rightarrow \infty$. Based on equation 14, a plot of ignition data as $t_{ig}^{-1/2}$ versus $\dot{q}''_{ext}$ is shown in figure 37. The intercept at $t_{ig}^{-1/2} = 0$ gives $q''_{ext} = q''_{cr}$.

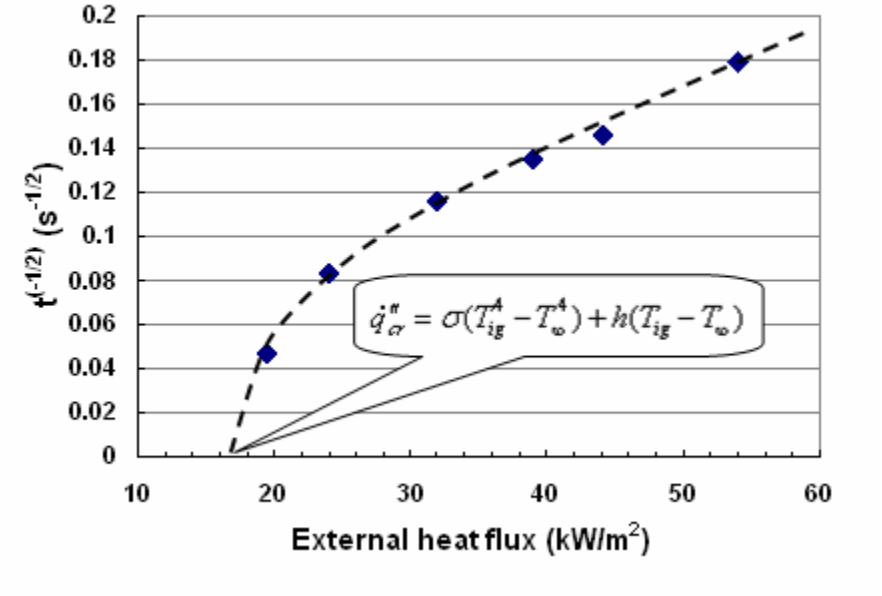

Figure 37. Critical Heat Flux by Intercept for 3.2-mm Nylon

4.3.3 Ignition Temperature.

In general, the net heat flux at the surface can be expressed as:

$$\dot{q}''_{net} = \dot{q}''_{ext} - h(T_S - T_\infty) - \sigma(T_S^4 - T_\infty^4)$$

The critical heat flux for ignition was normally found by trial-and-error in the testing. It was found to be roughly 19 kW/m^2 for all samples, but this needs to be examined further, since there were not enough samples to truly find the threshold. The ignition temperature was deduced from an energy balance at the surface when the heat flux into the material is theoretically zero. This was the limiting state under radiant heating. The equation then becomes:

$$\dot{q}''_{cr} = \sigma(T_{ig}^4 - T_\infty^4) + h(T_{ig} - T_\infty) \tag{15}$$

For this analysis, an average value of the convective coefficient was h = 10 W/m^{2}K, as indicated in reference 2 and confirmed by an extensive analysis given in appendix B. The experimental value was based on an ambient temperature of T_∞ = 23ºC, the average laboratory state. Generally, the ignition temperature was estimated at about 460 ±10^o C for all samples.

4.3.4 Thermal Inertia, $k\rho c$.

From equation 14,

$$t_{ig}^{-1/2} = \frac{1}{(\frac{\pi}{4} k\rho c)^{1/2}(T_{ig} - T_\infty)} \dot{q}''_i \tag{16}$$

The slope for the plot $t_{ig}^{-1/2}$ versus q''_{ext} at high heat flux is $\left[(\frac{\pi}{4} k\rho c)^{1/2}(T_{ig} - T_\infty)\right]^{-1}$ (figure 38). With T_{ig} calculated from equation 15, $k\rho c$ can be determined.

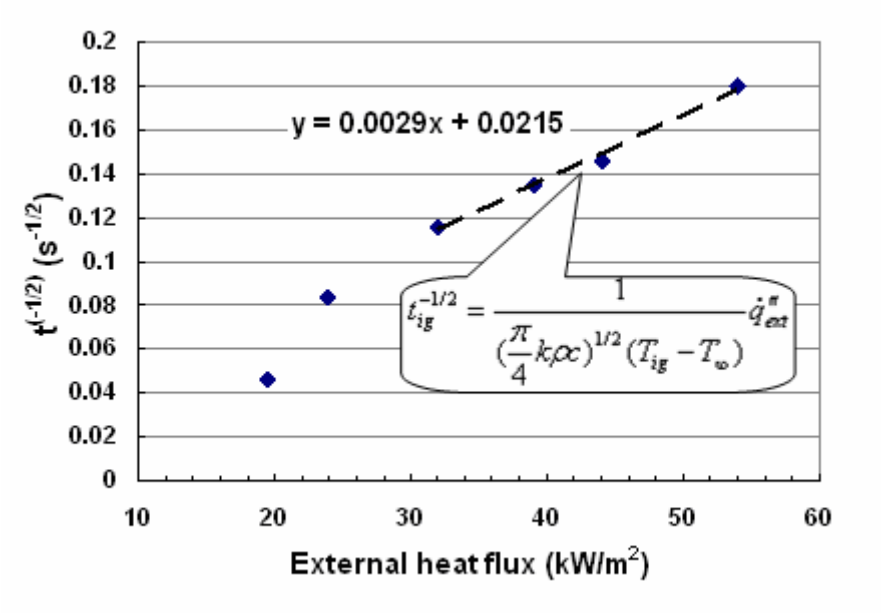

Figure 38. Slope Determination Thermal Inertia for 3.2-mm Nylon

Results for different samples are shown in figure 39 and listed in table 3. Sample density can be calculated by $\frac{mass}{volume}$ as measured.

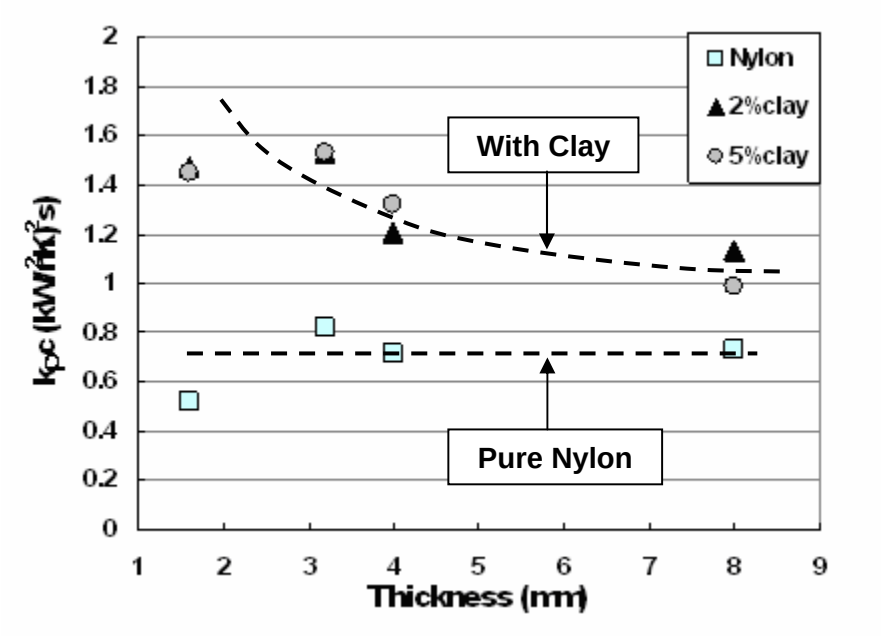

Figure 39. *kρc* Versus Thickness

Table 3. Density of Samples (kg/m^3)

Thickness	Nylon	Nylon +2% Clay	Nylon +5% Clay
24 mm	1103.1	1108.9	1108.9
8 mm	1110.8	1108.0	1110.8

Table 4 shows that the sample density (ρ) is independent of small amount of clay loading, and specific heat (c_p) is also known to not change much due to the small amount of clay. Figure 40 shows the thermal conductivity (k) data for nylon and nylon +5% clay from Kashiwagi [12]. There is not much difference. If the three properties are considered together as thermal inertia ($k\rho c$), there is an increase in thermal inertia as clay additive is increased, which is clearly seen in figure 38.

Table 4. Ignition Tendency and Thermal Inertia

Additive	Thickness (mm)	$\left[\left(\frac{\pi}{4}k\rho c\right)^{1/2}(T_{ig}-T_\infty)\right]^{-1}$ ($s^{1/2}kW/m^2$)	$k\rho c(T_{ig}-T_\infty)^2$ in 10^5 $(kW/m^2)^2s$)	$k\rho c$ $(kW/m^2K)^2s$)
0	8.0	0.0031	1.33	0.73
	4.0	0.0030	1.42	0.71
	3.2	0.0029	1.51	0.82
	1.6	0.0038	0.88	0.52
2% Clay	8.0	0.0025	2.04	1.13
	4.0	0.0023	2.41	1.21
	3.2	0.0021	2.89	1.53
	1.6	0.0022	2.63	1.47
5% Clay	8.0	0.0028	1.63	0.99
	4.0	0.0022	2.63	1.32
	3.2	0.0021	2.89	1.53
	1.6	0.0023	2.41	1.45

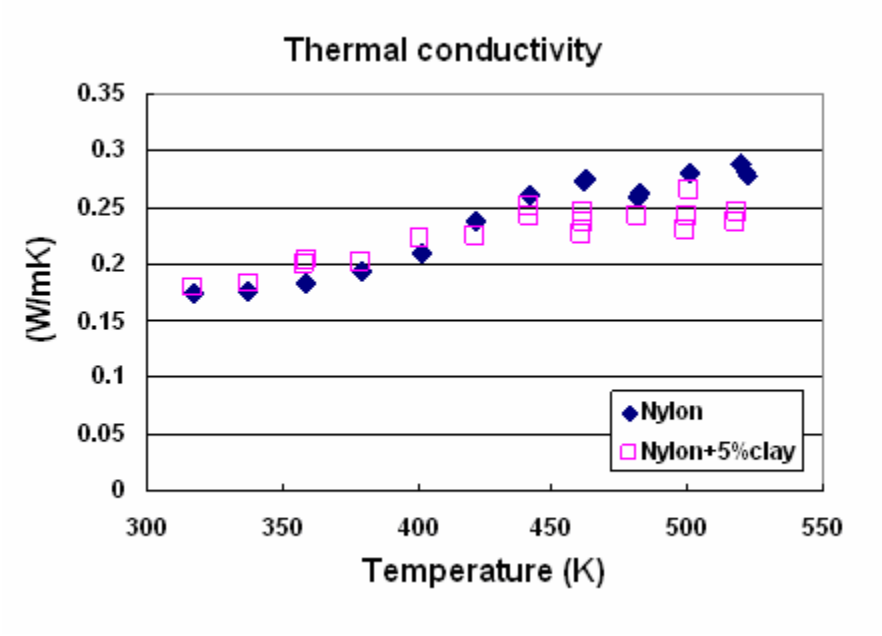

Figure 40. Thermal Conductivity of Nylon and Nylon +5% Clay

The term $k\rho\, c$ derived from ignition time versus external flux is so called effective $k\rho\, c$ or apparent $k\rho\, c$. These values are quite different from the values derived from each value of k, ρ, and c_p. The reason is that the derivation from equation 16 is based on lumped approach solving thermal conduction equation with several assumptions. These assumptions are (1) external flux is absorbed at the surface (this may be not good for nylon or at high flux); (2) each thermal property is assumed to be constant, not a function of temperature (c_p changes significantly with temperature); and (3) radiative loss is approximated or not included.

During a sample burning, a dark skin formed on samples with clay before its ignition, but no such skin formed on pure nylon. Such skin could have significant effects and it might be one of reasons for the difference between the samples with clay and with nylon only.

5. THERMO-CHEMICAL PROPERTIES OF THE POLYMERS.

A full understanding of the thermo-chemical properties of the nylon and the composites is needed for any modeling purposes. These include the kinetic properties associated with the decomposition of the polymer, its heat of decomposition, and its thermal properties. The approach for obtaining the kinetic data was based on Boonmee [13]. The kinetic data are taken from Kashiwagi [12] along with thermal conductivity and specific heat data as a function of temperature. Data for the heat of decomposition are absent.

5.1 THERMAL PROPERTIES.

From Kashiwagi [12] results for thermal conductivity and specific heat of pure nylon, thermal conductivity ranges from approximately 0.18 to 0.25 W/m-K over temperatures of roughly 25° to 250ºC, respectively. Over the same range of temperatures, the specific heat ranges were from approximately 1.5 to 3.5 J/g-K. The density of the nylon was 1110 kg/m^3. A computation from

the data of the $k\rho c$ property gives 0.97 $(kW/m^2K)^2$-s. This compares to overall values derived from ignition data of about 0.83 $(kW/m^2K)^2$-s for the thick samples with an ignition temperature of about 450°C. This demonstrated some indication of the consistency of the data and the accuracy of deriving thermal properties from the ignition data.

5.2 KINETIC PARAMETERS FROM THEORY.

Thermal gravimetric analysis is a standard technique for measuring decomposition properties of materials. In these tests, the samples were continuously weighed, while their temperatures were increased. The properties for a first-order reaction were considered. They included the kinetic parameters (activation energy E_a and pre-exponential factor a_P).

In this section, the methods used to determine the kinetic parameters are discussed. This analysis follows from Boonmee [13].

5.2.1 Mass Conversion Fraction (α).

The sample's total mass changed as it underwent the pyrolysis process. A continuum representation for decomposition considered the sample with the char in a fixed volume. The mass conversion fraction (α) is defined as:

$$\alpha = \frac{m - m_{\text{int}}}{m_f - m_{\text{int}}} \tag{17}$$

where:

m is the total mass of the sample, which is changing with the pyrolysis process
m_{int} is the initial mass of sample
m_f is the final mass of sample

The value of α goes from zero to the final value (char fraction) as the total mass m goes from m_{int}, the initial mass of the sample, to m_f, the final mass of sample. The rate of change of the conversion factor can be expressed in a general differential equation form as:

$$\frac{d\alpha}{dt} = f(\alpha)k(T) \tag{18}$$

where:

$f(\alpha)$ is a reaction order function
$k(T)$ can be expressed as the Arrhenius rate equation

$$k(T) = a_p \exp(-E_a / RT) \tag{19}$$

where:

a_p is the pre-exponential factor
E_a is the activation energy
R is the universal gas constant

Substitute equation 19 into equation 18:

$$\frac{d\alpha}{dt} = f(\alpha)a_p \exp(-E_a / RT) \tag{20}$$

5.2.2 Differential Method.

Take the natural logarithms on both sides of equation 20:

$$\ln\left(\frac{d\alpha}{dt}\right) = \ln\left(f(\alpha)a_P\right) - \frac{E_a}{R}\left(\frac{1}{T}\right) \tag{21}$$

For one sample, pick $\ln\left(\frac{d\alpha}{dt}\right)$ at three different α_i's and plot them against $1/T$ (α_i) (T (α_i) is corresponding to α_i), the linear slope is, and the intercept is $1n\left(f(\alpha_i)\, a_p\right)$. $f(\alpha)$ is defined as:

$$f(\alpha) = \frac{(1-\alpha)}{(1-X_C)} \tag{22}$$

$$X_C = \frac{m_f}{m_{\text{int}}} \text{ is the char fraction}$$

Then E_a and a_p are easily calculated.

$$E_a = -R \times slope \tag{23}$$

$$a_p = \frac{\exp(\text{intercept})}{f(\alpha)} \tag{24}$$

5.3 DIFFERENTIAL METHOD.

The thermogravimetric analysis (TGA) data of nylon and nylon +5% clay are from Kashiwagi, NIST [12]. The data are obtained from nonisothermal tests with a series of constant heating rates (β) of 1^o, 2^o and 5^oC/min from NIST. At these low heating rates (<10^oC/min), the sample mass

gradually decreases as the decomposition process is controlled by kinetics. For a given heating rate (e.g., 2°C/min in figure 41), the sample mass decreases uniformly with one slope until its remaining mass reaches approximately 2% of the original mass.

In order to get activation energy E_a and pre-exponential factor a_p using equation 20, $\frac{d\alpha}{dt}$ is needed from the TGA data.

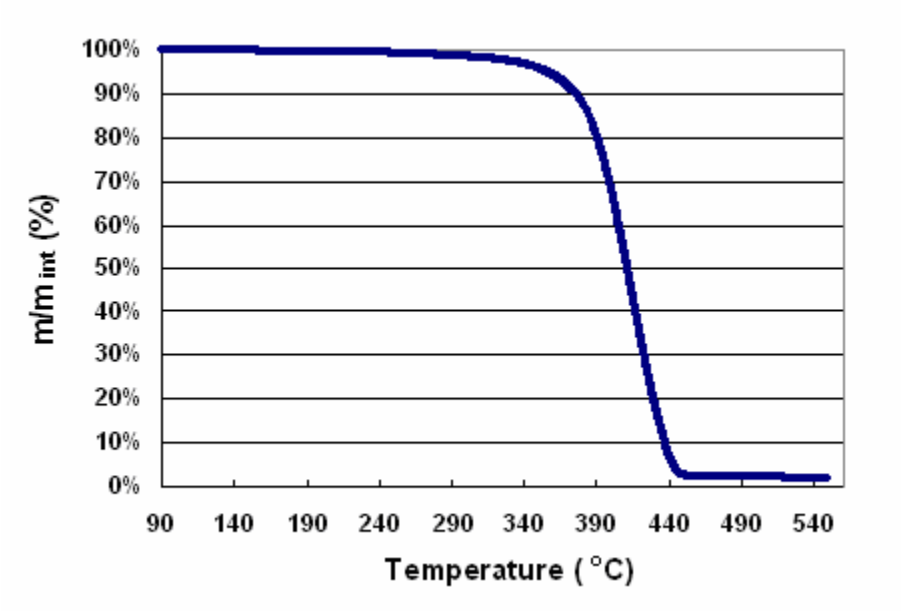

Figure 41. Mass Fraction of Nylon Heated at 2°C/min

Since α is defined as

$$\alpha = \frac{m - m_{\text{int}}}{m_f - m_{\text{int}}}$$

$$\frac{d\alpha}{dt} = \frac{1}{m_f - m_{\text{int}}} \frac{dm}{dt}$$

TGA data show mass fraction as a function of temperature, and temperature is a function of time.

$$\frac{dm}{dt} = \frac{dm}{dT}\frac{dT}{dt} = m_{\text{int}} \frac{d\frac{m}{m_{\text{int}}}}{dT}\frac{dT}{dt}$$

where:

$\frac{dT}{dt}$ is the heating rate (e.g. 5°C/min)

$\frac{d\frac{m}{m_{\text{int}}}}{dT}$ is the derivative of weight (%/°C), directly from TGA data shown in figure 42.

Combining these terms gives:

$$\frac{d\alpha}{dt} = \frac{m_{\text{int}}}{m_f - m_{\text{int}}} \frac{d\frac{m}{m_{\text{int}}}}{dT} \frac{dT}{dt} \tag{25}$$

Then following differential method, pick α = 0.25, 0.5, 0.75, plot $\ln\left(\frac{d\alpha_i}{dt}\right)$ vs $\frac{1}{T_i}$

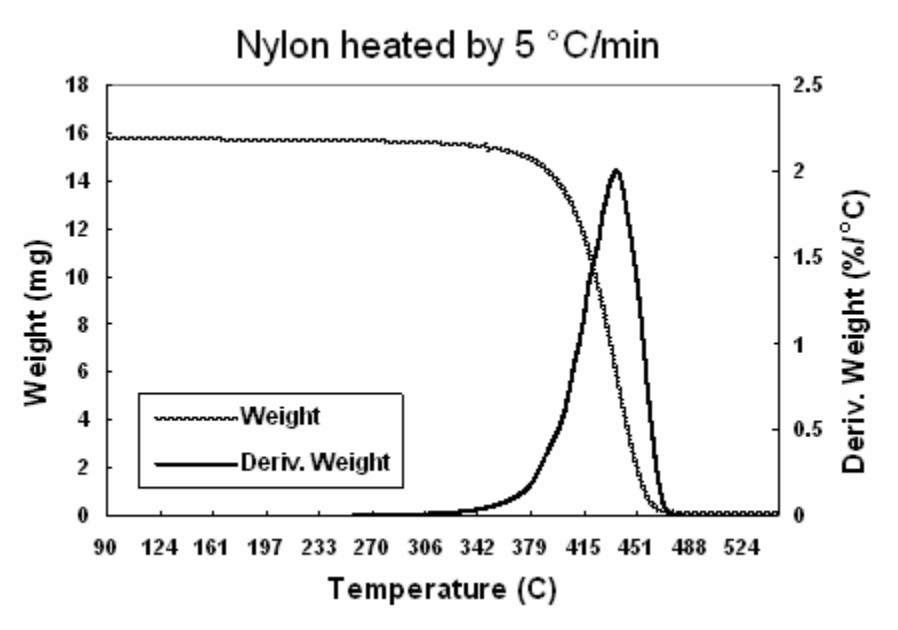

Figure 42. The TGA Data Nylon Heated at 5°C/min

Find the char fraction $X_C = \frac{m_f}{m_{\text{int}}}$ for each material and substitute it into equation 22. Then $f(\alpha)$ is easily calculated for three different α values. Read slope and intercept in figure 43. Use slope in equation 23 to get E_a. Use intercept in equation 24 to get a_p. Those values are listed in table 5.

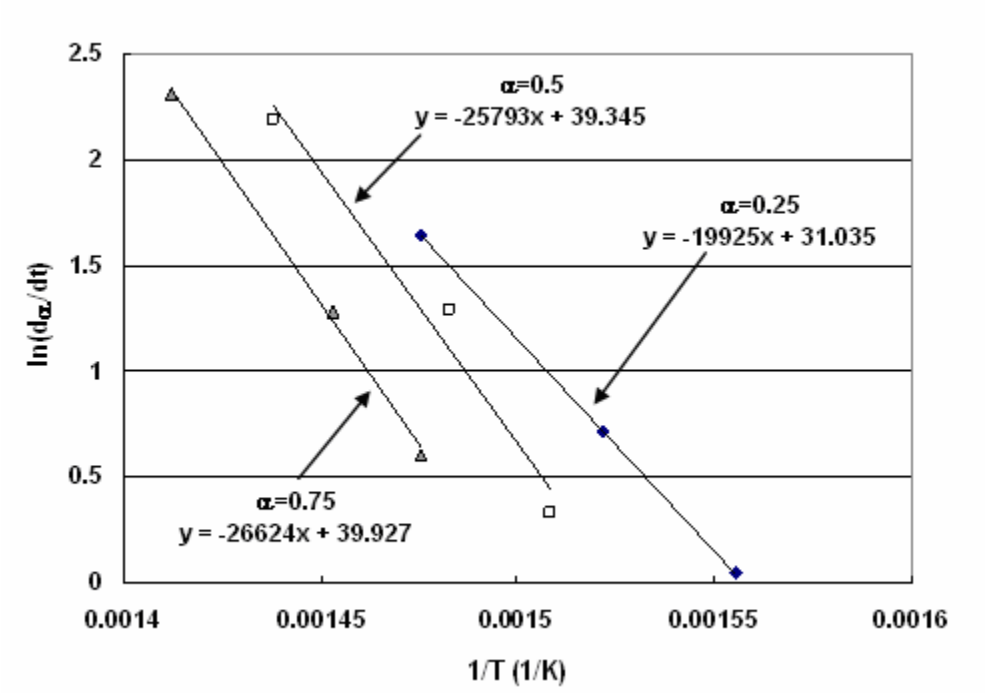

Figure 43. Nylon +5% Clay

Table 5. Kinetic Parameters

Nylon X_c=0.017					
α	slope	intercept	E_a (J/mol)	$f(\alpha)$	a_p
0.25	-22282	34.209	185163.4	0.76297	9.4248E+14
0.5	-28752	43.188	238929.1	0.508647	1.12174E+19
0.75	-30770	45.233	255698.7	0.254323	1.73403E+20
Nylon +5% clay Xc=0.06					
α	slope	intercept	E_a (J/mol)	$f(\alpha)$	a_p
0.25	-19925	31.035	165576.8	0.797872	3.77E+13
0.5	-25793	39.345	214339.8	0.531915	2.3E+17
0.75	-26624	39.927	221245.4	0.265957	8.23E+17

Now there are three sets of E_a and a_p for each sample. Substitute each set back into equation 20, and combine with equation 22.

$$\frac{d\alpha}{dt} = \frac{1-\alpha}{1-X_C} a_p \exp(-E_a / RT) \tag{26}$$

In equation 26, X_C, E_a, and a_p are fixed for each material, $\frac{d\alpha}{dt}$ is only a function of temperature (time).

$\frac{d\alpha}{dt}$ from TGA data calculation, from $\alpha = 0.25$, from $\alpha = 0.5$, and from $\alpha = 0.75$ are compared in figure 44.

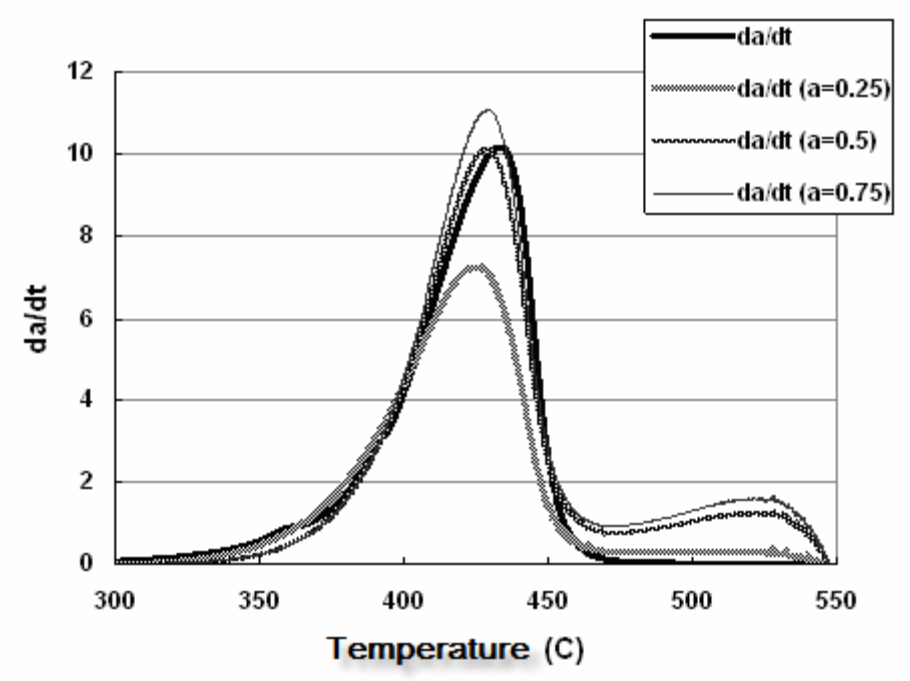

Figure 44. Nylon 6 +5% Clay Heated by 5°C/min

Comparing these three sets of values with the one calculated from TGA data (the darkest curve), the curve at $\alpha = 0.5$ matches the TGA data well. So X_C, E_a, and a_p at $\alpha = 0.5$ are set to be the value used in the simulation model later.

6. MODELING BURNING RATE.

6.1 INTRODUCTION.

Previous work showed that the addition of clay to nylon in a nanocomposite reduced its energy release rate, and the thickness of the sample influenced these results [1]. The current study sought to investigate the effect of thickness and heat flux on the burning and ignition behavior for pure nylon and as a nanocomposite of nylon and 2% and 5% clay. The principal effect of the clay has been the formation of a char-like residue that inhibits heat flow and therefore reduces the burning rate. The char residue was found to be nearly the same as the clay loading, suggesting it is solely clay. It should be pointed out that these samples are charring weakly compared to wood, which can have 20% to 40% char yield decreasing with heat flux according to Spearpoint and Quintiere [14].

Table 6 summarizes the findings for thicknesses varying from 1.6 to 24 mm and heat fluxes ranging from 17 to 55 kW/m^2.

Table 6. Summary of Effects on Ignition and Burning

Material	Char Residue %	$k\rho c$ $(kW/m^2K)^2s$	Critical Flux (kW/m^2)	Heat of Combustion (kJ/g)	Heat of Gasification (kJ/g)
Nylon	0-0.5	0.7-0.8	17.7	27-29	1.5-3.5
2% clay	2	1.1-1.5	17.5	27-29	1.5-4.0
5% clay	4-5	1.0-1.5	16.0	27-29	2.5-3.5

The critical flux for ignition is not significantly different within the samples, and a corresponding ignition temperature of about 430°C can be computed. This is consistent with the decomposition temperatures found in TGA tests as they commence at about 350°C and peak at about 430°C. The values for thermal inertia suggest an increase in the thermal conductivity with the addition of clay, as density and specific heat are basically constant. However, figure 40 indicated that the measured thermal conductivity of pure nylon and the nanocomposite with 5% clay are virtually the same. The clay addition increases the time to ignite over the pure nylon as seen in figures 35, 45, 46, and 47. These figures show that curve fits indicate the ignition behavior is following that of thermally thick samples, but there is a definite thickness effect, i.e., ignition time decreases as the thickness decreases. In general, as the heat flux increased, the ignition time could increase by a factor of 1.3 to 2 over the pure nylon for both the 2% and 5% composite loadings. While the ignition-derived $k\rho c$ values suggested a larger k for the loaded clay samples, direct k measurements refuted this. It appeared that the $k\rho c$ values actually masked the effects of decomposition and perhaps the charring. Thus, the thermal inertia deduced from the ignition data was not a true thermal property, but included other effects. Probably, the reduction in mass loss along with the addition of the clay are leading to a longer ignition time than it would take to build up to the lower flammable limit needed for piloted ignition.

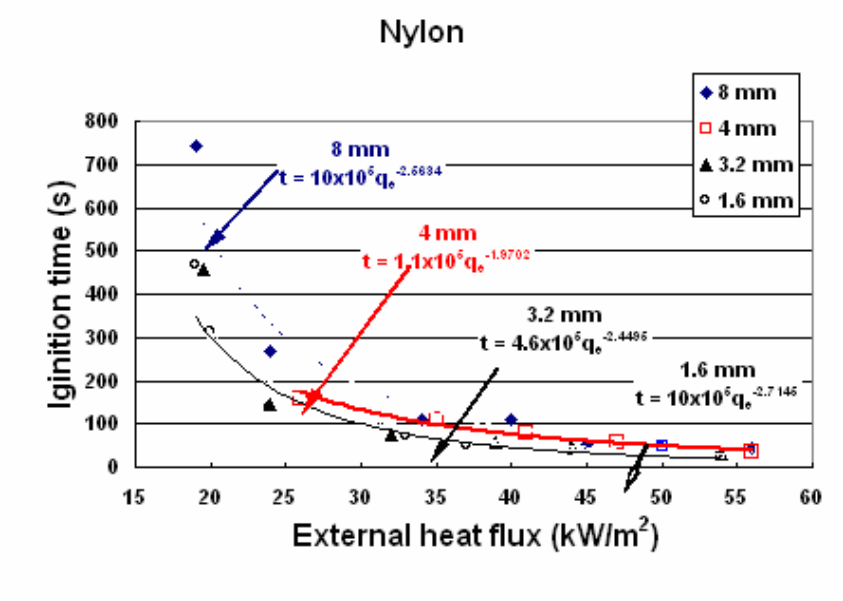

Figure 45. Ignition of Nylon Samples

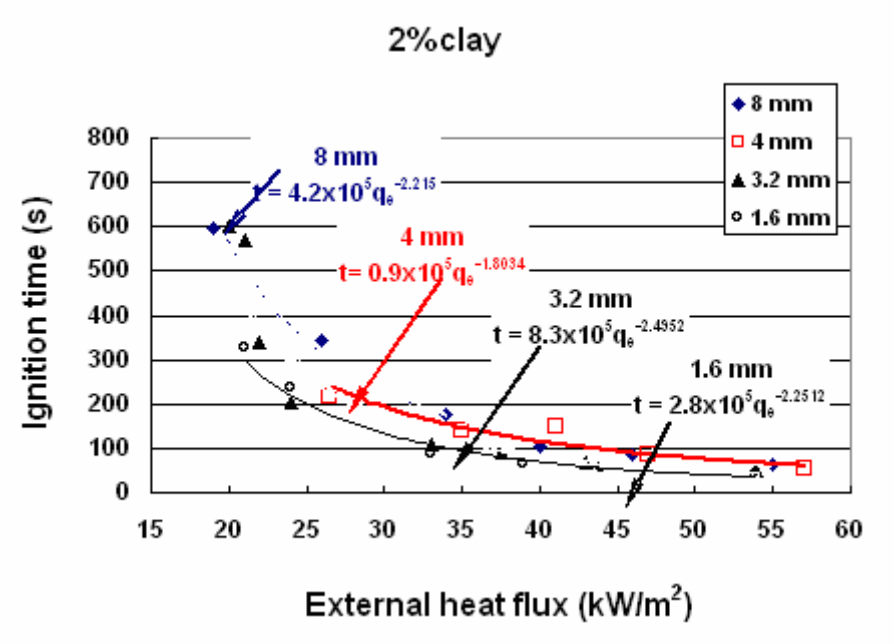

Figure 46. Ignition of 2% Clay Samples

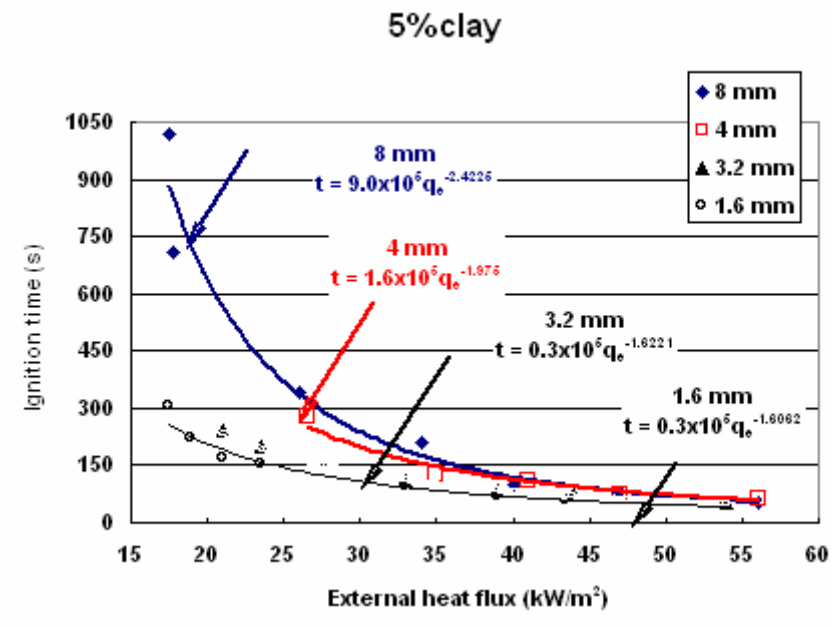

Figure 47. Ignition of 5% Clay Samples

For the energy release rate or the burning rate, table 6 indicates that the reductions are principally related to the decomposition rate as indicated by the heat of gasification differences. The heats of combustion were virtually the same for all the samples. This is expected, because the mass loss is essentially nylon, and the heat of combustion is based on the mass loss. The variations in the heats of gasification are due to the uneven burning rates over time. These heats of

gasification are representative of the peak burning at the beginning of the process and at the end due to back-face effects. It hides a lot of processes, and only can be relied on as an approximate property to give a general behavior. The values given do indicate a reduction in burning rate with the addition of clay. The factors affecting the burning behavior show that two mechanisms are responsible for the burning rate. One is based on heat transport into the solid that is absorbed into the heat of vaporization or decomposition of the material. The other is based on the kinetics of decomposition. The first (heat transport) applies to thick samples before the heating wave reaches the back face of the sample. The second (the kinetic process) occurs for thin samples that have been sufficiently preheated. The back-face effect for an insulated sample is also an example of the dominant kinetics. In the kinetics-controlled case, the material tends to heat more uniformly during decomposition. In the heat conduction case, a sharp temperature gradient exists at the decomposition front. These thermal features are illustrated in figure 48.

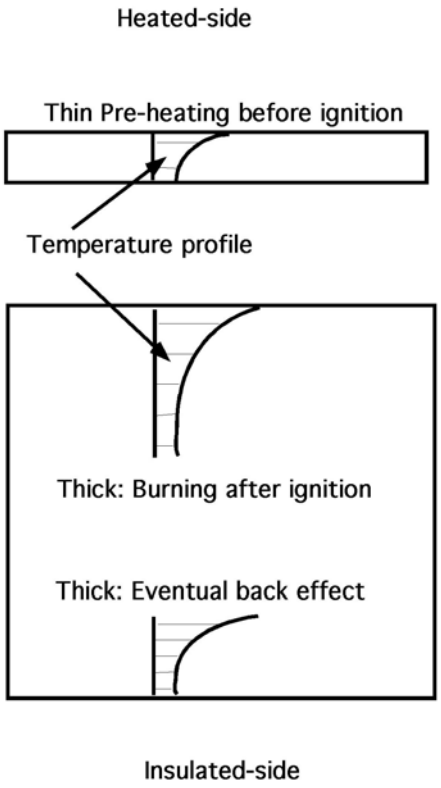

Figure 48. Thermally Thin and Thick Effects

6.2 BURNING RATE MODEL.

The burning rate model is based on the wood decomposition model used by Boonmee [13]. The model was redeveloped here, and it will help to explain the burning behavior of the samples. Later, some numerical results will illustrate a complete quantitative solution. However, the qualitative and empirical features of the model together with the data are considered more valuable, as the stiffness of the first-order kinetic term will limit an accurate numerical result at this time. Staggs gives an approximate solution for the quasi-steady degradation of a

noncharring polymer with first-order kinetics [15]. He ignored the preheating during ignition, and that was examined here.

6.2.1 Charring Model.

The model considers the decomposing solid as a perfect mixture of original solid fuel, active species (*a*) and char (*c*). The char forms a layer, filling the same volume of the original material. If no char is produced, the heated surface simply regresses. Gaseous fuel is generated within and flows through the solid under constant pressure. Darcy flow was not considered, as cracks and porous char allowed ease of flow. The gas has negligible mass in the solid mixture. Decomposition is given in terms of an Arrhenius first-order chemical reaction. The chemical stoichiometry is given as follows:

$$\text{1-g active (original) solid} \rightarrow X_c \text{ g char} + (1-X_c) \text{ g gaseous fuel.} \tag{27}$$

Conservation of mass is derived for a differential one-dimensional (1-D) element (figure 49) of solid fuel containing active solid (*a*) and char (*c*) of mixture density,

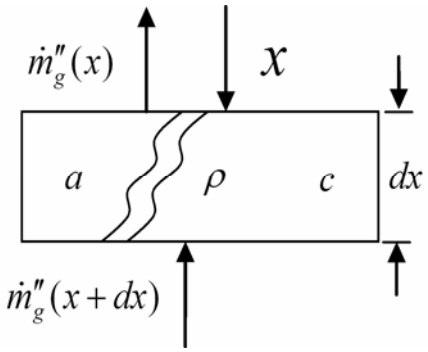

Figure 49. Differential Element

$$\rho = \rho_a + \rho_c \tag{28}$$

Fuel gases escapes at a mass flux over the domain as $m''_g(x)$. The conservation of mass for a control volume surrounding the element can be written for:

$$\frac{dm}{dt} + \dot{m}_{out} - \dot{m}_{in} = 0 \tag{29}$$

Substituting for an area of unit cross section gives

$$\frac{dm}{dt} + \dot{m}_{out} - \dot{m}_{in} = 0 \quad \Rightarrow \quad \frac{\partial(\rho \cdot 1 \cdot dx)}{dt} + \dot{m}''_g(x) \cdot 1 - \dot{m}''_g(x+dx) \cdot 1 = 0$$

Expanding:

$$\dot{m}''_g(x) - \dot{m}''_g(x+dx) = -\frac{\partial \dot{m}''_g}{\partial x} dx$$

$$\therefore \quad \frac{\partial \rho}{\partial t} = \frac{\partial \dot{m}''_g}{\partial x} \tag{30}$$

This gives a relationship between the gaseous fuel flow and the rate of decomposition per unit volume. The latter is determined from TGA data for uniformly heated small samples.

The TGA analysis of section 5 expressed the decomposition in terms of:

$$\frac{d\alpha}{dt} = f(\alpha) a_p \exp(-E_a / RT)$$

$$f(\alpha) = \frac{(1-\alpha)}{(1-X_C)} \tag{31}$$

where $\alpha \equiv \frac{m - m_{\text{int}}}{m_f - m_{\text{int}}} = \frac{\rho - \rho_{\text{int}}}{\rho_f - \rho_{\text{int}}}$, and $X_C \equiv \frac{m_f}{m_{\text{int}}}$ is the char fraction. The conservation of active species gives:

$$\frac{\partial \rho_a}{\partial t} = -\dot{m}''' \Big/ (1 - X_c) \tag{32}$$

$$= \left(\frac{\text{mass of gaseous fuel evolved}}{\text{volume} \cdot \text{time}} \right) \Bigg/ \left(\frac{\text{mass of gaseous fuel}}{\text{mass of active fuel decomposed}} \right)$$

The kinetics is usually expressed in terms of the mass generation rate per unit volume as:

$$\dot{m}''' = -\frac{\partial \rho}{\partial t} = \rho_a a_p e^{-\frac{E}{RT}} \tag{33}$$

This is equivalent to the previous TGA expression in equation 31 as seen by the following. From equations 32 and 33, the active and mixture densities are related as:

$$\frac{\partial \rho_a}{\partial t} = \frac{1}{(1-X_c)} \frac{\partial \rho}{\partial t} \tag{34}$$

Integrating from any time to the final state gives:

$$0-\rho_a=\frac{\rho_f-\rho}{(1-X_c)} \tag{35}$$

Substituting this into equation 31 gives exactly equation 33, which will be used henceforth.

In a similar manner, conservation of the char species gives:

$$\frac{\partial\rho_c}{\partial t}=-(\frac{X_c}{1-X_c})\frac{\partial\rho}{\partial t} \tag{36}$$

Conservation of energy will be considered. First, a charring medium is considered in which the overall volume remains fixed, and the coordinate x is measured from the heated fixed surface. Later, a noncharring medium will be considered in which the coordinate is measured from the regressing surface. The charring medium is depicted in figure 50.

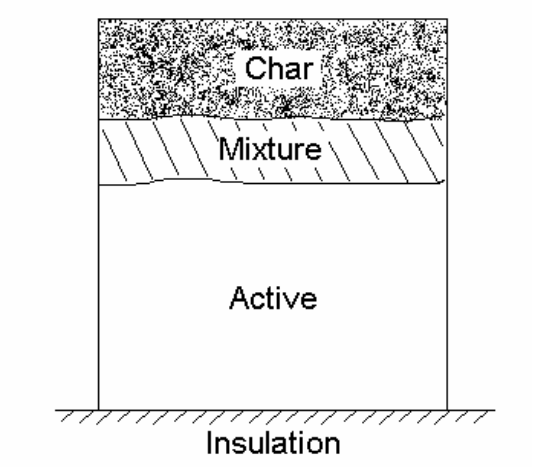

Figure 50. Charring Medium

A differential element depicted in figure 51 shows gaseous fuel with enthalpy (h_g) leaving, and h is enthalpy of active char mixture. The enthalpies are taken in terms of the heats of formation of the species. The energy equation flows for a constant pressure system.

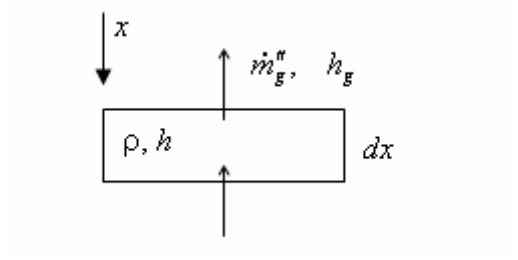

Figure 51. Differential Element for Energy Balance

$$\frac{\partial(\rho h)}{\partial t} - \frac{\partial(\dot{m}''_g h_g)}{\partial x} = \frac{\partial}{\partial x}(k\frac{\partial T}{\partial x}) \tag{37}$$

The enthalpies are expressed in terms of the heat of formation and the sensible enthalpy due to temperature change. For each species:

$$h_i = \Delta h^o_{f,i} + h_{s,i} \tag{38a}$$

The sensible enthalpy ($h_{s,i}$) can be written as:

$$h_{s,i} = \int_{25^oC}^{T} c_{p,i}\, dT \tag{38b}$$

Also, for the mixture of char and active material,

$$\rho h = \rho_a h_a + \rho_c h_c \tag{39}$$

Equation 37 can then be written as:

$$\frac{\partial(\rho h_s)}{\partial t} - \frac{\partial(\dot{m}''_g h_{s,g})}{\partial x} = \frac{\partial}{\partial x}(k\frac{\partial T}{\partial x}) + \frac{\Delta h_d}{(1-X_c)}\frac{\partial \rho}{\partial t} \tag{40}$$

where

$$\Delta h_d \equiv -\left[\Delta h^o_{f,a} - X_c \Delta h^o_{f,c} - (1-X_c) h^o_{f,g}\right] \tag{41}$$

is the heat of decomposition per unit of mass of original material at 25°C. The quantity $\frac{\Delta h_d}{(1-X_c)}$ is the heat of decomposition per unit of mass lost.

Now expanding the first term in equation 40 gives

$$\frac{\partial(\rho h_s)}{\partial t} = \rho\frac{\partial h_s}{\partial t} + h_{s,a}\frac{\partial \rho_a}{\partial t} + h_{s,c}\frac{\partial \rho_c}{\partial t} \tag{42}$$

and substituting from the conservation of species, equations 34 and 36, the left-hand side become:

$$\rho \frac{\partial h_s}{\partial t} + \frac{h_{s,a}}{(1-X_c)} \frac{\partial \rho}{\partial t} + \frac{h_{s,c} X_c}{(1-X_c)} \left(-\frac{\partial \rho}{\partial t} \right) \tag{43}$$

Also, one can write:

$$\frac{\partial}{\partial x}(\dot{m}''_g h_{s,g}) = \dot{m}''_g \frac{\partial h_{s,g}}{\partial x} + h_{s,g} \frac{\partial \dot{m}''_g}{\partial x}$$

$$= \dot{m}''_g \frac{\partial h_{s,g}}{\partial x} + h_{s,g} \frac{\partial \rho}{\partial t} \tag{44}$$

Then equation 40 becomes

$$\rho \frac{\partial h_s}{\partial t} - \dot{m}''_g \frac{\partial h_{s,g}}{\partial x} = \frac{\partial}{\partial x}(k \frac{\partial T}{\partial x}) + \frac{\partial \rho}{\partial t} \left[\frac{\Delta h_d}{(1-X_c)} - \frac{h_{s,a}}{(1-X_c)} + \frac{X_c h_{s,c}}{(1-X_c)} + h_{s,g} \right] \tag{45}$$

The term in the bracket can be called the heat of vaporization. It includes the heat of decomposition and any phase changes in the region (δx), where $\frac{\partial \rho}{\partial t}$ is significantly changing. This region for the thin δx can be interpreted as a vaporization front at a vaporization temperature T_v. The temperature is not constant, but generally varies over the decomposing region. However, if the region is thin, a constant, uniform vaporization temperature might be valid.

Define the heat of vaporization at this temperature as:

$$\Delta h_{vap}(T_v) = \Delta h_d - h_{s,a}(T_v) + X_c h_{s,c}(T_v) + (1-X_c) h_{s,g}(T_v) \tag{46}$$

Note, if there is no chemical decomposition ($\Delta h_d = 0$) and no char ($X_c = 0$), only a vaporization phase change from solid (a) to gaseous fuel (g) occurs, then

$$\Delta h_{vap}(T_v) = h_{s,g}(T_v) - h_{s,a}(T_v) \tag{47}$$

the thermodynamic heat of vaporization in a phase change.

Recognizing that the sensible enthalpy can be expressed as:

$$\frac{\partial h_s}{\partial t} = c_p \frac{\partial T}{\partial t}$$

Equation 27 becomes:

$$\rho c_p \frac{\partial T}{\partial t} - \dot{m}_g'' c_{p,g} \frac{\partial T}{\partial x} = \frac{\partial}{\partial x}(k \frac{\partial T}{\partial x}) + \frac{\partial \rho}{\partial t} \frac{\Delta h_{vap}}{(1 - X_c)} \tag{48}$$

6.2.2 Noncharring Model.

The conservation of energy for a noncharring material with chemical decomposition and surface regression is depicted in figure 52 where the original length is *l*. Equation 48 still applies but in a fixed frame of reference, x_o. It is more suitable to express the noncharring case in a moving reference frame measured from the vaporization regressing surface and in terms of the regression speed,

$$x = x_o - \int_0^t v dt \tag{49}$$

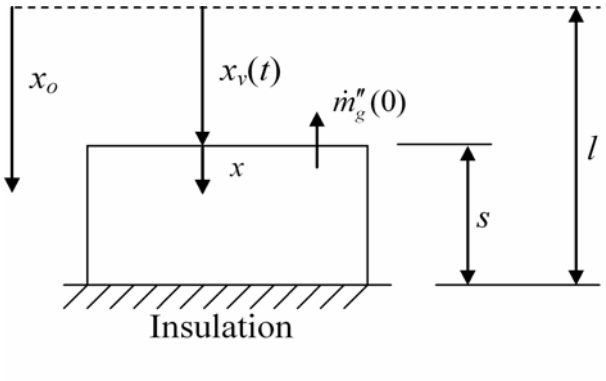

Figure 52. Noncharring Model and Coordinate System

where $v = \frac{dx_v}{dt}$ is the speed. Equation 48 is in terms of $T(x_o, t)$. Transforming to $T(x(x_o), t)$ by:

$$\left(\frac{\partial T}{\partial t}\right)_{x_o} = \left(\frac{\partial T}{\partial t}\right)_x + \left(\frac{\partial T}{\partial t}\right)_t \frac{\partial x}{\partial t} \tag{50}$$

From equation 49

$$\frac{dx}{dt} = -v$$

and

$$\left(\frac{\partial T}{\partial x_o}\right)_t = \left(\frac{\partial T}{\partial x}\right)_t$$

By conservation of mass at the moving surface $x = 0$,

$$\rho v = \dot{m}''_g(0)$$

Then equation 48 becomes for the moving frame

$$\rho c_p \frac{\partial T}{\partial t} - c_p \dot{m}''_g(0)\frac{\partial T}{\partial x} - \dot{m}''_g c_{p,g}\frac{\partial T}{\partial x} = \frac{\partial}{\partial x}(k\frac{\partial T}{\partial x}) + \frac{\partial \rho}{\partial t}\frac{\Delta h_{vap}}{(1-X_c)} \tag{51}$$

6.3 SOLUTIONS.

From equations 48 and 51, a form of a solution can be given for the total mass flux lost $m''_g(0)$ due to a constant incident heat flux q''_i. The incident heat flux here can be considered the total flame and external heat flux, where it is realized that the flame heat flux might vary as the mass flux changes. This variation is not considered. In the burning problem, the flame heat flux will change, so a constant incident flux made up of the flame and external radiant flux will not necessarily be valid. But this assumption will be sufficient to explain the burning behavior here. Further, it should be pointed out that the inclusion of the energy equations with heat conduction must allow a gradient for temperature. Hence, these solutions investigated are for the thermally thick case of burning.

6.3.1 Thermally Thick Solutions.

Consider some appropriate assumptions for the thermally thick case. Take Δh_{vap} constant at a thin reaction region where T_v is uniform. This will apply for rapid decomposition under high heating rates. Further expand the term

$$\dot{m}''_g \frac{\partial T}{\partial x} = \frac{\partial}{\partial x}(\dot{m}''_g T) - T\frac{\partial \dot{m}''_g}{\partial x} \tag{52}$$

and substitute this and equation (30) into equations (48) and (51). Integrate over $0 \le x \le l$, where at $x = l$, $\frac{\partial T}{\partial x} = 0$, and $\dot{m}''_g = 0$.

The charring result is

$$\int_0^l \rho c_p \frac{\partial T}{\partial t} dx + c_{p,g}\dot{m}''_g(0)T(0) - c_{p,g}T_v\dot{m}''_g(0) = \left(\dot{q}''_i - \sigma T^4(0)\right) + \frac{\Delta h_{vap}}{(1-X_c)}\left(0 - \dot{m}''_g(0)\right)$$

or

$$\dot{m}_g''(0)\left(\frac{\Delta h_{vap}}{(1-X_c)}+c_{p,g}(T(0)-T_v)\right)=\dot{q}_i''-\sigma T^4(0)-\int_0^l \rho c_p\frac{\partial T}{\partial t}dx \tag{53}$$

The noncharring (X_c = 0) case performs the integration over $s = l - x_v(t)$. Here the only difference is the term:

$$\int_0^s c_p\dot{m}_g''(0)\frac{\partial T}{\partial x}dx=c_p\dot{m}_g''(0)\big(T(s)-T(0)\big)$$

Further, taking the temperature at the surface to be the vaporization temperature gives

$$\dot{m}_g''(0)\big[\Delta h_{vap}+c_{p,g}(T(0)-T_v)+c_p\big(T(0)-T(s)\big)\big]=\dot{q}_i''-\sigma T^4(0)-\int_0^s \rho c_p\frac{\partial T}{\partial t}\mathrm{d}x$$

$$\dot{m}_g''(0)\big[\Delta h_{vap}++c_p\big(T_v-T(s)\big)\big]=\dot{q}_i''-\sigma T_v^4-\int_0^s \rho c_p\frac{\partial T}{\partial t}\mathrm{d}x \tag{54}$$

The solution forms given in equations 53 and 54 show the behavior of the mass loss rate over time. For example, the noncharring solution shows the classical steady solution and how the unsteady temperature derivative reduces the burning rate until it becomes zero. Explicitly,

$$\dot{m}_g''(0)=\left[\dot{q}_i''-\sigma T_v^4-\int_0^s \rho c_p\frac{\partial T}{\partial t}\mathrm{d}x\right]/L \tag{55}$$

where:

$$L\equiv\big[\Delta h_{vap}++c_p\big(T_v-T(s)\big)\big]$$

and L is the traditional heat of gasification as a property. Typically, the back-face temperature is the initial ambient for a thick material.

The corresponding result for the charring material shows that

$$\dot{m}_g''(0)=\left(\dot{q}_i''-\sigma T^4(0)-\int_0^l \rho c_p\frac{\partial T}{\partial t}\mathrm{d}x\right)/\left(\frac{\Delta h_{vap}}{(1-X_c)}+c_{p,g}(T(0)-T_v)\right) \tag{56}$$

Here, it is seen that the build up of char will cause an increase in the surface temperature over the temperature where decomposition is occurring. This factor will diminish the burning rate over time, and the char reduction factor ($1\text{-}X_c$) will drop the mass loss over a comparable noncharring material. Spearpoint and Quintiere [14] have shown that for wood, the mass loss rate will follow a particular behavior in time, after an initial peak, of $t^{-1/2}$.

The heats of gasification derived in this study from peak or overall burning behavior can now clearly be seen to be effective values as they are the slopes of mass loss rate with heat flux. The effective values are seen to be for noncharring materials:

$$L \equiv \left[\Delta h_{vap} + + c_p\left(T_v - T(s)\right)\right] \text{ under steady state,}$$

and for charring materials it is higher as:

$$L = \frac{\Delta h_{vap}}{(1 - X_c)} + c_{p,g}(T(0) - T_v)$$

However, both of these results ignore the transient effects that are inexplicitly included in the data analysis.

6.3.2 Thermally Thin Solutions.

For a thermally thin material, the temperature would ideally be uniform throughout. During burning this will be taken as the vaporization temperature. Equations 30 and 33 give

$$\frac{\partial \dot{m}''_g}{\partial x} = -\rho_a a_p e^{-E/RT} \tag{57}$$

This integrates over the region to give the mass flux at the surface.

$$\dot{m}''_g(0) = \int_0^l \rho_a a_p e^{-E/RT} dx \tag{58}$$

Since $T = T(t)$ only, equation 58 used for a thin region becomes

$$\dot{m}''_g(0) \approx \rho_a a_p e^{-E/RT_v} \cdot l_{thin} \tag{59}$$

where l_{thin} can be the thickness from the start of burning, or it can be a region near the back face when the thermal wave arrives. Its magnitude will be considered shortly. It should be recognized that the active density will not be constant over this burning period as it is depleted, and hence equation 59 is approximate. It will decrease and this effect can be derived from the species equation 35 as follows:

$$\frac{\partial \rho_a}{\partial t} = \left(\frac{-1}{1 - X_c}\right) \rho_a a_p e^{-E/RT_v} \tag{60}$$

where at $t = 0$, $\rho_a = \rho_o$ and at $t = \infty$, $\rho_a = 0$. Integrating over time gives:

$$\int_{\rho_o}^{\rho_a} \frac{d\rho_a}{\rho_a} = \int_0^{\Delta t} \left(\frac{-K}{1-X_c} \right) dt$$

or

$$\rho_a = \rho_o e^{-\frac{K\Delta t}{1-X_c}} \quad \text{with } K \equiv a_p e^{-E/RT}$$

with ρ_o, the density of original material before decomposition.

$$\therefore \dot{m}''_g(0) = \rho_o \left(1 - e^{-\frac{K\Delta t}{1-X_c}} \right) K l_{thin} \tag{61}$$

The time period is not directly determined here, but the maximum or initial value gives a measure of the mass flux for the thin case.

$$\dot{m}''_{g,\max}(0) \approx \rho_o l_{thin} a_p e^{-E/RT} \tag{62}$$

For TGA data indicating a_p = 1.1x10^{19} and E = 2.4x10^5 J/mole-K, the result for a peak vaporization temperature of about 425^{o}C is [13.3 kg/m^{2}s l_{thin}(mm)] and for an onset vaporization temperature of 350^{o}C, [95 g/m^{2}s l_{thin}(mm)]. This shows the potentially high values for the thermally thin case, but they would be mitigated by the decrease in the active fuel. It also shows the difficulty in a numerical computation with this sudden jump effect. The form of the solution shows that the thin domain will give a sudden peak followed by a rapid decrease in the mass flux.

6.4 CRITERIA FOR THERMALLY THICK AND THIN BURNING.

The thickness of the reaction zone in the thin case depends on two effects. First, during the heating to ignition, the back face of the sample could have the thermal wave reach it at ignition. The material then would have behaved as thermally thick for ignition, but now the burning is occurring with the sample fully heated at the start. Second, the sample could be thermally thick during most of the burning following ignition, but the thermal wave during burning eventually reaches the back face. The depths of these thermal layers indicate the magnitude of the reaction zone in thermally thin burning.

6.4.1 Thermally Thin at Ignition.

Spearpoint and Quintiere [14] report an approximate solution for ignition in terms of a thermal depth. The thermal depth varies as:

$$\delta = \sqrt{3\left(\frac{k}{\rho c}\right)\left(\frac{2-\beta}{1-\beta}\right)t} \tag{63}$$

where:

$$\beta = \frac{\sigma(T^4 - T_o^4) + h_c(T - T_o)}{\dot{q}_i''}$$

The time at ignition is given as:

$$t_{ig} = \frac{4}{3} k\rho c \left(\frac{1-\beta}{2-\beta} \right) \frac{(T_{ig} - T_o)^2}{\dot{q}_i''^2} \tag{64}$$

The sample will burn as a thin material if $\delta(t_{ig}) = l$, then

$$l_{thin} = \sqrt{3\left(\frac{k}{\rho c} \right)\left(\frac{2-\beta}{1-\beta} \right)\frac{4}{3}\left(\frac{1-\beta}{2-\beta} \right)\frac{(T_{ig} - T_o)^2}{\dot{q}_i''^2}}$$

or the criterion for burning as a thin sample is that the thickness, l, must be less than

$$l_{thin} = 2\frac{(T_{ig} - T_o)k}{\dot{q}_i''} \tag{65}$$

Here, the incident heat flux is the external radiant flux. If the temperature at the onset of degradation is used, then it can be estimated that for the nylon samples that:

$$l_{thin}\,(\text{mm}) \approx \frac{2(325^o C - 25^o C)(0.2 \times 10^{-3}\ \text{kW/mK})}{\dot{q}_i''\,(\text{kW/m}^2)} \approx \frac{120}{\dot{q}_i''\,(\text{kW/m}^2)}$$

This suggests samples of 2 to 6 mm could act as thermally thin immediately following ignition. Figure 53 shows an example of burning 3.2-mm-thick nylon at different heat fluxes. For the higher heat fluxes, steady burning is clearly indicated, but for the lowest flux, a thermally thin behavior is seen. This dependence on heat flux is clearly seen in the criterion. Also shown in the high heat flux curves is the thermally thin burning behavior that occurs when the back face begins heating.

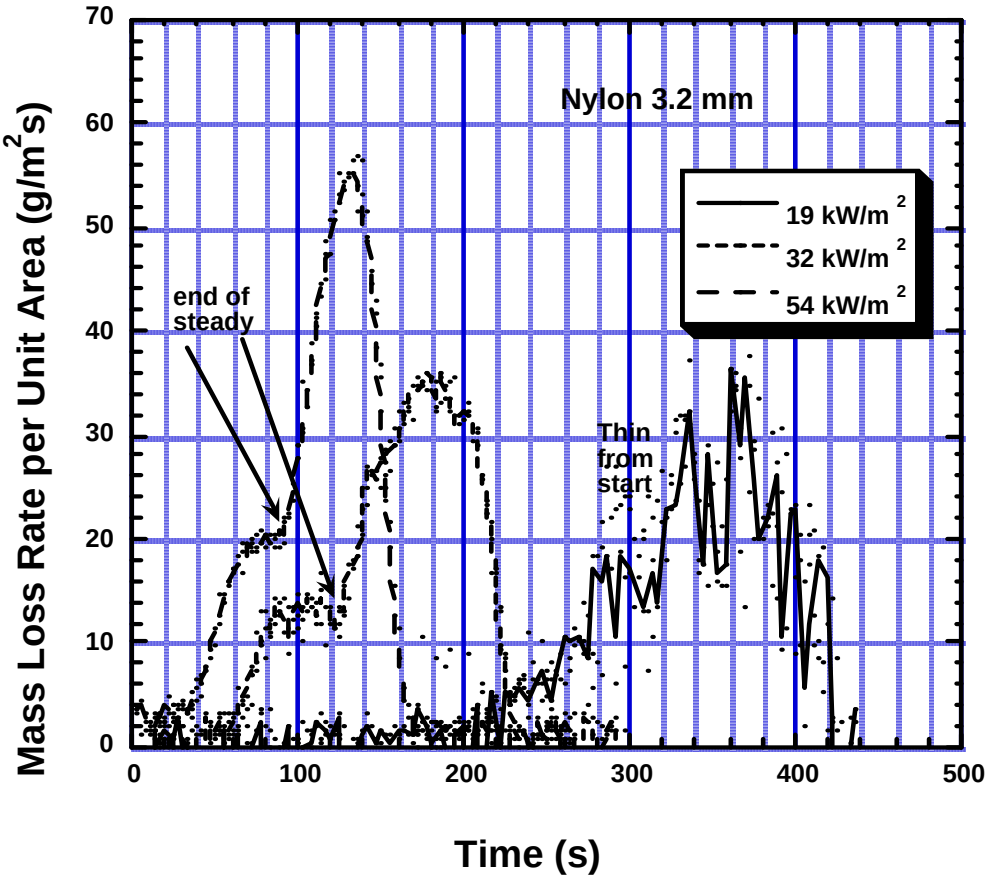

Figure 53. Thermally Thick and Thick Burning Behavior

6.4.2 Back-Face Thermally Thin Effect.

As the degradation progress in a sample of original thickness, *l*, a thermal depth will advance from the vaporization region, as illustrated in figure 48, and will eventually reach the back face. At that point, the insulated back surface temperature will increase over the steady solution within the thermal depth region and the kinetic effects will proceed to control the burning rate. For a thick sample, the thermal depth will reach a constant value during steady burning. Hopkins and Quintiere [2] give this steady depth as:

$$\delta_s = \frac{2kL}{c(\dot{q}_i'' - \sigma T_v^4)} \tag{66}$$

Staggs [15] obtained a similar result, in the terminology, as $\delta_s = \frac{2k(T_v - T_o)}{(\dot{q}_i'' - \sigma T_v^4)}$. Staggs states that when this value is less than 0.25*l*, the solid will burn quasi-steady. At some point, this quasi-

steady behavior will succumb to its insulated back face and burn as thermally thin. From figure 53, this transition to thermally thin burning will occur when:

$$l = x_v + \delta_s \tag{67}$$

for steady burning in a noncharring material. Under these conditions, the regression front is given from equation. (55) as:

$$x_v = \left(\dot{q}_i'' - \sigma T_v^4\right) t / \rho_o L \tag{68}$$

where t is the time to reach the back face. This vaporization distance is the dominant factor for thick samples in indicating when the back face effects occur. All data, including the plotted charring samples, ignored the smaller thermal depth, as q''^{t}_{i} versus l in figure 54. Although charring material, from Spearpoint and Quintiere [14], would indicate that the vaporization front and the thermal depth both are a weak function of the heat flux and grow as $\sqrt{\frac{kt}{\rho c}}$. This is not seen for the weakly charring clay nanocomposites in figure 54. Perhaps higher char yields would produce the indicated charring behavior. The initial thermally thin regions for small l values have been estimated and shown in figure 54 for the thin thickness ignition criterion. From equation 68, the slope of the linear data fits allows a computation for a heat of gasification. For density of 1108 kg/m^3, the L values are 1.88, 2.38, and 2.71 kJ/g for 0%, 2%, and 5% clay. These are not unreasonable in view of table 6. When the time indicated in figure 54 is achieved for a given thickness and heat flux, thermally thin burning will ensue. This burning rate can be estimated from equation 62 with now l_{thin} taken from equation 66.

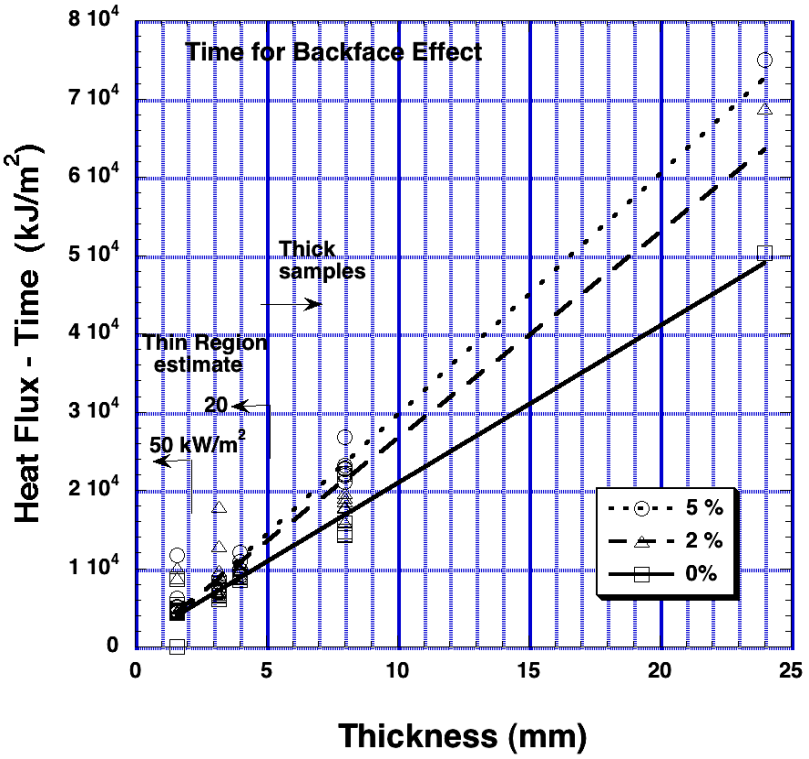

Figure 54. Time for the Thermal Depth to Reach the Back Face for a Given Original Thickness and Incident Heat Flux

6.5 STEADY BURNING AND KINETICS.

It is interesting to note that for a thermally thick sample, no kinetic parameters explicitly show up in the solution forms. Only the heats of vaporization or gasification are present. In contrast, for the thermally thin solution, the thermodynamic parameters do not show up; only the kinetic parameters are present. The case of the noncharring solid burning at steady state can show the connection between the thermodynamic and kinetic properties. The steady noncharring solution gives:

$$T - T_\infty = (T_v - T_\infty) e^{-\frac{c_p \dot{m}''_g(0)}{k} x} \tag{69}$$

Equation (58) gives:

$$\dot{m}''_g(0) = \int_{T_v}^{T_o} \frac{\rho_a a_p e^{-E/RT}}{\left(\frac{dT}{dx}\right)} dT \tag{70}$$

that clearly show as the sample becomes thermally thin $\frac{dT}{dx} \to 0$ and the burning rate can increase. However, at steady state where

$$\dot{m}_g''(0) = \left(\dot{q}_i'' - \sigma T_v^4\right)/ L \tag{71}$$

the steady temperature derivative can be found from equation 69. Furthermore, approximating

$$e^{-E/RT} \approx e^{\theta} e^{-E/RT_v}$$
$$\theta \equiv \left(\frac{T - T_v}{T_v}\right)\frac{E}{RT_v} \tag{72}$$

it can be shown that

$$\left(\left(\dot{q}_i'' - \sigma T_v^4\right)/ L\right)^2 \approx \frac{\rho_a a_p e^{-E/RT_v} k}{c_p\left(\frac{T_v - T_o}{T_v}\right)\left(\frac{E}{RT_v}\right)}\left(1 - \exp\left(-\frac{E}{RT_v}\left(\frac{T_v - T_o}{T_v}\right)\right)\right) \tag{73}$$

This shows that the vaporization temperature is not a constant, but will increase as the incident heat flux increases. This occurs for given kinetic properties a_p and E and the thermodynamic parameter L. The heat of gasification will be a true property; however, as equation 46 shows, the heat of vaporization depends on the vaporization temperature. Thus, the heat of gasification will only be a unique property for materials having a constant vaporization temperature as pure liquids. Hence, these parameters are linked through the resultant vaporization temperature.

Under steady burning for pure nylon, the value for L can be determined by the mass loss rate over the constant burning period after the initial transient and before the back-face effect. For the 8-mm sample, such data are shown in figure 55. The slope of these data is usually used to determine L from equation 55, but only if the incident heat flux remained constant. During burning in the cone configuration, a tall flame will retain a constant heat flux for varying external heat flux exposures [16]. Consequently, the low heat flux data point is ignored, and the value for L should be 3.4 kJ/g. From TGA data, a vaporization temperature of 425°C, and an initial temperature of 25°C with an extrapolated c_p of 4 J/g-K from figure 63, then a heat of vaporization is computed as 2.8 kJ/g.

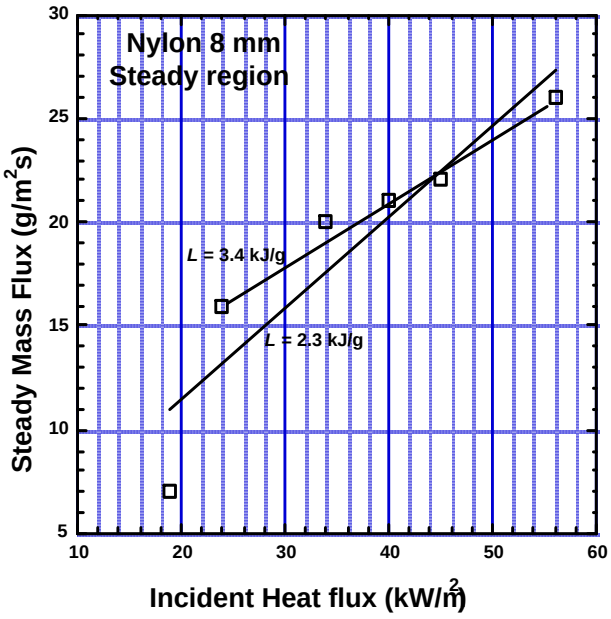

Figure 55. Heat of Gasification for Nylon From Steady Burning

6.6 OVERALL BURNING BEHAVIOR AND THE EFFECT OF THICKNESS.

The two kinds of burning behavior—thick and thin—make it difficult to describe the effect of the nanoclay addition to nylon in a universal way. It is clear that the weak char residue of the clay is the principal factor in reducing the burning rate for the thick samples as the char accumulates. However, the thermally thin burning behavior and its dependence on both char yield and kinetic properties are another factor. TGA data, for its samples, gave a char yield of pure nylon of 0.017, and with 5% clay, a char yield of 0.060; slightly higher than the samples burned in the cone calorimeter. The kinetic properties are $a_p = 1.1\text{x}10^{19}$ and $E = 2.4\text{x}10^5$ J/mole-K for pure nylon and $a_p = 2.3\text{x}10^{17}$ and $E = 2.1\text{x}10^5$ J/mole-K for the 5% clay. The clay shows a distinct reduction in the burning rate according to the pre-exponential factor.

6.6.1 Illustrations of Burning Differences.

Figure 56 shows a sampling of the burning behavior for nylon and the nanocomposite with 5% clay as a function of thickness. For thick samples over 8 mm, the nylon burns at roughly 600 to 700 kW/m^2 during its quasi-steady period with the clay sample reduced by about 30%. Also, the clay sample shows very little back face enhanced burning, while the nylon achieves up to 2000 kW/m^2, a jump of more than threefold.

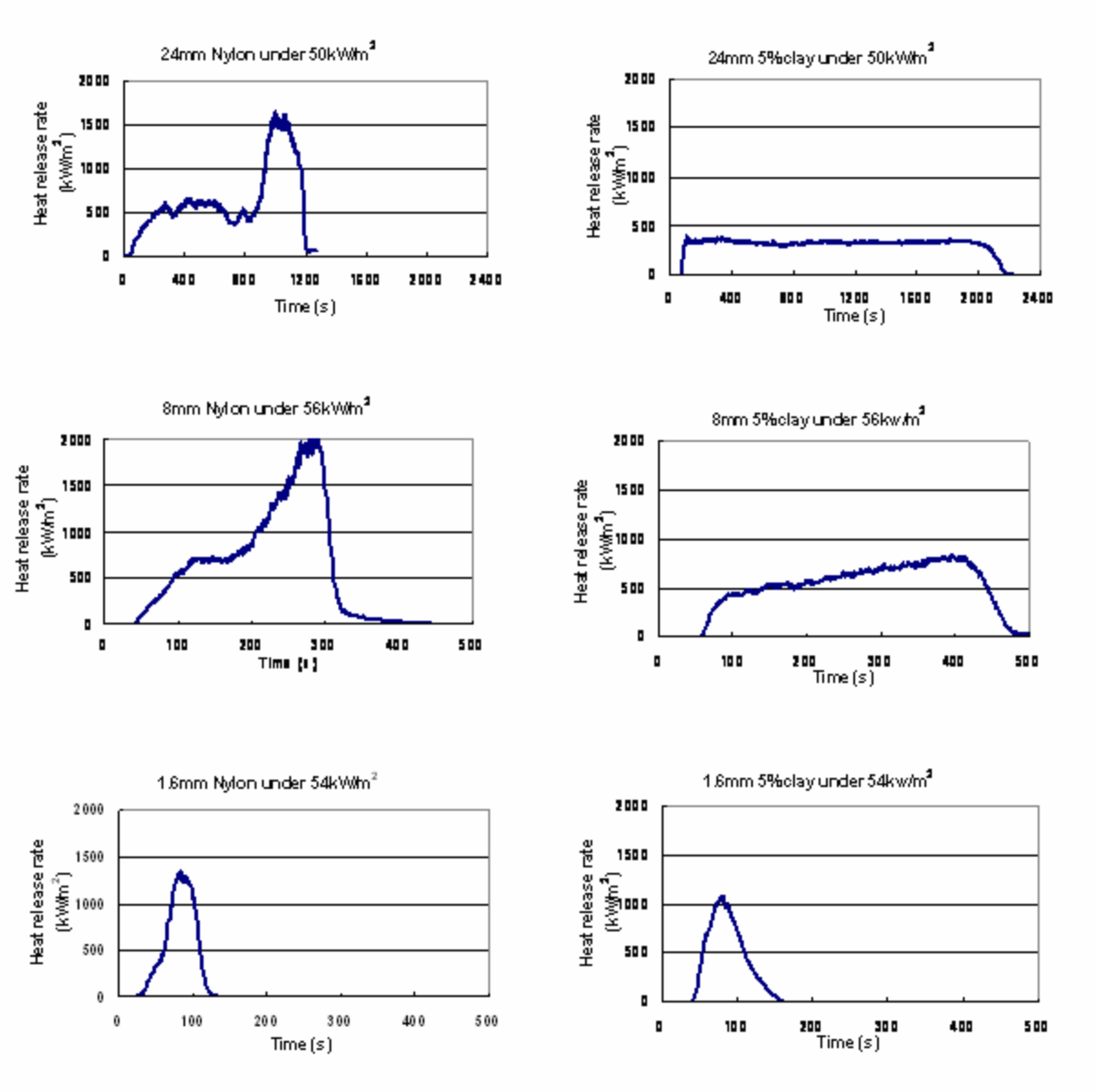

Figure 56. Heat Release Rate Dependence Thickness and Clay Content for 50-56 kW/m^2

For the 1.6-mm sample, thermally thin burning is displayed and the peak condition shows the nylon at 1300 kW/m^2 and the 5% clay sample at 1000 kW/m^2. Significant reductions in the burning rates (as the heats of combustion are nearly identical) are achieved with the clay. The effect of heat flux is illustrated in figure 57. It is clearly seen that the heat flux has a proportional effect on the burning rate. This effect for steady burning should be linear. It is also seen that at the lower heat flux, the preheating of the sample before ignition causes thermally thin burning to mostly prevail for all thicknesses.

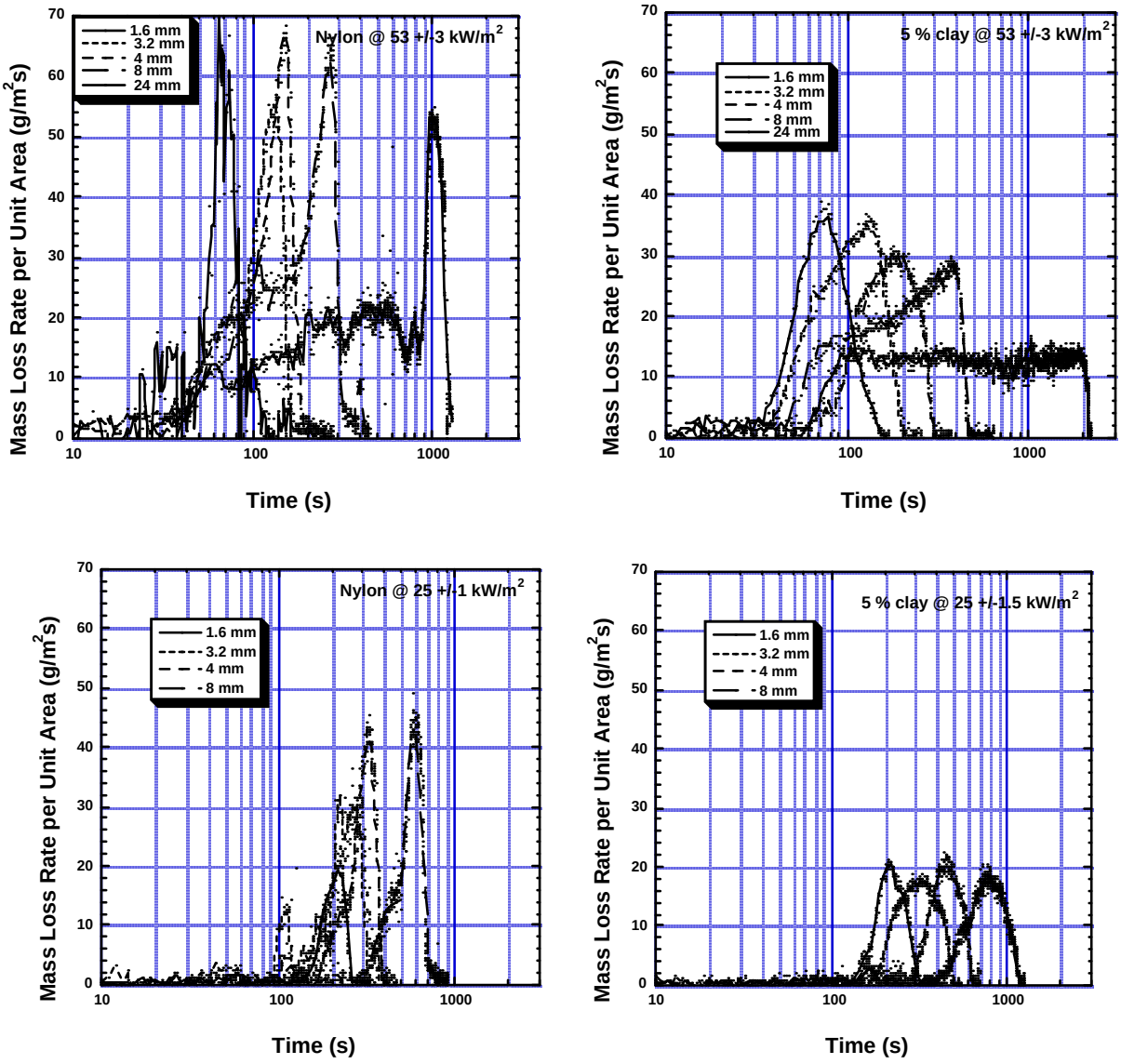

Figure 57. The Effect of Heat Flux for the Nylon and 5% Composite Samples

6.6.2 Overall Burning Rate and Effective Heat of Gasification.

Attempts were made to characterize the burning rates in terms of the heats of gasification. Commonly, this is done for the steady burning period or for a distinct peak region of burning. However, the thickness and back-face effects caused up to two peak regions. Initially, the two peak conditions were used to obtain heats of gasification, and their ranges are listed in table 6. This was not a satisfactory way to characterize the burning behavior. Therefore, an overall burning rate was computed as an integrated average over the entire burning period. This captures the entire effects of thickness, steady burning, and back-face conditions. It gives a better way to access the effects of clay addition and thickness together. Figures 58, 59, and 60 show the results for pure nylon and 2% and 5% clay composites, respectively. With a curious,

unexplainable exception at either 4- or 8-mm thickness, the overall heats of gasification are roughly 2.4 kJ/g for nylon, 1.8 kJ/g for 2%, and 2.6 kJ/g for 5%. The reduction in mass loss rates can be seen, for example at 50 kW/m^2 with nylon at 29 g/m^{2}s, +2% clay at 22 g/m^{2}s, and +5% clay at 18 g/m^{2}s. The pure nylon, with insignificant char, displays a decrease in the mass loss rate as the thickness decreases. But the opposite trend is seen for the charring composites, except at 1.6 mm where the trend is mixed.

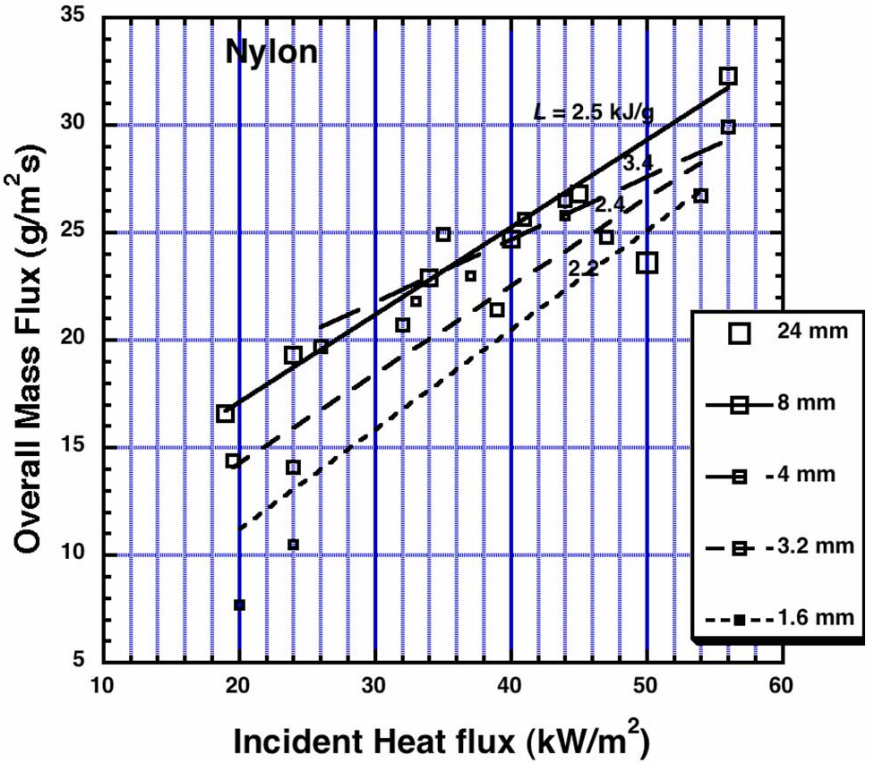

Figure 58. Overall Average Burning Rate for Nylon Samples

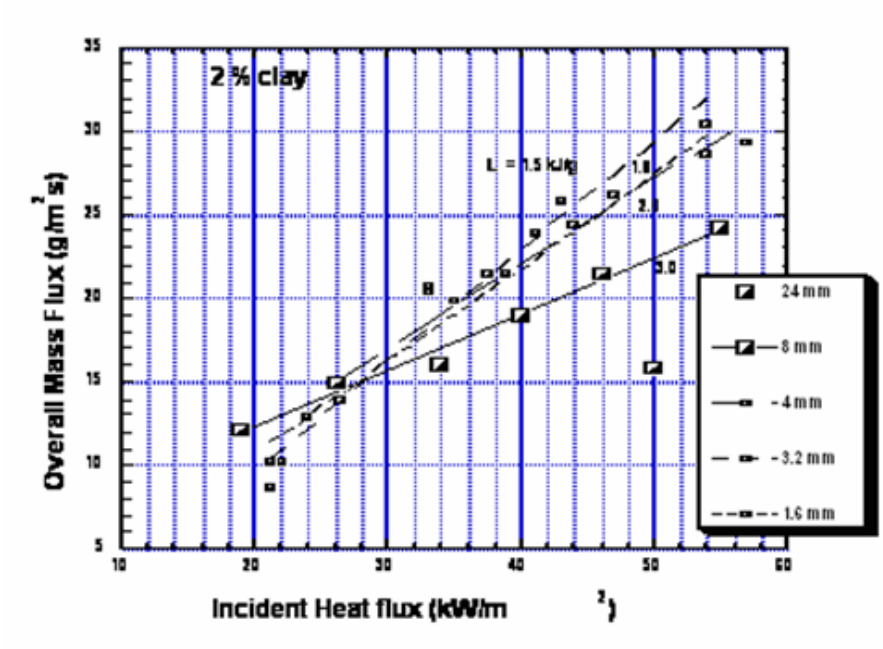

Figure 59. Overall Average Burning Rate for 2% Composite Samples

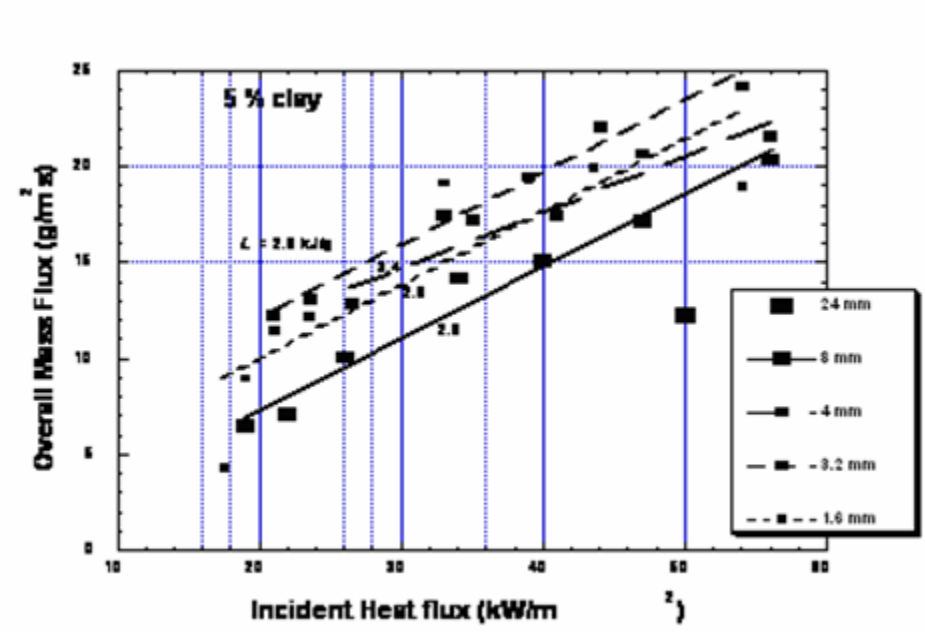

Figure 60. Overall Average Burning Rate for 5% Composite Samples

It is well known for wood sticks that the average burning rate increases as the thickness decreases. This is likely due to the decrease in burning rate with time until the back-face effect causes an increase. For sticks, this back-face effect is manifested by the thermal depth reaching the center of the stick. Generally, it is found for wood that the burning rate per unit area varies as $l^{-0.5}$ where l is the stick diameter. Figure 58 presents a plot of all the average burning rate data.

The mass flux is divided by the incident heat flux to include its roughly linear effect. Power law fits, giving rough trends, are shown in figure 61.

The approximate empirical formulas are in the form:

$$\dot{m}''(\mathrm{g/m^2 s}) = C\dot{q}_i''(\mathrm{kW/m^2})l^n(\mathrm{mm}) \tag{74}$$

where C = 0.52 for nylon, 0.61 for 2%, and 0.52 for 5%; and n = + 0.095 for nylon, -0.11 for 2% and -0.17 for 5%. Figure 61 shows that there can be as much as a 50% reduction in burning rate for the addition of 5% nanoclay compared to nylon for a given heat flux and thickness.

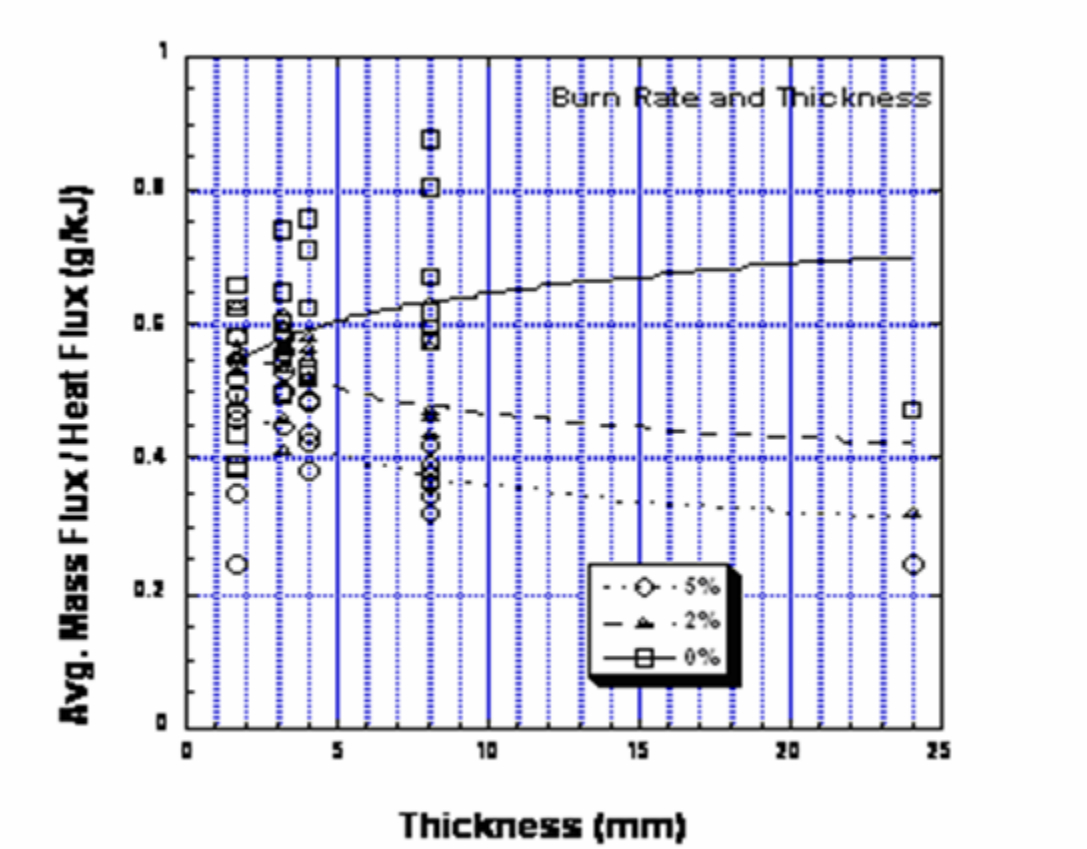

Figure 61. Power Law Behavior With Thickness for Samples

6.7 NUMERICAL MODELING.

A theoretical solid phase model had been used that accounts for kinetic decomposition and heat and mass transfer in the material subjected to a radiant heat source [13]. The model includes variations of thermal properties of material and char. The model will be executed to obtain some illustrated numerical results. Precise results for the nylon samples were not possible because numerical errors occurred due to the stiffness of the kinetic term.

For a thermal gravimetric analysis, very small samples (milligram quantities) are heated in an inferior TGA instrument to find out whether or not thermal degradation will start at a given temperature. In this section, a FORTRAN program was used to simulate the combustion process of real size samples. This FORTRAN program was developed by Boonmee [13] for his wood material. The input properties were selected to best match the nylon samples. The nylon activation energy (E_a) and pre-exponential factor (a_p) were also used in the program, which was calculated in section 5.

The following assumptions were imposed in order to simplify the problem:

- The problem could be formulated as a 1-D transient heat conduction problem.
- The continuum volume of the sample consisted of three species: active, char, and gas.
- Local thermal properties and density varied with temperature.
- Convective and radiative heat losses were taken into account at the sample surface.
- No heat or mass losses occurred at the back of the sample.

The theoretical model involved the following equations:

Kinetics Decomposition

$$\frac{\partial \rho_j}{\partial t} = -\rho_{a,j} a_{P,j} \exp(-E_{a,j} / RT)$$

Mass Conservation

$$\frac{\partial \rho}{\partial t} + \frac{\partial (\rho_a v_a)}{\partial x} + \frac{\partial (\rho_C v_C)}{\partial x} + \frac{\partial (\rho_g v_g)}{\partial x} = 0$$

Energy Conservation

$$\frac{\partial (\rho_a h_a + \rho_c h_c)}{\partial t} = \frac{\partial}{\partial x}\left(k \frac{\partial T}{\partial x} \right) + \frac{\partial}{\partial x}\left(\dot{m}''_g h_g \right) - Q_P \left(-\frac{\partial \rho}{\partial t} \right)$$

where Q_p was the heat of pyrolysis positive for endothermic decomposition and negative for exothermic decomposition and that was the same as $\frac{\Delta h_d}{(1 - X_c)}$ that was introduced in the previous analysis, and where $\rho_a h_a = \sum_{j=1}^{3} X_j \rho_{a,j} h_{a,j}$ was the total enthalpy of the active part and $\rho_C h_C = \sum_{j=1}^{3} X_j \rho_{C,j} h_{C,j}$ was the total enthalpy of char and the subscript *a* was for the active part, *c* is for char, and *g* was for gas.

6.7.1 FORTRAN Model Input Properties.

Use input of nylon as an example.

- Ambient temperature (K) 298
- Sample thickness (m) 0.024, 0.008, 0.004, and 0.0016
- Virgin density (kg/m3) 1136
- Char fraction 0.017
- Final density (kg/m^3) 0.017 x 1136
- Activation energy (J/mol) 2.4E+5
- Pre-exponential factor (1/s) 1.1E+19
- Incident heat flux (W/m2) 50×10^3
- Flame heat flux (W/m^2) 5×10^3
- Heat transfer coefficient (W/m^2K) 10
- Emissivity 1.0

The other two thermal properties are thermal conductivity and specific heat. These are shown in figure 62 and 63, the dot data are from NIST [12]. A linear equation is used in the former FORTRAN program. Since the linear variation in temperature for the properties used in the FORTRAN program for wood still match well with the data from NIST for nylon, and the aim of this simulation is to qualitatively show the thickness effect, the properties were written for the wood input. (Changing those properties slightly cause numerical issues that were not resolvable at this time.)

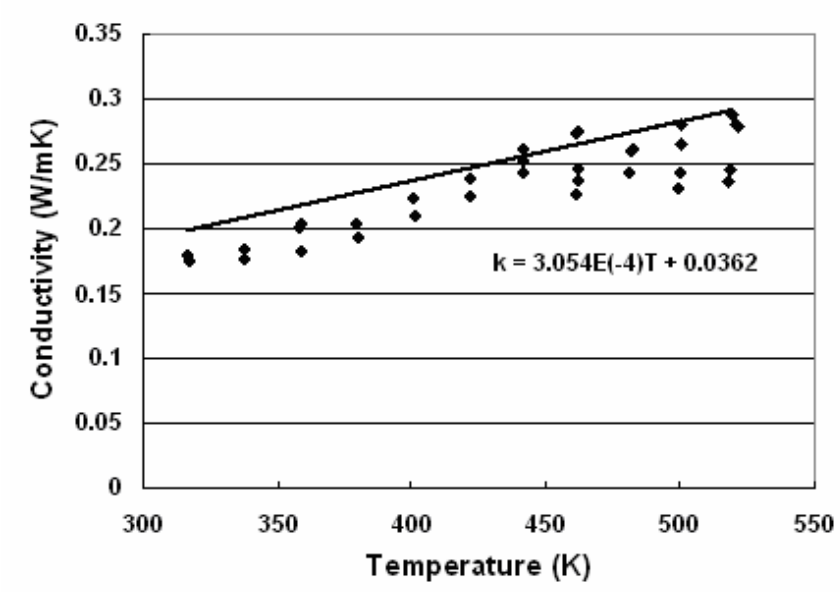

Figure 62. Conductivity of Nylon

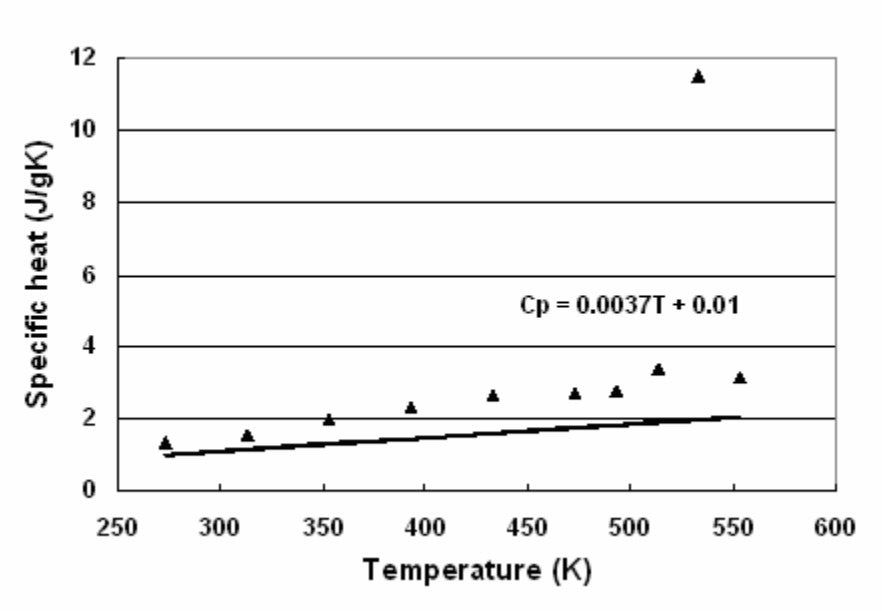

Figure 63. Specific Heat of Nylon

6.7.2 Results Analysis.

Comparison of data from an experiment and the results from a FORTRAN model are displayed in figure 64 using 8-mm nylon +5% clay under 50kW/m^2 as an example.

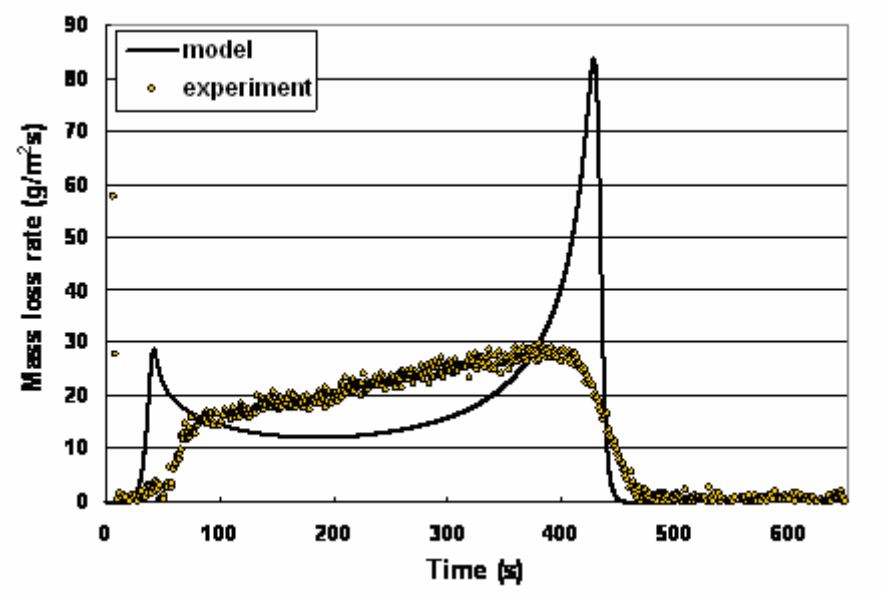

Figure 64. An 8-mm Nylon +5% Clay Under 50 kW/m^2

There are three factors that can affect the results.

1. Thickness effect

Figure 65 shows two FORTRAN program simulation of a mass loss rate of nylon +5% clay with different thickness. Figure 66 shows the experimental results for the same material. In comparing these two figures, the trend of thickness effect was the same. A thicker sample had a lower mass loss rate. The big jump for each curve in figure 65 was from the back face insulation boundary condition, which was caused by numerical simulation.

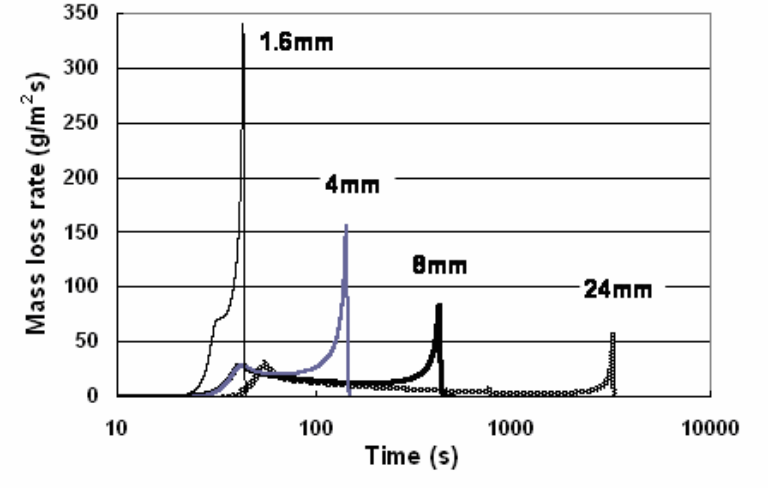

Figure 65. Nylon +5% Clay With Different Thicknesses From Simulation of Mass Loss Rate

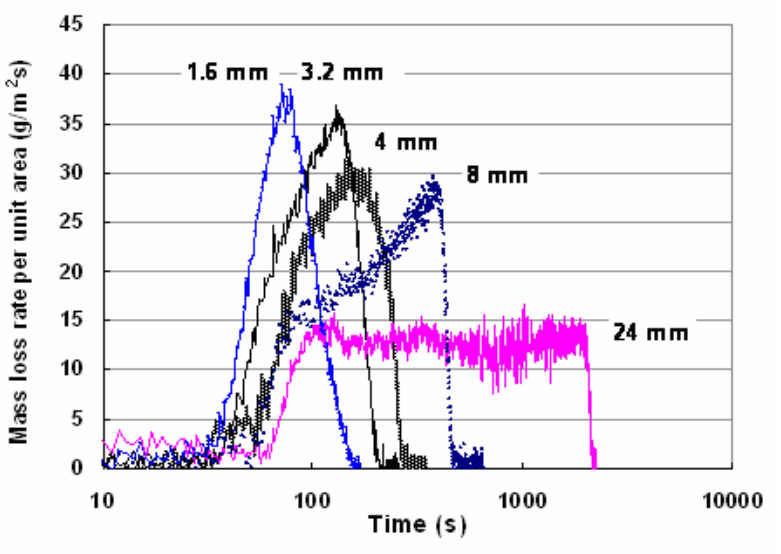

Figure 66. Different Thicknesses of Nylon +5% Clay Under 53 ±3 kW/m^2 From Experiment Results

2. E_a and a_p effect

Since different α (0.25, 0.5, and 0.75) gives a different set of E_a and a_p, the curve calculated by different E_a and a_p may be different too. Consider the value of 8-mm Nylon +5% clay under 50 kW/m^2 as an example. Figure 67 shows that a smaller α has a lower value of E_a and a_p, thus mass loss rate is smaller.

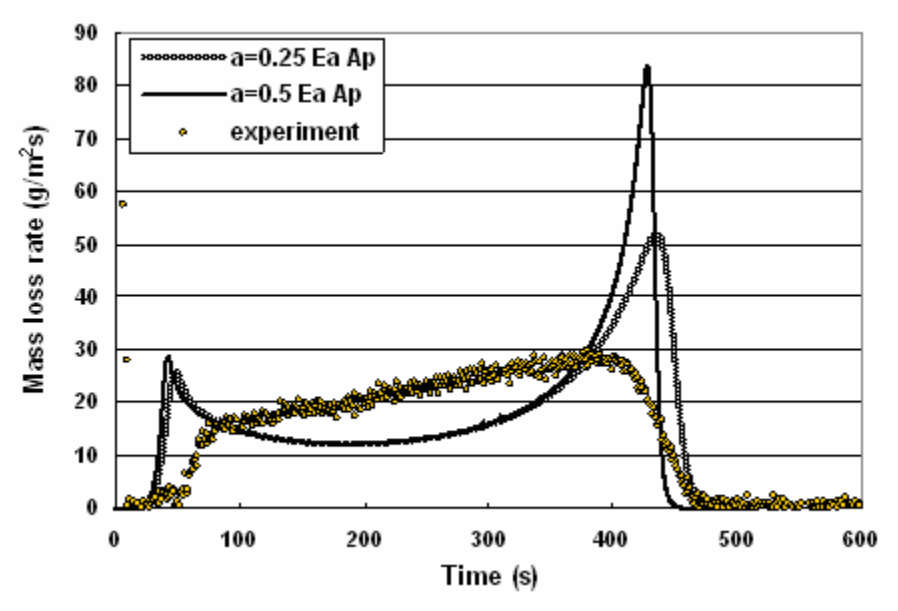

Figure 67. Comparison of Results of Different Sets of E_a and a_p 8-mm Nylon +5% Clay Under 50 kW/m^2

3. Effect of heat of pyrolysis

Q_p is the heat of pyrolysis (positive for endothermic decomposition and negative for exothermic decomposition). It is an unknown for the nylon samples. Hence, the heat of pyrolysis was changed from a large positive number to a large negative number to see if it would affect the final results.

Figure 68 shows the change of the solid heat of pyrolysis setting in the program, with Q_p = 1500 J/kg (Endothermic), Q_p = 0 and Q_p = -1500 J/kg (exothermic). The results do not show much difference. Therefore, Q_p = 0 was used for all simulations. (In hindsight, it was likely that this value would have been much higher, in the order of 1.5 kJ/g, and this would have dropped the mass loss rate computed.)

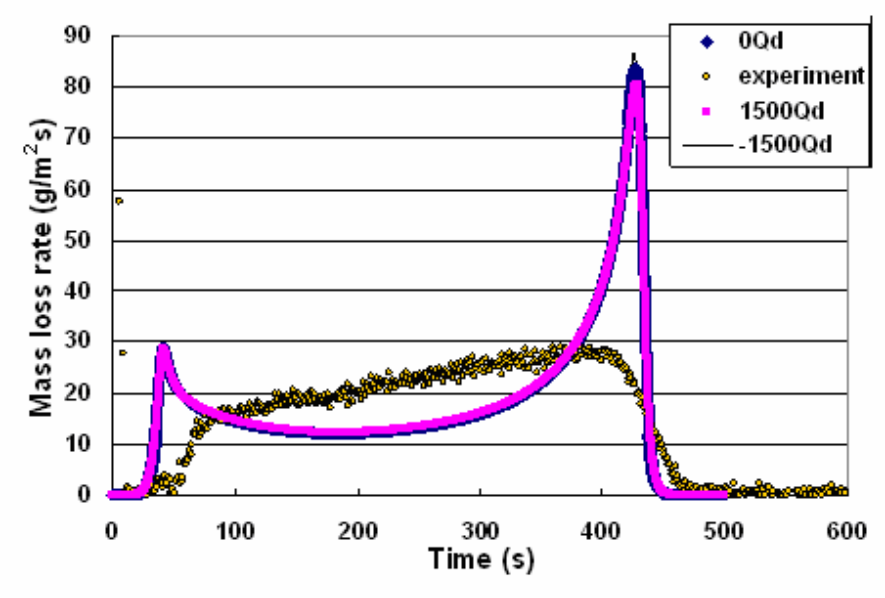

Figure 68. Comparison of Different Heat of Pyrolysis 8-mm Nylon +5% Clay Under 50 kW/m^2 Results

7. SUMMARY.

Polymer layered-silicate (clay) nanocomposites have the unique combination of reduced flammability and improved physical properties. A summary of the properties is listed in table 7. The heats of combustion and gasification pertain to heat release rate (fire power) potential, and the ignition temperature and thermal properties pertain to flame spread and ignition behavior. The heats of gasification refer only to that based on the second, or back face, mass loss rate peak. Solely, it is not a complete indication of the overall behavior. Following are some distinct conclusions.

- Char yield will inhibit burning rate, but can enhance flame spread by providing a low-density matrix of fuel over a melted pool. It is clear from these properties that residue fraction is an important effect. The residue, char-like fraction yield is almost coincident with the clay loading. For pure nylon it ranges from 0 to 0.005 and 0.11 to 0.015 for 2% loading and 0.04 to 0.05 for 5% loading.

- The heat of combustion varies slightly for the samples. It is roughly about 33, 30, and 29 kJ/g for nylon, 2%, and 5% composite, respectively. Also, the total energy released per unit volume of the original sample stays fairly constant at about 30 to 35 MJ/m^3, decreasing slightly with clay loading.

- The peak burning rate or heat release rate is affected considerably by the clay loadings. For example, at a heat flux of about 40 kW/m^2, pure nylon peaks at about 1500 kW/m^2, at about 900 kW/m^2 for 2% clay, and about 600 kW/m^2 for 5% clay. This is attributed to the reduction in gaseous fuel and was mostly likely due to the inhibited heat transfer of

the char residue. The 2% loading causes a char skin with a hollow core to form over the melting solid, whereas the char matrix is more homogeneous for the 5% loading.

- It is found that that there can be as much as a 50% reduction in average burning rate for the addition of 5% nanoclay to nylon for a given heat flux and thickness.

- The clay addition increases the time to ignite over the pure nylon. Ignition time also decreases as the thickness decreases. In general, the ignition time could increase by a factor of 1.3 to 2 over the pure nylon for both of the composite loadings.

- The critical flux for ignition is not significantly different for the samples, dropping form 17.7 to 16.0 kW/m^2 between 0 and 5% clay. The corresponding computed ignition temperature is about 430^{o}C. This is consistent with the decomposition temperatures found in TGA tests as they commence at about 350^{o}C and peak at about 430^{o}C.

- The addition of clay shows that there is an effective increase for the $k\rho c$ despite the formation of char in the addition of clay. Direct measurements of the thermal conductivity and specific heats suggest that $k\rho c$ should not change for the charring samples. Thus, this effective change is likely to reduce the flammable vapor rate that causes longer ignition time for the charring samples.

- The thickness of the sample also affects ignition behavior. It has been empirically found that the thickness effect is given approximately as m''(g/m^{2}s) = Cq''_i (kW/m^2)l^n (mm) where C = 0.52 for nylon, 0.61 for 2%, and 0.52 for 5%; and n = +0.095 for nylon, -0.11 for 2% and -0.17 for 5%.

- There were two kinds of burning manifested in the burning behavior of the test samples: a thermally thin and a thermally thick, and a model has been put forth to explain the two modes. The thermal wave reaching the back face, due to preheating before ignition, or later for a thicker sample will lead to thermally thin burning. Thermally thin burning is governed by kinetic properties, whereas thermally thick burning (and most particularly steady, noncharring burning) is governed by the heat of gasification. For steady burning, the corresponding heat of gasification, L, is estimated as 3.4 kJ/g. From TGA data, a vaporization temperature of 425^{o}C, an initial temperature of 25^{o}C with an extrapolated c_p of 4 J/g-K, then a heat of vaporization, Δh_{vap}, was computed as 2.8 kJ/g. These values might be considered true thermodynamic properties over the effective values for L found for different burning periods. Kinetic properties were found from TGA analyses as a_p=1.1x10^{19}, and E=2.4x10^5 J/mole-K for pure nylon and a_p=2.3x10^{17}, and E=2.1x10^5 J/mole-K for the 5% clay.

- A theoretical solid phase model accounting for kinetic decomposition and heat and mass transfer of nanocomposites subjected to a radiant heat source were used. The model includes variations of thermal properties of sample and char. Comparisons between the theoretical and experimental mass loss rate are given. The theoretical results qualitatively agree with the experiments.

Table 7. Summary of Properties

	Nylon	Nylon +2% Clay	Nylon +5% Clay
8-mm Samples			
Δh_c, second *peak avg.* (kJ/g)	32.5	29.3	28.4
$\dot{q}''_{cr}$ (kW/m^2)	17.7< $\dot{q}''_{cr}$ <19	17.5< $\dot{q}''_{cr}$ <19	16< $\dot{q}''_{cr}$ <17.5
T_{ig} (ºC)	450	450	430
$k\rho c$ (kW/m^{2}K)^{2}s	0.73	1.13	0.99
L (kJ/g), second peak	2.17	3.85	2.34
char fraction χ_c %	≈0	1.83~2.1	4.19~4.96
total HR Q'''(MJ/m^3)	31.9	31.1	29.8
4-mm Samples			
Δh_c, second *peak avg.* (kJ/g)	33	29.6	28.8
$\dot{q}''_{cr}$ (kW/m^2)	<26	<26.5	<26.5
T_{ig} (ºC)	467≈470	472≈470	472≈470
$k\rho c$ (kW/m^{2}K)^{2}s	0.71	1.21	1.32
L (kJ/g), second peak	2.25	1.77	3.6
char fraction χ_c	≈0	1.44~1.93	3.86~4.81
total HR Q'''(MJ/m^3)	34.4	32.9	32.6
3.2-mm Samples			
Δh_c, second *peak avg.* (kJ/g)	33.7	29.7	29.3
$\dot{q}''_{cr}$ (kW/m^2)	≤19	≤20	≤20
T_{ig} (ºC)	452≈450	457≈460	457≈460
$k\rho c$ (kW/m^{2}K)^{2}s	0.82	1.53	1.53
L (kJ/g), second peak	2.63	1.92	1.85
char fraction χ_c	0~1.2	0.6~1.9	4.0~4.8
total HR Q'''(MJ/m^3)	31.2	30.2	34.5

Table 7. Summary of Properties (Continued)

	Nylon	Nylon +2% Clay	Nylon +5% Clay
1.6-mm Samples			
Δh_c, second *peak avg.* (kJ/g)	30.1	30.2	29.0
$\dot{q}''_{cr}$ (kW/m^2)	≤19	≤19	≤17.5
T_{ig} (°C)	446.6≈450	446.6≈450	430
$k\rho c$ (kW/m^{2}K)^{2}s)	0.52	1.47	1.45
L (kJ/g), second peak	2.27	1.7	1.7
char fraction χ_c	0~1.0	1.0~3.0	4.0~5.0
total HR Q'''(MJ/m^3)	33.5	37.5	37.7

From the point of view of material flammability, the improvements due to the clay loading for the clay nanocomposite with nylon are very satisfactory. First, the ignition time is increased, which means during a real fire, the escape time is increased. Second, the total amount of energy is not changing by adding clay, but the peak heat release rate is greatly reduced. It can lower the risk of flashover occurrence. This is an important factor for safety of life.

8. REFERENCES.

1. Gilman, J.W., Kashiwagi, T., Morgan, A.B., Harris, R.H., Brassell, L., Jackson, C.L. and VanLandingham, M., "Flammability of Polymer Clay Nanocomposites Consortium: Year One Annual Report." *National Institute of Standards and Technology*: Gaithersburg, MD, 2000.

2. Hopkins, D. and Quintiere, James G., "Material Fire Properties and Predictions for Thermoplastics," *Fire Safety Journal*, 1996. 26(3): p. 241-268.

3. Giannelis, Emmanuel P., "Polymer Layered Silicate Nanocomposites," *Advanced Materials*, 1996.

4. Dillon, S.E., Kim, W.H., and Quintiere, J.G., "Determination of Properties and the Prediction of the Energy Release Rate of Materials in the ISO 9705 Room-Corner Test." *National Institute of Standards and Technology*, Gaithersburg, MD, 1998.

5. Kashiwagi, T., Harris, R. H., Zhang, X., Briber, R.M., Cipreiano, B.H., Raghavan, S.R., Awad, W.H., Shields, J.R., "Flame Retardant Mechanism of Polyamide 6-Clay Nanocomposites," *Polymer*, 2004.

6. Margenau, Henry and Murphy, George Moseley, *The Mathematics of Physics and Chemistry*, ed. S. Edition.

7. Janssens, Marc, "Calorimetry," in *SFPE Handbook of Fire Protection Engineering*.

8. Jannssens, Marc and Parker, William J., "Oxygen Consumption Calorimetry," in *Heat Release in Fires*, Grayson, V.B.a.S.J., editor, Elsevier Applied Science, London, New York.

9. Quintiere, James G., *Fundamentals of Fire Phenomena*, 2002.

10. ASTME1354-90, "Standard Test Method for Heat and Visible Smoke Release Rates for Materials and Products Using and Oxygen Consumption Calorimeter," in *Annual Book of ASTM Standards*, A.S.f.T.a. Materials, Editor, Philadelphia, 1990, pp. 803-817.

11. Spearpoint, M.J. and Quintiere, J.G., "Predicting the Piloted Ignition of Wood in the Cone Calorimeter Using an Integral Model—Effect of Species, Grain Orientation and Heat Flux," *Fire Safety Journal*, 36 (2001), 2000, pp. 391-415.

12. Kashiwagi, Takashi, Private Communication, "TGA Data for Nylon and Nylon +5% Clay With a Series of Constant Heating Rates," 2004.

13. Boonmee, Nathasak, "Theoretical and Experimental Study of Autoignition of Wood," in *Fire Protection Engineering*, University of Maryland, College Park, 2004, p. 88.

14. Spearpoint, M.J. and Quintiere, J.G., "Predicting the Burning of Wood Using an Integral Model," *Combustion and Flame*, 123, 2000, pp. 308-324.

15. Staggs, J.E.J., "A Theory for Quasi-Steady Single-Step Thermal Degradation of Polymers." *Fire and Materials*, 22, 1998, pp. 109-118.

16. Rhodes, B.T. and Quintiere, James G., "Burning Rate and Flame Heat Flux for PMMA in a Cone Calorimeter," *Fire Safety Journal*, 26(3), 1996, pp. 221-240.

APPENDIX A—METHOD FOR MEASURING HEAT RELEASE RATE

Materials are exposed to controlled levels of radiant heating, with or without an external igniter, and the products and responses of these materials can be measured. This oxygen consumption method is used to determine the ignitability, heat release rate, mass loss rate, and the effective heat of combustion of the materials. The rate of heat release is found by measurement of the oxygen consumption as determined from the oxygen concentration and the flow rate in the exhaust product stream. The effective heat of combustion is determined by combining the specimen's mass loss rate and its heat release rate.

In 1917, Thornton showed that, for a large number of organic liquids and gases, a more or less constant net amount of heat is released per unit mass of oxygen consumed for complete combustion. Thornton's rule implies that it is sufficient to measure the oxygen consumed in a combustion system in order to determine the net heat released [A-1].

In the literature, such as ASTM E1354-99 and section 3/chapter 2 of the SFPE Handbook, the heat release equation based on oxygen consumption method is given:

$$\dot{Q} = \Delta h_{O_2} \left[\frac{\phi}{1 + \phi(\alpha - 1)} \right] \dot{m}_e \frac{M_{O_2}}{M_a} X^0_{O_2} (1 - X^0_{H_2O} - X^0_{CO_2}) \qquad \text{(A-1)}$$

with

$$\phi = \frac{X^0_{O_2} - X_{O_2}}{(1 - X_{O_2}) X^0_{O_2}}$$

where

ϕ = oxygen depletion factor
α = volumetric expansion factor

These sources give the heat release equation with an average value for the expansion factor ($\alpha = 1.105$).

In the analysis below, the same oxygen consumption measurement method was used to determine the heat release rate equation but with a different analysis procedure. By comparing this heat release equation with equation A-1 shown in the ASTM E1354-99 standard demonstrates how the expansion factor α varies by material.

In this method (figure A-1), only the O_2 is measured, and all water vapor and CO_2 must be removed from the sample stream before the O_2 can be measured. The water vapor was removed by a cooling unit and a moisture sorbent. The CO_2 was removed by a chemical sorbent. This leads to the assumption that the sample gas consists only of O_2 and N_2. Another assumption was that the CO production is negligible and these assumptions are consistent with the literature.

The heat release rate can be calculated either by fuel consumption or by oxygen consumption.

$$\dot{Q} = \dot{m}_F \Delta h_c = \dot{m}_{O_2,used} \Delta h_{O_2} \tag{A-2}$$

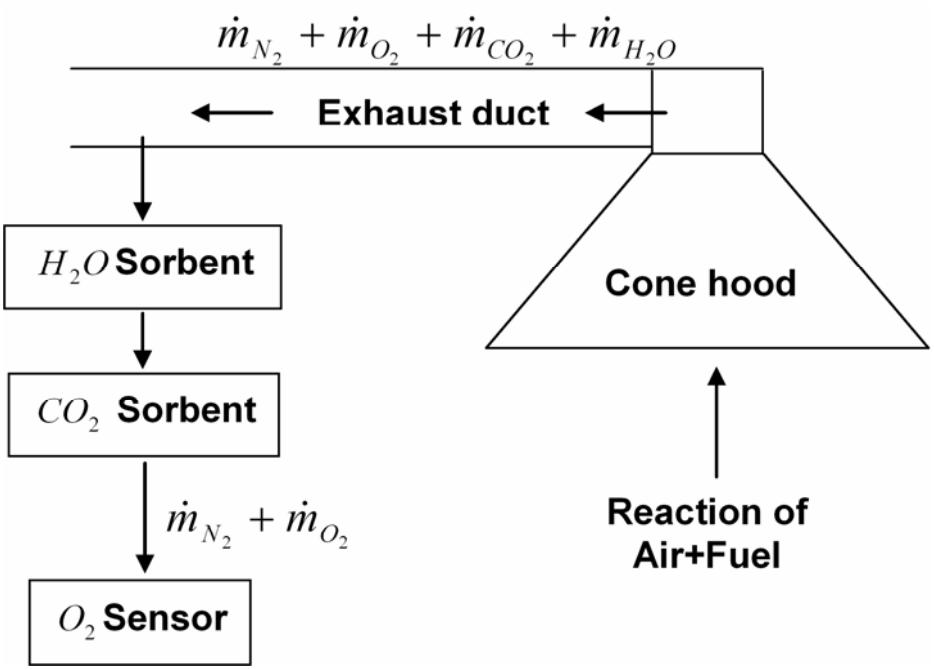

Figure A-1. Equipment Arrangement for O_2 Measurement

Mass conservation:

$$\dot{m}_e = \dot{m}_a + \dot{m}_F$$

where

$\dot{m}_a$ = Mass flow rate of the incoming air (kg/s)
$\dot{m}_F$ = Mass flow rate of the fuel gas (kg/s)
$\dot{m}_e$ = Mass flow rate in the exhaust duct (kg/s)

Oxygen conservation:

$$\dot{m}_{O_2,used} = \dot{m}^0_{O_2} - \dot{m}_{O_2} = \dot{m}_a Y_{O_2,\infty} - \dot{m}_e Y_{O_2}$$
$$= (\dot{m}_e - \dot{m}_F) Y_{O_2,\infty} - \dot{m}_e Y_{O_2} = \dot{m}_e (Y_{O_2,\infty} - Y_{O_2}) - \dot{m}_F Y_{O_2,\infty} \tag{A-3}$$

$\dot{m}^0_{O_2}$ = Mass flow rate of O_2 in the incoming air (kg/s)
$\dot{m}_{O_2}$ = Mass flow rate of O_2 in the exhaust duct (kg/s)

$Y_{O_2,\infty}$ = Measured mass fraction of O_2 in the incoming air
Y_{O_2} = Measured mass fraction of O_2 in the exhaust gases

Chemical equation:

$$\nu_F F + \nu_{O_2} O_2 \rightarrow \nu_{H_2O} H_2O + \nu_{CO_2} CO_2$$

The exhaust gas is a mixture, including CO_2, H_2O, N_2, O_2, etc.

Exhaust gas:

$$\dot{m}_{CO_2} = \dot{m}_e Y_{CO_2} \tag{A-4}$$

$$\dot{m}_{H_2O} = \dot{m}_e Y_{H_2O} \tag{A-5}$$

$\dot{m}_{CO_2}$ = Mass flow rate of CO_2 in the exhaust duct (kg/s)
$\dot{m}_{H_2O}$ = Mass flow rate of H_2O in the exhaust duct (kg/s)
Y_{CO_2} = Measured mass fraction of CO_2 in the exhaust gases
Y_{H_2O} = Measured mass fraction of H_2O in the exhaust gases

CO_2 and water vapor are absorbed before the O_2 in the exhaust gas was measured:

$$\dot{m}_e Y_{O_2} = (\dot{m}_e - \dot{m}_{CO_2} - \dot{m}_{H_2O}) Y'_{O_2} \tag{A-6}$$

Y'_{O_2} is the mass fraction in the oxygen analyzer after the CO_2 and the H_2O were removed from the exhaust gas. The gas going through oxygen analyzer then only consists of O_2 and N_2.

Substitute equations A-4 and A-5 into equation A-6

$$Y_{O_2} = (1 - Y_{CO_2} - Y_{H_2O}) Y'_{O_2} \tag{A-7}$$

For the stoichiometric chemical reaction:

$$\nu_F F + \nu_{O_2} O_2 \rightarrow \nu_{H_2O} H_2O + \nu_{CO_2} CO_2$$

$$\frac{\nu_F}{\nu_{CO_2}} = \frac{\frac{\dot{m}_F}{M_F}}{\frac{\dot{m}_{CO_2}}{M_{CO_2}}} \Rightarrow \dot{m}_{CO_2} = \frac{\nu_{CO_2} M_{CO_2}}{\nu_F M_F} \dot{m}_F \tag{A-8}$$

$$\frac{\nu_F}{\nu_{H_2O}} = \frac{\frac{\dot{m}_F}{M_F}}{\frac{\dot{m}_{H_2O}}{M_{H_2O}}} \Rightarrow \dot{m}_{H_2O} = \frac{\nu_{H_2O} M_{H_2O}}{\nu_F M_F} \dot{m}_F \quad \text{(A-9)}$$

where M is the molecular weight.

Equations A-4 and A-5 show the composition of the exhaust gas:

$$\dot{m}_{CO_2} = \dot{m}_e Y_{CO_2}$$
$$\dot{m}_{H_2O} = \dot{m}_e Y_{H_2O}$$

Consequently, equations A-8 and A-9 become:

$$\dot{m}_{CO_2} = \dot{m}_e Y_{CO_2} = \frac{\nu_{CO_2} M_{CO_2}}{\nu_F M_F} \dot{m}_F \Rightarrow Y_{CO_2} = \frac{(\frac{\nu_{CO_2}}{\nu_F})(\frac{M_{CO_2}}{M_F})}{\dot{m}_e} \dot{m}_F \quad \text{(A-10)}$$

$$\dot{m}_{H_2O} = \dot{m}_e Y_{H_2O} = \frac{\nu_{H_2O} M_{H_2O}}{\nu_F M_F} \dot{m}_F \Rightarrow Y_{H_2O} = \frac{(\frac{\nu_{H_2O}}{\nu_F})(\frac{M_{H_2O}}{M_F})}{\dot{m}_e} \dot{m}_F \quad \text{(A-11)}$$

Combining equations A-2 and A-3

$$\dot{Q} = [\dot{m}_e (Y_{O_2,\infty} - Y_{O_2}) - \dot{m}_F Y_{O_2,\infty}] \Delta h_{O_2}$$

$$\dot{Q} = [\dot{m}_e Y_{O_2,\infty} - \dot{m}_e (1 - Y_{CO_2} - Y_{H_2O}) Y'_{O_2} - \dot{m}_F Y_{O_2,\infty}] \Delta h_{O_2}$$

$$= [\dot{m}_e (Y_{O_2,\infty} - Y'_{O_2}) + \dot{m}_e Y_{CO_2} Y'_{O_2} + \dot{m}_e Y_{H_2O} Y'_{O_2} - \dot{m}_F Y_{O_2,\infty}] \Delta h_{O_2}$$

$$\dot{Q} = [\dot{m}_e (Y_{O_2,\infty} - Y'_{O_2}) + (\frac{\nu_{CO_2}}{\nu_F})(\frac{M_{CO_2}}{M_F}) \dot{m}_F Y'_{O_2} + (\frac{\nu_{H_2O}}{\nu_F})(\frac{M_{H_2O}}{M_F}) \dot{m}_F Y'_{O_2} - \dot{m}_F Y_{O_2,\infty}] \Delta h_{O_2} \quad \text{(A-12)}$$

The stoichiometric ratio is defined as:

$$r_{CO_2} = \frac{m_{CO_2}}{m_F} = \frac{\nu_{CO_2}}{\nu_F} \frac{M_{CO_2}}{M_F} \quad \text{(A-13)}$$

$$r_{H_2O} = \frac{m_{H_2O}}{m_F} = \frac{\nu_{H_2O}}{\nu_F} \frac{M_{H_2O}}{M_F} \quad \text{(A-14)}$$

$$\Delta h_{O_2} = \frac{\Delta h_c}{r_{O_2}} \tag{A-15}$$

Substitute equations A-13, A-14, and A-15 into A-12, and the heat release equation becomes:

$$\dot{Q} = [\dot{m}_e (Y_{O_2,\infty} - Y'_{O_2}) + (r_{CO_2} + r_{H_2O})\dot{m}_F Y'_{O_2} - \dot{m}_F Y_{O_2,\infty}] \frac{\Delta h_c}{r_{O_2}}$$

All of the mass fractions (Y) are converted to mole fractions in the heat release equation because the oxygen sensor can only output the mole fraction of oxygen.

$$Y_{O_2,\infty} = \frac{X^0_{O_2}}{M_a} \qquad\qquad Y'_{O_2} = \frac{X_{O_2}}{M_e}$$

$X^0_{O_2}$ Measured mole fraction of O_2 in the incoming air

X_{O_2} Measured mole fraction of O_2 in the exhaust gases

$$\dot{Q} = \dot{m}_e \left(\frac{X^0_{O_2}}{M_a} - \frac{X_{O_2}}{M_e}\right) M_{O_2} \frac{\Delta h_c}{r_{O_2}} + \dot{m}_F (r_{CO_2} + r_{H_2O}) \frac{X_{O_2} M_{O_2}}{M_e} \frac{\Delta h_c}{r_{O_2}} - \dot{m}_F Y_{O_2,\infty} \frac{\Delta h_c}{r_{O_2}} \tag{A-16}$$

Because $\dot{m}_F \Delta h_c = \dot{Q}$, with the assumption $M_e \approx M_a$, equation A-16 becomes:

$$\dot{Q} = \frac{\Delta h_c}{r_{O_2}} \dot{m}_e \left(\frac{M_{O_2}}{M_a}\right)(X^0_{O_2} - X_{O_2}) + \dot{Q} \frac{r_{CO_2} + r_{H_2O}}{r_{O_2}} \left(\frac{M_{O_2}}{M_a}\right) X_{O_2} - \dot{Q} \frac{Y_{O_2,\infty}}{r_{O_2}}$$

$$\Downarrow$$

$$\dot{Q}\left[1 - \frac{r_{CO_2} + r_{H_2O}}{r_{O_2}} \left(\frac{M_{O_2}}{M_a}\right) X_{O_2} + \frac{Y_{O_2,\infty}}{r_{O_2}}\right] = \frac{\Delta h_c}{r_{O_2}} \dot{m}_e \left(\frac{M_{O_2}}{M_a}\right)(X^0_{O_2} - X_{O_2})$$

$$\Downarrow$$

$$\dot{Q} = \frac{\Delta h_c}{r_{O_2}} \dot{m}_e \left(\frac{M_{O_2}}{M_a}\right) \frac{X^0_{O_2} - X_{O_2}}{1 + \frac{Y_{O_2,\infty}}{r_{O_2}} - \frac{r_{CO_2} + r_{H_2O}}{r_{O_2}} \left(\frac{M_{O_2}}{M_a}\right) X_{O_2}} \tag{A-17}$$

In the heat release rate (equation A-17), for a given fuel, the molecular weights and stoichiometric ratios are known. The mole fraction of O_2 in the incoming air $X^0_{O_2}$ and the mole

fraction of O_2 in the exhaust gases X_{O_2} can be measured by the oxygen sensor. The only unknown is the mass flow rate in the exhaust duct $\dot{m}_e$.

A.1 FLOW-RATE MEASUREMENTS.

The exhaust mass flow rate can be measured via the pressure drop across and temperature at an orifice plate in the exhaust duct.

$$\dot{m}_e = C\sqrt{\frac{\Delta P}{T_e}} \tag{A-18}$$

where

$\dot{m}_e =$ Mass flow rate in the exhaust duct ($kg \cdot s^{-1}$)
C = Orifice plate coefficient ($kg^{1/2} \cdot m^{1/2} \cdot K^{1/2}$)
$\Delta p =$ Pressure drop across the orifice plate (Pa)
$T_e =$ Gas temperature at the orifice plate (K)

Substitute equation A-18 into equation A-17 and the heat release equation becomes:

$$\dot{Q} = \frac{\Delta h_c}{r_{O_2}}\left(C\sqrt{\frac{\Delta P}{T_e}}\right)\left(\frac{M_{O_2}}{M_a}\right)\frac{X_{O_2}^0 - X_{O_2}}{1+\frac{Y_{O_2,\infty}}{r_{O_2}} - \frac{r_{CO_2}+r_{H_2O}}{r_{O_2}}\left(\frac{M_{O_2}}{M_a}\right)X_{O_2}} \tag{A-19}$$

In ASTM E1354 P836, an average value of expansion factor is used (α=1.105) for equation A-1, and the heat release equation is simplified with $\frac{M_{O_2}}{M_a} \approx 1.10$, $X_{O_2}^0 = 0.21$. The final version of this equation found in ASTM E1354 P836 is:

$$\dot{Q} = \frac{\Delta h_c}{r_{O_2}}\left(C\sqrt{\frac{\Delta p}{T_e}}\right)1.10\frac{X_{O_2}^0 - X_{O_2}}{1.105 - 1.5X_{O_2}} \tag{A-20}$$

In reference [A-1], heat release rate is shown as:

$$\dot{Q} = \Delta h_{O_2}\left[\frac{\phi}{1+\phi(\alpha-1)}\right]\dot{m}_e\frac{M_{O_2}}{M_a}X_{O_2}^0$$

with

$$\phi = \frac{X_{O_2}^0 - X_{O_2}}{(1-X_{O_2})X_{O_2}^0}$$

After simplification of ϕ and $\frac{M_{O_2}}{M_a} \approx 1.10$, the equation becomes:

$$\dot{Q} = \left[\frac{\Delta h_c}{r_{O_2}} \left(C \sqrt{\frac{\Delta p}{T_e}} \right) 1.10 \right] \frac{X_{O_2}^0 - X_{O_2}}{\alpha - \left[1 + \frac{(\alpha - 1)}{X_{O_2}^0} \right] X_{O_2}} \qquad \text{(A-21)}$$

Comparison of equations A-21 and A-20 with equation A-19 shows only the differences in the denominator. From this comparison, the expansion factor can be defined as

$$\alpha = 1 + \frac{Y_{O_2,\infty}}{r_{O_2}}.$$

A.2 CALIBRATION CONSTANT C.

In order to use equations A-19, A-20, or A-21, the calibration constant C must be known. The calibration constant C can be calculated from the heat release equation A-19 based on methane.

$$\frac{M_{O_2}}{M_a} \approx 1.10$$

$$c = \frac{\dot{Q}}{\left(\frac{\Delta h_c}{r_{O_2}}\right)} \sqrt{\frac{T_e}{\Delta P}} \frac{\left(\alpha - 1.10 \frac{r_{CO_2} + r_{H_2O}}{r_{O_2}} X_{O_2} \right)}{1.10 (X_{O_2}^0 - X_{O_2})}$$

For methane,

$$\frac{\Delta h_c}{r_{O_2}} = 12.54 \times 10^3 \, kW / kgO_2$$

$$\frac{r_{CO_2} + r_{H_2O}}{r_{O_2}} = 1.25$$

$$\alpha = 1 + \frac{Y_{O_2,\infty}}{r_{O_2}} = 1 + \frac{0.233}{4} = 1.05825$$

The specification $\dot{Q} = 5.0$ is then made, based on ASTM E1354, where 5.0 corresponds to 5.0 kW methane supplied.

$$c = \frac{5.0}{12.54 \times 10^3} \sqrt{\frac{T_e}{\Delta P}} \frac{1.05825 - 1.375 X_{O_2}}{1.10(X_{O_2}^0 - X_{O_2})}$$

ASTM E1354 also suggests that the methane calibration be performed daily in order to check for the proper operation of the instrument and to compensate for minor changes in mass flow determination.

A.3 PROOF OF THE DEFINITION FOR THE EXPANSION FACTOR α.

To get the definition of the expansion factor α, a stoichiometric chemical reaction was used in the above analysis to get the heat release rate equation. To prove the validity of the definition of expansion factor α, the same oxygen consumption method was used. Instead of the analysis of the stoichiometric chemical reaction, the heat release rate equation was found from the conservation of mass. The definition of α was also used in the analysis. If the final heat release equation appears the same as equation 20 in ASTM E1354 P836 or equation 21 in reference A-1, then the definition for the expansion factor α given above is reasonable.

Start with the oxygen consumption method. Changes in the oxygen concentration found in the combustion gases can be used to determine the heat release rate

$$\dot{Q} = \Delta h_{O_2} \dot{m}_{O_2,used} = \Delta h_{O_2} (\dot{m}_{O_2}^0 - \dot{m}_{O_2})$$

Only O_2 is measured. All water vapor and CO_2 must be removed from the sample stream before this measurement is taken. The sample gas only consists of O_2 and N_2.

Before combustion:

$$X_{O_2}^0 = \frac{\frac{\dot{m}_{O_2}^0}{M_{O_2}}}{\frac{\dot{m}_{O_2}^0}{M_{O_2}} + \frac{\dot{m}_{N_2}^0}{M_{N_2}}}, \qquad \text{(A-22)}$$

$X_{O_2}^0$ = Initial reading from the oxygen analyzer before combustion

$\dot{m}_{O_2}^0$ = Mass flow rate of O_2 in the incoming air (kg/s)

$\dot{m}_{N_2}^0$ = Mass flow rate of the N_2 in the incoming air (kg/s)

After combustion:

$$X_{O_2} = \frac{\frac{\dot{m}_{O_2}}{M_{O_2}}}{\frac{\dot{m}_{O_2}}{M_{O_2}} + \frac{\dot{m}_{N_2}}{M_{N_2}}}, \tag{A-23}$$

X_{O_2} = Reading during the test from the oxygen analyzer.

$\dot{m}_{O_2}$ = Mass flow rate of the O_2 in the exhaust duct (kg/s)

$\dot{m}_{N_2}$ = Mass flow rate of the N_2 in the exhaust duct (kg/s)

As N_2 is conserved and does not participate in the combustion reactions, $\dot{m}^0_{N_2}$ is equal to $\dot{m}_{N_2}$. Rearranging equations A-22 and A-23 while subtracting equation A-23 from equation A-22 leads to:

$$\dot{m}^0_{O_2} - \dot{m}_{O_2} = \left[\frac{X^0_{O_2} - X_{O_2}}{\left(1 - X^0_{O_2}\right)\left(1 - X_{O_2}\right)}\right]\dot{m}_{N_2}\frac{M_{O_2}}{M_{N_2}} \tag{A-24}$$

Because all water vapor and CO_2 has been removed from the sample stream before O_2 is measured, the component of the sample gas (in terms of mole fraction) before combustion becomes:

$$X^0_{N_2} + X^0_{O_2}$$

$$X^0_{N_2} + X^0_{O_2} = \left(\frac{\dot{m}_a}{M_a}\right)\left(1 - X^0_{H_2O} - X^0_{CO_2}\right) = \frac{\frac{\dot{m}_{N_2}}{M_{N_2}}}{\left(1 - X^0_{O_2}\right)} \tag{A-25}$$

$\dot{m}_a$ = Mass flow rate of the incoming air (kg/s)

$X^0_{O_2}$ = Mole fraction of O_2 in the incoming air

$X^0_{H_2O}$ = Mole fraction of H_2O in the incoming air

$X^0_{CO_2}$ = Mole fraction of CO_2 in the incoming air

Combining the right-hand sides of equations A-24 and A-25 to cancel the $\frac{\frac{\dot{m}_{N_2}}{M_{N_2}}}{\left(1 - X^0_{O_2}\right)}$ term, transforms equation A-24 into the following:

$$\dot{m}_{O_2}^0 - \dot{m}_{O_2} = \left[\frac{X_{O_2}^0 - X_{O_2}}{\left(1 - X_{O_2}\right)} \right] \dot{m}_a \frac{M_{O_2}}{M_a} (1 - X_{H_2O}^0 - X_{CO_2}^0) \tag{A-26}$$

According to the oxygen consumption principle, combining with equation A-26, the heat release rate then becomes:

$$\dot{Q} = \Delta h_{O_2} \dot{m}_{O_2,used} = \Delta h_{O_2} (\dot{m}_{O_2}^0 - \dot{m}_{O_2}) = \Delta h_{O_2} \left[\frac{X_{O_2}^0 - X_{O_2}}{\left(1 - X_{O_2}\right)} \right] \dot{m}_a \frac{M_{O_2}}{M_a} (1 - X_{H_2O}^0 - X_{CO_2}^0) \tag{A-27}$$

The mole fractions of H_2O ($X_{H_2O}^0$) and of CO_2 ($X_{CO_2}^0$) in the incoming air are both negligible.

The heat release rate equation is then shown as:

$$\dot{Q} = \Delta h_{O_2} \left[\frac{X_{O_2}^0 - X_{O_2}}{\left(1 - X_{O_2}\right)} \right] \dot{m}_a \frac{M_{O_2}}{M_a} \tag{A-28}$$

The oxygen depletion factor ϕ is defined as in reference A-1:

$$\phi = \frac{\dot{m}_{O_2}^0 - \dot{m}_{O_2}}{\dot{m}_{O_2}^0} = \frac{X_{O_2}^0 - X_{O_2}}{(1 - X_{O_2}) X_{O_2}^0}$$

An assumption is required regarding the expansion due to combustion of the fraction of the air that is fully depleted of its oxygen (See ASTM E1354 Page 838 and "Heat Release in Fires," Chapter 3). This expansion depends on the composition of the fuel and the actual stoichiometry of the combustion.

The expansion factor is defined as $\alpha = 1 + \frac{Y_{O_2,\infty}}{r_{O_2}}$ (As gained from former analysis).

For the stoichiometric reaction, the stoichiometric ratio is:

$$r_{O_2} = \frac{m_{O_2}}{m_F} = \frac{\dot{m}_{O_2,used}}{\dot{m}_F}$$

Substituting r_{O_2} into α

$$\alpha = 1 + \frac{Y_{O_2,\infty} \dot{m}_F}{\dot{m}_{O_2,used}} = 1 + \frac{Y_{O_2,\infty} \dot{m}_F}{\dot{m}_{O_2}^0 - \dot{m}_{O_2}} = \frac{\dot{m}_{O_2}^0 + Y_{O_2,\infty} \dot{m}_F - \dot{m}_{O_2}}{\dot{m}_{O_2}^0 - \dot{m}_{O_2}}$$

Mass conservation:

$$\dot{m}_e = \dot{m}_a + \dot{m}_F$$

$$\dot{m}^0_{O_2} = \dot{m}_a Y_{O_2,\infty}$$

$$\alpha = \frac{\dot{m}_a Y_{O_2,\infty} + Y_{O_2,\infty}\dot{m}_F - \dot{m}_{O_2}}{\dot{m}^0_{O_2} - \dot{m}_{O_2}} = \frac{Y_{O_2,\infty}(\dot{m}_a + \dot{m}_F) - \dot{m}_{O_2}}{\dot{m}^0_{O_2} - \dot{m}_{O_2}} = \frac{Y_{O_2,\infty}\dot{m}_e - \dot{m}_{O_2}}{\dot{m}^0_{O_2} - \dot{m}_{O_2}}$$

$$\alpha - 1 = \frac{Y_{O_2,\infty}\dot{m}_e - \dot{m}_{O_2}}{\dot{m}^0_{O_2} - \dot{m}_{O_2}} - 1 = \frac{Y_{O_2,\infty}\dot{m}_e - \dot{m}^0_{O_2}}{\dot{m}^0_{O_2} - \dot{m}_{O_2}} \tag{A-29}$$

Multiplying each side of equation A-29 by $\frac{\dot{m}^0_{O_2} - \dot{m}_{O_2}}{\dot{m}^0_{O_2}}$ and substituting $\dot{m}^0_{O_2} = \dot{m}_a Y_{O_2,\infty}$

$$(\alpha - 1)\frac{\dot{m}^0_{O_2} - \dot{m}_{O_2}}{\dot{m}^0_{O_2}} = \frac{Y_{O_2,\infty}\dot{m}_e - \dot{m}^0_{O_2}}{\dot{m}^0_{O_2}} = \frac{Y_{O_2,\infty}\dot{m}_e - \dot{m}_a Y_{O_2,\infty}}{\dot{m}_a Y_{O_2,\infty}} \tag{A-30}$$

Canceling $Y_{O_2,\infty}$ from the right-hand side of equation A-30:

$$(\alpha - 1)\frac{\dot{m}^0_{O_2} - \dot{m}_{O_2}}{\dot{m}^0_{O_2}} = \frac{\dot{m}_e - \dot{m}_a}{\dot{m}_a} \tag{A-31}$$

Substituting $\phi = \frac{\dot{m}^0_{O_2} - \dot{m}_{O_2}}{\dot{m}^0_{O_2}}$ into equation A-31

$$(\alpha - 1)\dot{m}_a\phi = \dot{m}_e - \dot{m}_a \tag{A-32}$$

Rearranging equation A-32

$$\dot{m}_a = \frac{\dot{m}_e}{1 + (\alpha - 1)\phi} \tag{A-33}$$

This relationship between $\dot{m}_a$ and $\dot{m}_e$ is important, because the mass flow rate of the incoming air cannot be measured; however, the exhaust flow rate in the exhaust duct can be measured.

Substituting equation A-33 into equation A-28

$$\dot{Q} = \Delta h_{O_2} \left[\frac{\phi}{1+\phi(\alpha-1)} \right] \dot{m}_e \frac{M_{O_2}}{M_a} X_{O_2}^0 \tag{A-34}$$

Substituting the measured mass flow rate $\dot{m}_e = C\sqrt{\frac{\Delta p}{T_e}}$ into equation A-34

The heat release rate equation becomes:

$$\dot{Q} = \Delta h_{O_2} \left[\frac{\phi}{1+\phi(\alpha-1)} \right] \left(C\sqrt{\frac{\Delta p}{T_e}} \right) \frac{M_{O_2}}{M_a} X_{O_2}^0 \tag{A-35}$$

For the stoichiometric reaction, $\Delta h_{O_2} = \frac{\Delta h_c}{r_{O_2}}$

Rearranging equation A-35 with $\phi = \frac{X_{O_2}^0 - X_{O_2}}{(1-X_{O_2})X_{O_2}^0}$

$$\dot{Q} = \left[\frac{\Delta h_c}{r_{O_2}} \left(C\sqrt{\frac{\Delta p}{T_e}} \right) \frac{M_{O_2}}{M_a} \right] \frac{\phi X_{O_2}^0}{1+\phi(\alpha-1)}$$

$$= \left[\frac{\Delta h_c}{r_{O_2}} \left(C\sqrt{\frac{\Delta p}{T_e}} \right) \frac{M_{O_2}}{M_a} \right] \frac{\dfrac{X_{O_2}^0 - X_{O_2}}{1-X_{O_2}}}{1+\dfrac{X_{O_2}^0 - X_{O_2}}{(1-X_{O_2})X_{O_2}^0}(\alpha-1)}$$

$$= \left[\frac{\Delta h_c}{r_{O_2}} \left(C\sqrt{\frac{\Delta p}{T_e}} \right) \frac{M_{O_2}}{M_a} \right] \frac{X_{O_2}^0 - X_{O_2}}{1-X_{O_2}+(1-\dfrac{X_{O_2}}{X_{O_2}^0})(\alpha-1)}$$

$$\Downarrow$$

$$\dot{Q} = \left[\frac{\Delta h_c}{r_{O_2}} \left(C\sqrt{\frac{\Delta p}{T_e}} \right) \frac{M_{O_2}}{M_a} \right] \frac{X_{O_2}^0 - X_{O_2}}{\alpha - \left[1+\dfrac{(\alpha-1)}{X_{O_2}^0} \right] X_{O_2}} \tag{A-36}$$

In ASTM E 1354, page 836, an average value of α=1.105 is used.

With $\frac{M_{O_2}}{M_a} \approx 1.10$, $X^0_{O_2} = 0.21$, equation A-36 becomes

$$\dot{Q} = \frac{\Delta h_c}{r_{O_2}} \left(C \sqrt{\frac{\Delta p}{T_e}} \right) 1.10 \frac{X^0_{O_2} - X_{O_2}}{1.105 - 1.5 X_{O_2}}$$

This form is identical to the equation found on ASTM E 1354, page 836.

In conclusion, the definition for the expansion factor $\alpha = 1 + \frac{Y_{O_2,\infty}}{r_{O_2}}$ is reasonable.

In table A-1, values of α and $1 + \frac{(\alpha - 1)}{X^0_{O_2}}$ are listed for different fuels. These values come from equation A-19 with the stoichiometric ratios.

$$\alpha = 1 + \frac{Y_{O_2,\infty}}{r_{O_2}}$$

$$1 + \frac{(\alpha - 1)}{X^0_{O_2}} = \frac{r_{CO_2} + r_{H_2O}}{r_{O_2}} \left(\frac{M_{O_2}}{M_a} \right)$$

Table A-1. Coefficient for Different Fuel

Fuel	Formula	α	$1+\frac{(\alpha-1)}{X_{O_2}^0}$
Normal Alkanes			
Methane	CH4	1.05825	1.375
Ethane	C2H6	1.062411	1.394643
Propane	C3H8	1.064075	1.4025
Butane	C4H10	1.064971	1.406731
Pentane	C5H12	1.065531	1.409375
Hexane	C6H14	1.065914	1.411184
Heptane	C7H16	1.066193	1.4125
Octane	C8H18	1.066405	1.4135
Nonane	C9H20	1.066571	1.414286
Decane	C10H22	1.066706	1.414919
Undecane	C11H24	1.066816	1.415441
Dodecane	C12H26	1.066909	1.415878
Tridecane	C13H28	1.066988	1.41625
Kerosene	C14H30	1.067055	1.41657
Hexadecane	C16H34	1.067166	1.417092
AVG		1.065464	1.409058
Normal Alkenes			
Ethylene	C_2H_4	1.06793	1.4207
Propylene	C_3H_6	1.06793	1.4207
Butylene	C_4H_8	1.06793	1.4207
Pentene	C_5H_{10}	1.06793	1.4207
Hexene	C6H12	1.06793	1.4207
Heptane	C7H14	1.06793	1.4207
Octene	C8H16	1.06793	1.4207
Nonene	C9H18	1.06793	1.4207
Decene	C10H20	1.06793	1.4207
Dodecene	C12H24	1.06793	1.4207
Tridecene	C13H26	1.06793	1.4207
Tetradecene	C14H28	1.06793	1.4207
Hexadecene	C16H32	1.06793	1.4207
Octadecene	C18H36	1.06793	1.4207
AVG		1.06793	1.4207

Table A-1. Coefficient for Different Fuel (Continued)

Fuel	Formula	α	$1+\frac{(\alpha-1)}{X_{O_2}^0}$
Normal Alkynes			
Acetylene	C2H2	1.075725	1.4575
Heptyne	C7H12	1.0699	1.43
Octyne	C8H14	1.069647	1.428804
Decyne	C10H18	1.069297	1.427155
Dodecyne	C12H22	1.069068	1.426071
AVG		1.070727	1.433906
Arenes			
Benzene	C6H6	1.075725	1.4575
Toluene	C7H8	1.074431	1.451389
Ethylbenzene	C8H10	1.073506	1.447024
Xylene	C8H10	1.073506	1.447024
Propylbenzene	C9H12	1.072813	1.44375
Trimethylbenzene	C9H12	1.072813	1.44375
Cumene	C9H12	1.072813	1.44375
Butylbenzene	C10H14	1.072273	1.441204
Diethylbenzene	C10H14	1.072273	1.441204
p-Cymene	C10H14	1.072273	1.441204
Pentylbenzene	C11H16	1.071842	1.439167
Triethylbenzene	C12H18	1.071489	1.4375
AVG		1.07298	1.444539
Polycarbonate	CH0.88O0.19	1.103097	1.586726
Polypropylene	CH	1.075649	1.453571
Polyvinylchloride	CH1.5Cl0.50	1.302597	1.411429
Nylon	CH1.8O0.17N0.17	1.119487	1.528718
GM21	CH1.8O0.30N0.05	1.113659	1.60439
Polyethylene	CH2	1.06793	1.4207

A.2 REFERENCES.

A-1. Jannssens, Marc and Parker, William J., "Oxygen Consumption Calorimetry," in *Heat Release in Fires*, Grayson, V.B.a.S.J., editor, Elsevier Applied Science, London, New York.

APPENDIX B—CONVECTIVE HEAT TRANSFER COEFFICIENT OF THE CONE CALORIMETER

B-1. THEORETICAL VALUE.

B.1.1 COMBINED NATURAL AND FORCED CONVECTION.

Figure B-1 shows the configuration using a Cil-plate to measure the heat transfer coefficient in the cone. For such cases, an external flow is superposed on the buoyancy-driven flow, and there exists a well-defined forced convection velocity. Generally, the combined effects of natural and forced convection must be considered when $(Gr_L / Re_L^2) \approx 1$. If the inequality $(Gr_L / Re_L^2) << 1$ is satisfied, natural convection effects may be neglected and $Nu_L = f(Re_L, \Pr)$. Conversely, if $(Gr_L / Re_L^2) >> 1$, forced convection effects may be neglected and $Nu_L = f(Gr_L, \Pr)$ [B-1].

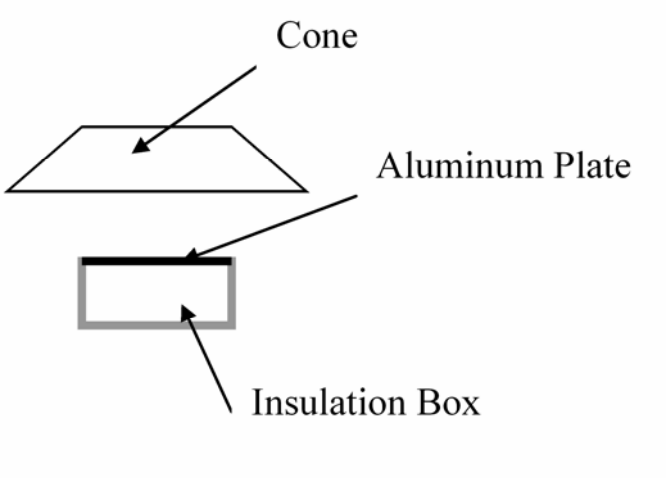

Figure B-1. Sketch of the Experimental Assembly

B.1.2 PROPERTIES.

Air:

$$T_S = 500^\circ\text{C}\quad T_\infty = 26^\circ\text{C}\qquad T = \frac{T_S + T_\infty}{2} = 263^\circ\text{C} = 536\ K$$

Air properties @ 550 K

$$\rho = 0.6329\ \text{kg/m}^2 \qquad \nu = 45.57 \times 10^{-6}\ \text{m}^2/\text{s}$$
$$\Pr = 0.683 \qquad k = 43.9 \times 10^{-3}\ \text{w/mK}$$

Aluminum Plate:

$$L = 7.7\ \text{cm}$$
$$Area = 7.7\ \text{cm} \times 7.7\ \text{cm}$$

$Mass = 7.4\ g$

Exhaust duct

Diameter = 0.1106 m

B.1.3 ANALYSIS.

Grashof Number:

$$Gr = \frac{g\beta(T - T_\infty)L^3}{\nu^2} = \frac{9.8\times(7.7\times10^{-2})^3(T - T_\infty)}{(45.57\times10^{-6})^2 T_\infty} = 2.154\times10^6 \frac{T - T_\infty}{T_\infty}$$

U_∞ air flow velocity

Air flow rate is not easily measured, however, use of the conservation of mass allows for a much more tangible measurement of the mass flow rate in the exhaust duct of the cone $\dot{m}_e$ to suffice.

Mass conservation:

$$\dot{m}_e = \rho A_{duct} U_{duct} = \rho A_{test} U_\infty$$

$\dot{m}_e$ = Mass flow rate in the exhaust duct (kg/s)

A_{duct} = Cross sectional area of exhaust duct

U_{duct} = Flow rate in the exhaust duct (m/s)

A_{test} = Bottom area of the small test compartment of the cone. Air comes into the small compartment vertically through the bottom.

A_{test} = 23 in. × 17 in. = (23×2.54) cm × (17×2.54) cm=0.252m^2

U_∞ = Air flow velocity around the plate

From the mass conservation equation, air flow velocity can be calculated as:

$$U_\infty = \frac{\dot{m}_e}{\rho A_{test}}$$

Reynold's Number

$$Re = \frac{U_\infty L}{\nu}$$

Nusselt Number

$$Nu_L = \frac{h_c L}{k}$$

Since both natural and forced convection exist (figure B-2), (natural convection due to buoyancy and forced convection due to the exhaust fan) both will effect the convection condition.

Natural Convection

For the hot upper surface case [B-2].

$Nu_L = 0.54 Ra_L^{1/4}$ $\quad (10^5 \le Ra_L \le 10^7)$

$Nu_L = 0.15 Ra_L^{1/3}$ $\quad (10^7 \le Ra_L \le 10^{10})$

$Ra = Gr \Pr$

Forced Convection

Normal flat plate [B-3].

$Nu_L = 0.20 Re^{2/3}{}_L$

Combined Natural and Forced Convection [B-4]

$$Nu^n_{combined} = Nu^n_{natural} + Nu^n_{forced}$$

+ sign applies when the flows are in the same direction.

n = 7/2 may be better suited for transverse flows involving horizontal plates.

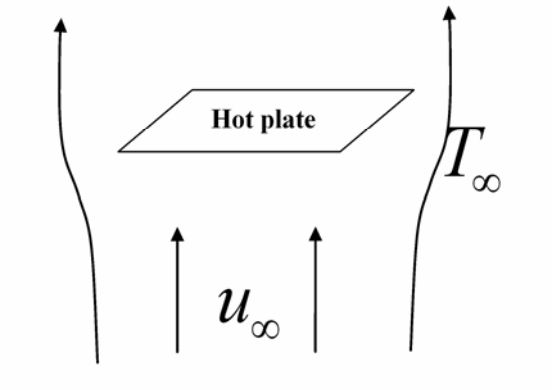

Figure B-2. Natural and Forced Convection

With this combined Nusselt Number, the combined convective heat transfer coefficient can be calculated:

$$h_c = \frac{Nu \cdot k}{L}$$

h_c versus $T_s - T_{amb}$ is plotted on log-log scale in figure B-3.

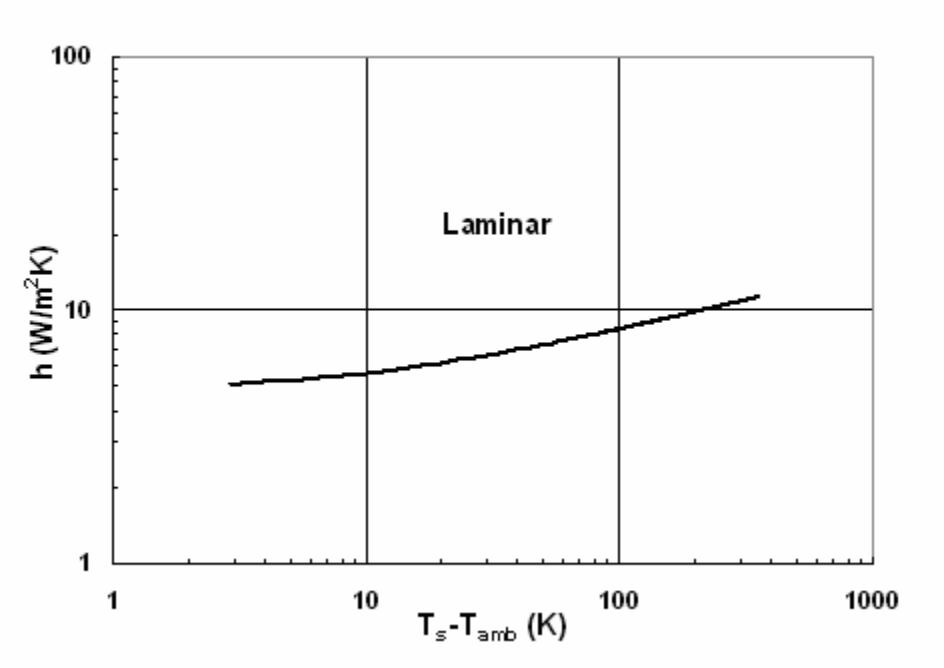

Figure B-3. Theoretical Convective Heat Transfer Coefficient With Exhaust Speed $\dot{m}_e = 25 g/s$

B.2 EXPERIMENTAL APPROACH.

B.2.1 EXPERIMENTAL SETUP.

A $7.7\,\text{cm} \times 7.7\,\text{cm}$ thin, aluminum plate was used in the experiment. Soot was added on the surface by a candle flame to increase the surface absorptivity. The opposite side of the plate was insulated by 4 layers of Kaowool blanket to minimize heat loss effects. A small box was made of thin Kaowool board to hold the aluminum plate and Kaowool blanket. Three thermocouples were used in the experiments. Two of them are shown in figure B-4. One thermocouple was welded on the back face of the aluminum plate to measure the aluminum temperature. Another thermocouple was inserted into the middle of the Kaowool blanket layers to measure the heat loss. The third thermocouple was used to measure the temperature in the small compartment of the cone (figure B-1). The experimental procedure consisted of exposing a sample in the horizontal orientation to a constant external irradiance from the cone heater.

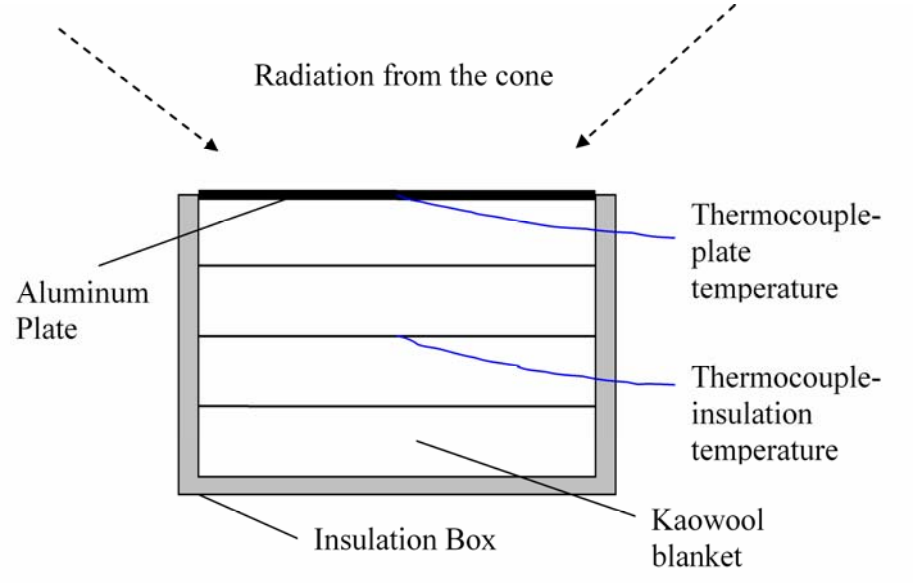

Figure B-4. Experimental Setup of Convective Heat Transfer Coefficient

Data from National Instruments LabVIEW:

Time (sec), ambient temperature (ºC), insulation temperature (ºC), and aluminum surface temperature (ºC).

B.2.2 DATA ANALYSIS.

Energy Conservation

Considering the conductive heat loss from the back side (insulation) of the aluminum plate

$$m'' c \frac{dT}{dt} = \alpha q''_{ext} - \varepsilon\sigma (T^4 - T_o^4) - h(T - T_\infty) - k \frac{T - T_{insulaion}}{l}$$

T is the temperature of the aluminum plate

T_o in the $\varepsilon\sigma(T^4 - T_o^4)$ term is the room temperature (about 25ºC)

T_∞ in the $h(T - T_\infty)$ term is the temperature around the sample holder in the small compartment of the cone. It is higher than room temperature.

l is the thickness of the insulation

k is the thermal conductivity of the Kaowool (insulation)

α is the absorptivity of the hot surface

ε is the emissivity of the hot surface

Without considering the conductive heat loss from the back side

$$m'' c \frac{dT}{dt} = \alpha q''_{ext} - \varepsilon\sigma(T^4 - T_o^4) - h(T - T_\infty)$$

Heat capacity of aluminum

Heat capacity of aluminum increases as a function of temperature.

$$c_p = -0.0005T^2 + 0.6099T + 884 \text{, } T \text{ in } ^oC$$

Surface absorptivity α

In order to find α, use the energy equation at the beginning, when all the temperatures are nearly the same.

$$\dot{m}'' c_p \frac{dT}{dt} = \alpha \dot{q}''_{ext}$$

$\frac{dT}{dt}$ is the initial slope value read from the time-temperature curve

$$\alpha = \frac{\dot{m}'' c_p \frac{dT}{dt}}{\dot{q}''_{ext}}$$

The average value of α under different external heat flux tests is 0.93.
Assume the surface emissivity is equal to the absorptivity.

Convective heat transfer coefficient

In the energy equations with or without the consideration of back face conduction heat loss, all of the values are known except for *h*. An average value of α=0.93 is used and all temperatures are measured with time by the thermocouples and recorded by the data acquisition program. The derivative is calculated as:

$$\frac{dT}{dt} \approx \frac{\Delta T}{\Delta t} = \frac{T_{i+4} - T_i}{4 \times \text{interval}}$$

Then *h* can be calculated.

Without conduction:

$$m''c\frac{dT}{dt} = \alpha q''_{ext} - \varepsilon\sigma(T^4 - T_o^4) - h(T - T_\infty) - k\frac{T - T_{insulaion}}{l}$$

With conduction:

$$m''c\frac{dT}{dt} = \alpha q''_{ext} - \varepsilon\sigma(T^4 - T_o^4) - h(T - T_\infty)$$

The definition of ambient temperature is of great importance in this analysis. Although it is common practice to define the ambient temperature as the room temperature, when the heater is on, the temperature in the small compartment of the cone is much higher than room temperature. Therefore, this elevated temperature should be used as the real ambient temperature around the heated sample.

In these calculations, the temperature underneath the sample in the compartment is defined as T_∞ when in steady state, which is about 50ºC.

Figure B-5 shows that the conductive heat loss is not small. The curve with conductive heat loss is closer to the theoretical value. The conductive heat loss cannot be neglected. Therefore, all values for the convective coefficient, *h*, were determined based on the consideration of this heat loss.

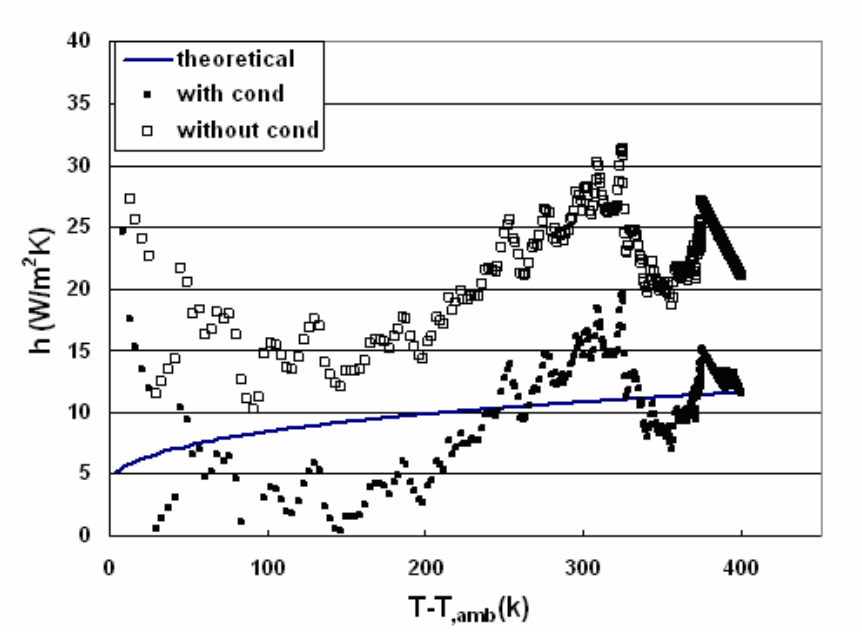

Figure B-5. *h* Versus ΔT 20.5 kW/m^2 External Heat Flux, 25 g/s Exhaust Flow

As shown in figures B-5, B-6, and B-7, the average value of the convective heat transfer coefficient is about 11 W/m^{2}K, which is also close to the theoretical value (shown in figure B-3). In the literature, h = 10 W/m^{2}K is always used as an average value for the cone. This value is indeed very close to the results of this analysis. Therefore, h = 10 W/m^{2}K is used in the analysis in order to maintain consistency between other literature results and this data analysis.

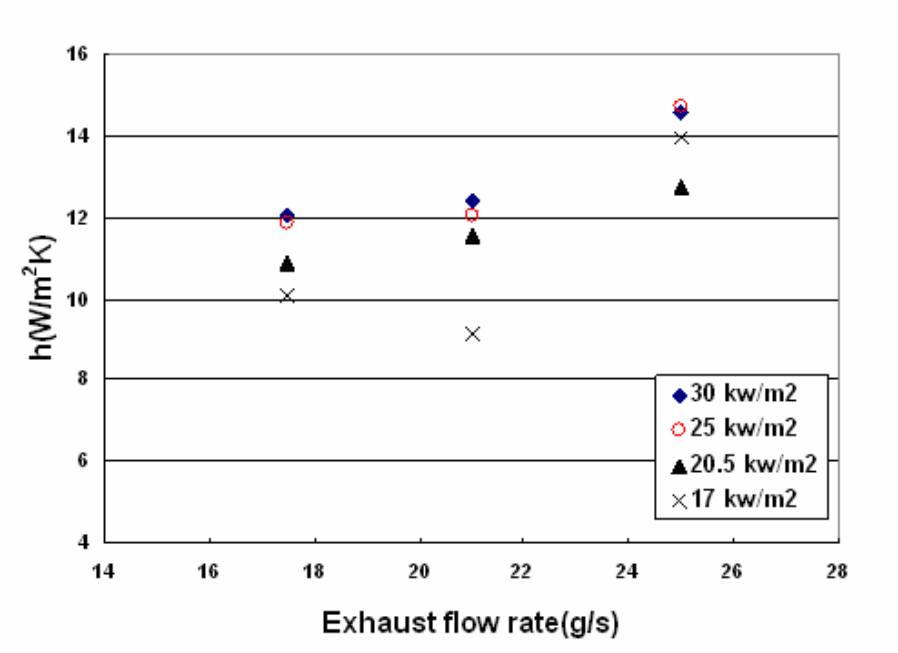

Figure B-6. *h* Versus Exhaust Flow Rate Under Different External Heat Flow

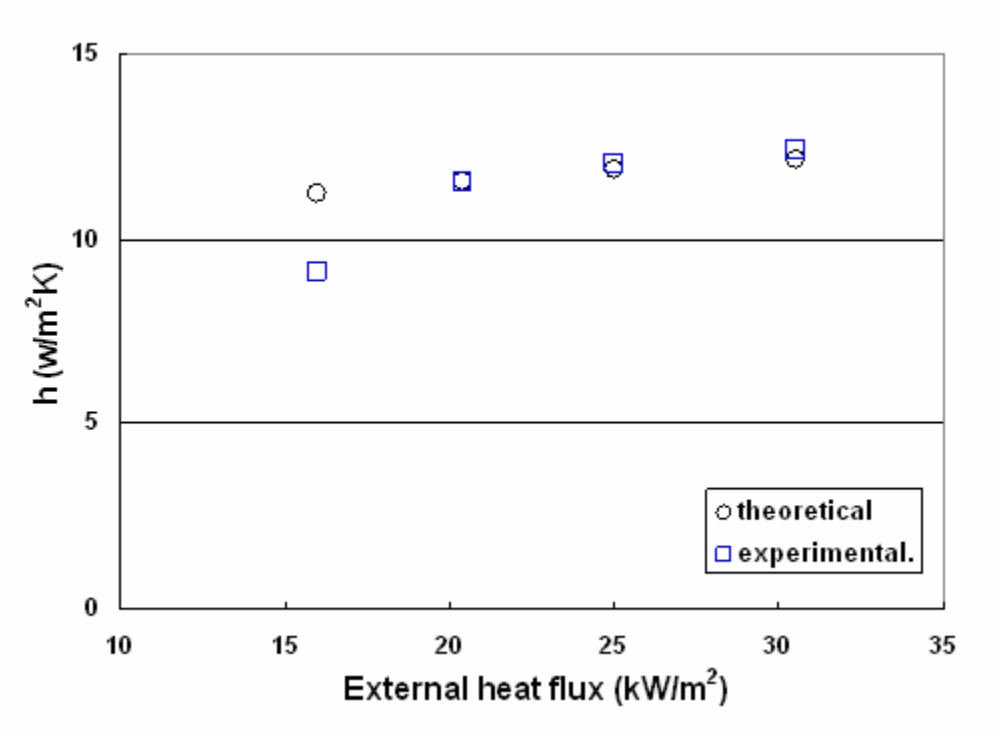

Figure B-7. *h* Versus External Heat Flux Exhaust Flow = 21 g/s

B.3 REFERENCES.

B-1. Incropera, Frank P. and DeWitt, David P., "Fundamentals of Heat and Mass Transfer," October 2006, pp. 487.

B-2. Kreith, Frank and Bohn, Mark S., "Principles of Heat Transfer," January 1991, pp. 314.

B-3. Kreith, Frank and Bohn, Mark S., "Principles of Heat Transfer," January 1991, pp. 439.

B-4. Incropera, Frank P. and DeWitt, David P., "Introduction to Heat Transfer," 1990, pp. 524.

APPENDIX C—FORTRAN PROGRAM FOR KINETIC MODELING

```
      Program Nylon
c     This program aims to solve heat and mass transfer during the decompositoin
c     process of Nylon.
c     The output file is in "dat" format which can be opened by matlab M-file

      implicit none
      integer i,j,npmax,nt_prof
      parameter (npmax = 1600)
      parameter (nt_prof = 100)
      integer nt,npx,itermax,ntmax

      real*8 errTnorm,Ts2
      real*8 Tinf,kwd,cpwd,L,rhowd,timec,Mgc,tol,dtime
      real*8 timed,rhofd,Qpd,Ead,apd,qd,hd,epsilon
      real*8 time,rhof,Qp,q,H,Sigma,ap,Te,dx,Ts1,Mgs,dTs1,ks
      real*8 qflamed,qflame,qnet
      real*8  sumha,sumhc,sumhg,sumQp,SumT
      real*8 rho1(npmax+2),rho2(npmax+2),T1(npmax+2),T2(npmax+2)
      real*8 T1d(npmax+2),T2prim(npmax+2)
      real*8 Mg(npmax+2),A(npmax+2),xc(npmax+2),x(npmax+2)
      real*8 dT(npmax+2)
      real*8 D1(npmax+2),D2(npmax+2),D3(npmax+2),RHS(npmax+2)
      real*8 cpcd1(npmax+2),cpad1(npmax+2),cpgd1(npmax+2)
      real*8 cpc1(npmax+2),cpa1(npmax+2),cpg1(npmax+2)
      real*8 hcd1(npmax+2),had1(npmax+2),hgd1(npmax+2)
      real*8 hc1(npmax+2),ha1(npmax+2),hg1(npmax+2),hall1(npmax+2)
      real*8 ka(npmax+2),kc(npmax+2),kad(npmax+2),kcd(npmax+2)
      real*8 k(npmax+2),rhocps(npmax+2)
      real*8 errT(npmax+2)
      real*8 drhodt(npmax+2)
```

```
      character(50) filename
      character(4) order
      open (file = 'Nylon_characters.dat',unit = 200)
      npx = 500
      dtime = 1.0e-4
      tol = 1.0e-6
      itermax = 500

C     Characteristic variables
      Tinf = 298.d0                          ! K          ambient temperature
      kwd = 3.054e-4*Tinf + 0.0362           ! J/m.s.K    solid virgin conductivity
      cpwd = 10.d0 + 3.7d0*Tinf              ! J/kg.K     solid virgin heat capacity
      L = 8.0e-3                             ! m          solid thickness
      rhowd = 1136.d0                        ! kg/m3      solid virgin density
      timec = cpwd*rhowd*(L**2)/kwd          ! s          characteristic time
      Mgc = kwd/(cpwd*L)                     ! kg/s-m2    characteristic massflux

C     Input varialbles
      timed = 500.d0                         ! s          total physical time
      rhofd = 0.017*rhowd                    ! kg/m3      solid final density
      Qpd = 0.d0                             ! J/kg       solid heat of pyrolysis
                                             ! + Endothermic and - Exothermic
      Ead = 2.4e5                            ! J/mole     solid activation energy
      apd = 1.0e19                           ! 1/s        solid pre-exponential
                                                          factor
      qd = 50.e3                             ! W/m2       incident heat flux
      qflamed = 5.e3                         ! W/m2       flame heat flux
      hd = 10.d0                             ! W/m2.K     heat transfer coefficient
      epsilon = 1.d0                         ! emissivity
C     Calculate Dimensionless Parameters
      time = timed/timec
```

```
      rhof = rhofd/rhowd
      Qp = Qpd/(cpwd*Tinf)
      q = qd*L/(kwd*Tinf)
      qflame = qflamed*L/(kwd*Tinf)
      H = hd*L/kwd
      Sigma = epsilon*(5.67e-8)*(Tinf**3)*(L)/kwd
      ap = apd*cpwd*rhowd*(L**2)/(kwd*(1-rhof))
      Te = Ead/(8.314*Tinf)

C     Generate Grid
      dx = 1.d0/npx
      do i=1,npx+3
      x(i) = (i-2)*dx
      enddo

      do i = 1,npx+2
      xc(i) = 0.5d0*(x(i+1)+x(i))
      enddo

C     Initialize Solution
      do i = 1,npx+2
            T1(i) = 1.d0
            T2(i) = 1.d0
            dT(i) = 0.d0
            rho1(i) = 1.d0
            rho2(i) = 0.d0
            Mg(i) = 0.d0
      enddo

      Ts1 = 1.d0
      Mgs = 0.d0
```

```
      dTs1 = 0.d0
      ntmax = ceiling(time/dtime)
      write(200,1000) timec,Mgc,Tinf,dtime,L,rhowd,cpwd,kwd,Qpd,apd,Ead
      close (200)
1000  format(11e15.3)
      open (file= 'Nylon_mass_temp.dat', unit = 100)

C     Start Advance in Time
      do nt = 1,ntmax
100   continue
      write(6,*) nt,ntmax
C     Arrhernius Kinetic Decomposition Rate
            do i = 1,npx+2                    ! include ghost points
            A(i) = -ap*dtime*exp(-2.d0*Te/(T2(i)+T1(i)))
            rho2(i) = (2.d0/(2.d0-A(i)))
     &      *(rho1(i)+A(i)*(0.5*rho1(i)-rhof))
            enddo

C     Mass Transfer Equation
C     Mg(L)-Mg(x) = integrate (drho/dtime)dx from x = x to x = L
                  do i = npx+1,2,-1
       Mg(i) = Mg(i+1)-((rho2(i)-rho1(i))/dtime)*dx
                  enddo

C     Calculate cp-heat capacity and h-enthalpy for active wood, char
C     ,and gas base on T1d (nth + dtime time step)
                  do i = 1,npx+2
                  T1d(i) = (T1(i)+dT(i))*Tinf
                  enddo
                  do i = 1,npx+2                  ! include ghost points
```

```
            cpcd1(i) = 1430.d0 + 0.355*T1d(i)-0.732*(T1d(i)**(-2.d0))
            cpad1(i) = 10.d0 + 3.7*T1d(i)
            cpgd1(i) = 66.8*(T1d(i)**(1.d0/2.d0)) - 136.d0

            hcd1(i) = (5.0e-4)*(2.86*1.e6*Tinf*(T1d(i)**2.d0)
     &      + 355.d0*Tinf*(T1d(i)**3.d0) + 1464.d0*Tinf -
     &      2.86e6*T1d(i)*(Tinf**2.d0)-355.d0*T1d(i)*(Tinf**3.d0)-
     &      1464.d0*T1d(i))/(T1d(i)*Tinf)

            had1(i) = 1.85*(T1d(i)**2.d0) - 1.85*(Tinf**2.d0)
     &      + 10.d0*(T1d(i)-Tinf)

            hgd1(i) = 44.53*(T1d(i)**(3.d0/2.d0)) - 136.d0*T1d(i) -
     &      44.53*(Tinf**(3.d0/2.d0)) + 136.d0*Tinf

c       None-dimensionalize cp and h
                  do i = 1,npx+2
                  cpc1(i) = cpcd1(i)/cpwd
                  cpa1(i) = cpad1(i)/cpwd
                  cpg1(i) = cpgd1(i)/cpwd

                  hc1(i) = hcd1(i)/(cpwd*Tinf)
                  ha1(i) = had1(i)/(cpwd*Tinf)
                  hg1(i) = hgd1(i)/(cpwd*Tinf)
                  enddo

                  do i = 2,npx+1
                  hall1(i) = (1.d0/(1.d0-rhof))*ha1(i)
     &             - (rhof/(1.d0-rhof))*hc1(i) - hg1(i)
                  enddo
```

```
C       Calculate k-thermal conductivity for active wood, char base on T1d (nth + dtime time
step)
                    do i = 1,npx+2
                    kcd(i) = ((9.46e-5)*T1d(i) + 4.88e-2)          ! W/m.K
                    kad(i) = 0.9d0*((3.054e-4)*T1d(i) + 3.62e-2)   ! W/m.K
                                                                   !Nylon conductivity
                    enddo

C       Non-dimensionalize k
                    do i = 1,npx+2
                    ka(i) = kad(i)/kwd
                    kc(i) = kcd(i)/kwd
                    enddo

C       Calculate k(i),rhocps and dk/dx base on average value between rho2 and rho1
        do i = 2,npx+1
                k(i) = ((0.5d0*(rho2(i)+rho1(i))-rhof)*ka(i))
     &           /(1.d0-rhof) + ((1.d0-0.5d0*(rho2(i)+rho1(i)))*kc(i))/(1.d0-rhof)

                rhocps(i) = ((0.5d0*(rho2(i)+rho1(i))-rhof)*cpa1(i))/(1.d0-rhof)
     &          + ((1.d0-0.5d0*(rho2(i)+rho1(i)))*cpc1(i))/(1.d0-rhof)
                enddo

C       Energy Eq
C       Calculate D1,D2,D3 (elements of tridiagonal temperature matrix)
        do i = 2,npx+1
        D1(i) =-(0.5d0*dtime/(rhocps(i)*(dx**2)))*0.5d0*(k(i+1)+k(i)) ! One above
        D2(i) = 1.d0+(0.5d0*dtime/(rhocps(i)*(dx**2)))*0.5d0*(k(i+1)+k(i))
     &  +(0.5d0*dtime/(rhocps(i)*(dx**2)))*0.5d0*(k(i)+k(i-1))     ! Diagonal
       D3(i) = -(0.5d0*dtime/(rhocps(i)*(dx**2)))*0.5d0*(k(i)+k(i-1))! One below          enddo
```

```
C       Back Boundary dT/dx = 0
        D3(npx+2) = -1.d0
        D2(npx+2) = 1.d0

C       Front Boundary q + qflame = -k(dT/dx) + H*(T-1) + Sigma(Ts^4-1).
C       Estimate Ts from Tsn+1 = Tsn + (dTs/dt)*dtime
        ks = 1.5d0*k(2)-0.5d0*k(3)
        D2(1) = 1.d0+ H*dx/(2.d0*ks)
        D1(1) = -1.+ H*dx/(2.d0*ks)

c       Fill in RHS vectior
        RHS(1) = q*dx/ks + H*dx/ks -
     &  (dx/ks)*Sigma*(((Ts1+ dTs1)**4)-1.d0) + (dx/ks)*(qflame)
        RHS(npx+2) = 0.d0

        do i = 2,npx+1
        RHS(i)= T1(i) + 0.5d0*(dtime/rhocps(i))*(1.d0/(dx**2))*
     &  ((0.5d0*(k(i+1)+k(i)))*(T1(i+1)-T1(i)) -
     &  (0.5d0*(k(i)+k(i-1)))*(T1(i)-T1(i-1)))
     &  + (1.d0/rhocps(i))*(rho2(i)-rho1(i))*(Qp-hall1(i))
     &  + ((Mg(i)*dtime)/rhocps(i))*(hg1(i+1)-hg1(i-1))/(2.d0*dx)
        enddo
        call tridag(D3,D2,D1,RHS,T2prim,npx+2)

C       check errT  relative error
        do i = 2,npx+1
        errT(i) = abs((T2(i)-T2prim(i))/T2(i))
        enddo
        errTnorm = 0.d0
        do i = 2,npx+1
```

```
            if (errTnorm.lt.errT(i)) errTnorm = errT(i)
            enddo

C           write (6,1500) nt,errTnorm
            do i = 1,npx+2
            T2(i)=T2prim(i)
            Ts2 = 1.5d0*T2(2)-0.5d0*T2(3)
c           Ts2 = 0.5d0*(T2(1)+T2(2))
            dTs1 = Ts2-Ts1
            enddo

            if (errTnorm.gt.tol) goto 100
            if (errTnorm.lt.tol) then

c           Calculate Temperature (Ts) and Mass flux (Mgs) at surface for each time step by linear interpolation
            do i = 2,npx+1
            drhodt(i) = (rho2(i)-rho1(i))/dtime
            enddo

           Mgs = 1.5d0*Mg(2)-0.5d0*Mg(3)

c           Setup T1 for the next time step
            do i = 1,npx+2
            dT(i) = T2(i)-T1(i)
            enddo
            Ts1 = Ts2
            do i = 1,npx+2
            T1(i) = T2(i)
            rho1(i) = rho2(i)
            enddo
```

```
      endif

c     Check Magnitude of energy term of time step nt
      sumha = 0.d0
      sumhc = 0.d0
      sumhg = 0.d0
      sumQp = 0.d0
      sumT = 0.d0

      do i = 2,npx+1
      sumha = sumha + cpwd*Tinf*dx*(ha1(i)/(1.d0-rhof))
      sumhc = sumhc + cpwd*Tinf*dx*(rhof*hc1(i)/(1.d0-rhof))
      sumhg = sumhg + cpwd*Tinf*dx*(hg1(i))
      sumQp = sumQp + cpwd*Tinf*dx*(Qp)
      sumT = sumT+Tinf*dx*T1(i)
      enddo

C     calculated qnet
      qnet = q-H*(Ts1-1.d0)-Sigma*((Ts1**4) - 1.d0)
      open (file='Nylon_energy.dat',unit = 500)
      write(500,2000) nt,sumha,sumhc,sumhg,sumQp,sumT,qnet,q,Ts2,Mgs

C     Writing Output File
      write(100,2500) nt,Ts2,Mgs
C     write In-depth profiles every nt_prof time step
      if (mod(nt,nt_prof).eq.0) then
      call int_to_char(order,nt,4)
      filename = 'Nylon_profile_'//order//'.dat'
      open (file = trim(filename) ,unit=150)

      do i = 2,npx+1
```

```
      write(150,3000) nt,xc(i),rho2(i),T2(i),drhodt(i)
      enddo
      close (150)
      endif
      Enddo ! Enddo of advancing in time
      close (100)
      close (500)

1500  format(i9,1e15.3)
2000  format(i9,9e18.8)
2500  format(i9,2e18.8)
3000  format(i9,9e18.8)
      End

c     ****************************************************************
      subroutine tridag(a,b,c,r,u,n)
      integer n,nmax
      real*8 a(n),b(n),c(n),r(n),u(n)
      parameter (nmax = 1600)
      integer j
      real*8 bet,gam(nmax)
      if(b(1).eq.0) pause 'tridag:rewrite equations'
      bet = b(1)
      u(1) = r(1)/bet
      do j = 2,n
            gam(j) = c(j-1)/bet
            bet = b(j)-a(j)*gam(j)
            if(bet.eq.0) pause 'tridag failed'
            u(j) = (r(j)-a(j)*u(j-1))/bet
      enddo
      do j = n-1,1,-1
```

```
u(j) = u(j)-gam(j+1)*u(j+1)
enddo
return
end

subroutine int_to_char(file_ext,num,max)
! converts a positive integer (num) to character (file_ext) of length max
! in other words, 0 < num < (10**max)-1
! routine uses function getchar (see below)
! note: this routine takes advantage of the fortran convention for passing arrays
!   through argument lists; in particular, in this routine file_ext is delcared
!   as a character array of length equal to the length of the single character
!   declaration of the calling routine; i'm sorry to have to do this, but it
!   made things very nice in this routine; in short:
!   character*max file_ext => character file_ext(max)
!-------------------------------------------------------------------------------
  implicit none
! declarations passed in
  character(*) file_ext
  integer num, max
! other declarations
  integer i, m, n, temp
  character getchar
!-------------------------------------------------------------------------------
! check for postiveness
  if(num.lt.0) then
  write(6,*) 'num passed into routine'
   write(6,*) 'set_file_extension_string is negative'
   stop
   endif
```

```
! check for maximum value of num
  if(num.gt.(10**max)-1) then
  write(6,*) 'num passed into routine set_file_extension_string'
  write(6,*) 'is greater than the character file_ext will allow'
  stop
  endif
!-------------------------------------------------------------------------------
! zero stuff (must do this!)
  n=0; temp=0
  do i=1,max,1
  file_ext(i:i)='0'
  enddo
! set file extension
  do i=max,1,-1
  temp=n
  n=(num/10**(i-1))
  m=max-i+1
  file_ext(m:m)=getchar(int(n-(temp*10)))
  enddo
!-------------------------------------------------------------------------------
  return
  end subroutine int_to_char
!===============================================================
  function getchar(n)
!===============================================================
! getchar returns a character corresponding to n
!-------------------------------------------------------------------------------
  implicit none
!-------------------------------------------------------------------------------
! declarations passed in
  character getchar
```

```
  integer n
!-------------------------------------------------------------------------------
  if(n.eq.0) getchar = '0'
  if(n.eq.1) getchar = '1'
  if(n.eq.2) getchar = '2'
  if(n.eq.3) getchar = '3'
  if(n.eq.4) getchar = '4'
  if(n.eq.5) getchar = '5'
  if(n.eq.6) getchar = '6'
  if(n.eq.7) getchar = '7'
  if(n.eq.8) getchar = '8'
  if(n.eq.9) getchar = '9'
!-------------------------------------------------------------------------------
  return
  end function getchar
```

APPENDIX D—EXPERIMENTAL DATA OF NANOCOMPOSITES

Data from all samples are shown in figures D-1 through D-24.

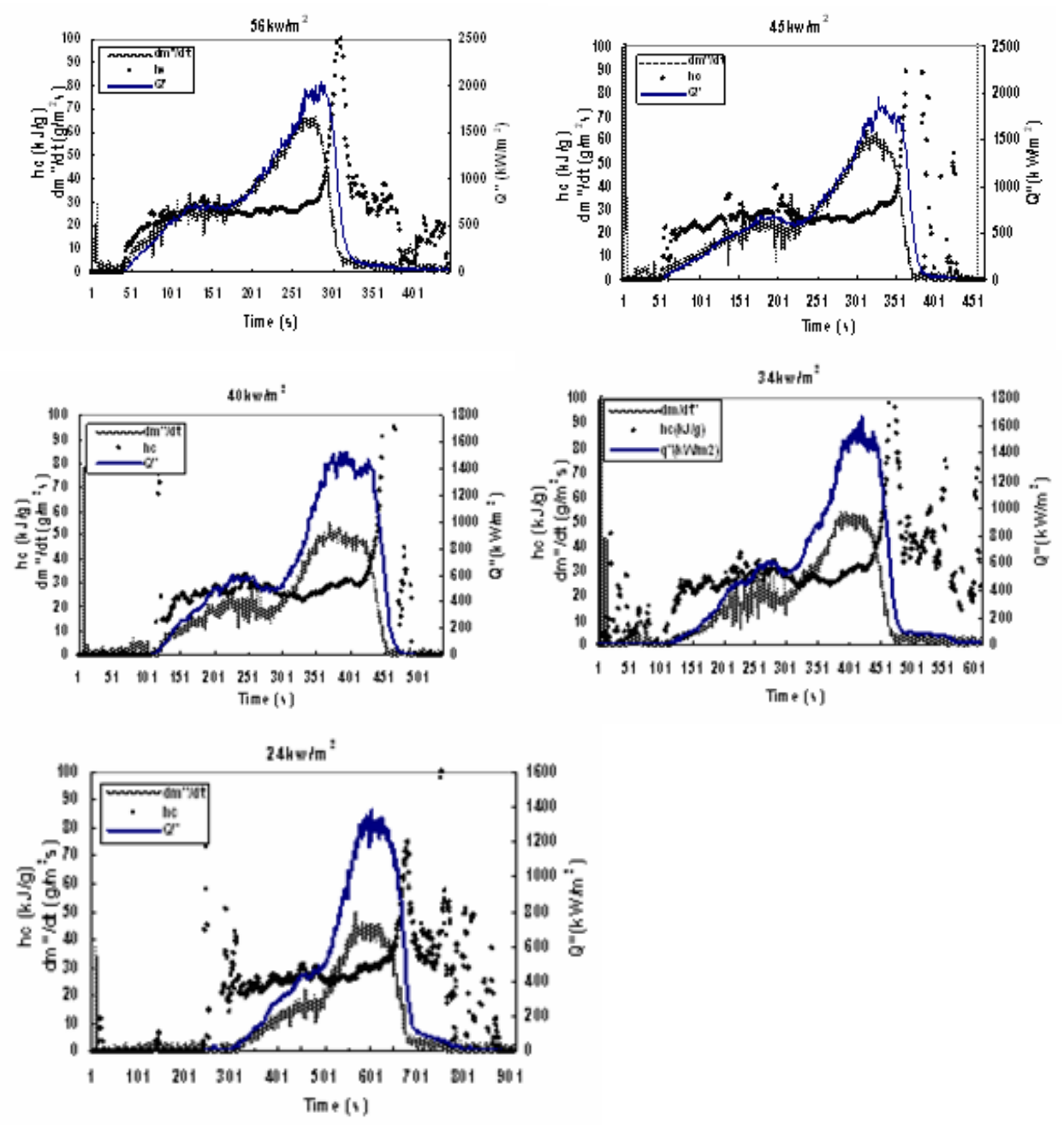

Figure D-1. Nylon Under Different External Heat Flux (Thickness 8 mm, Diameter 74 mm)

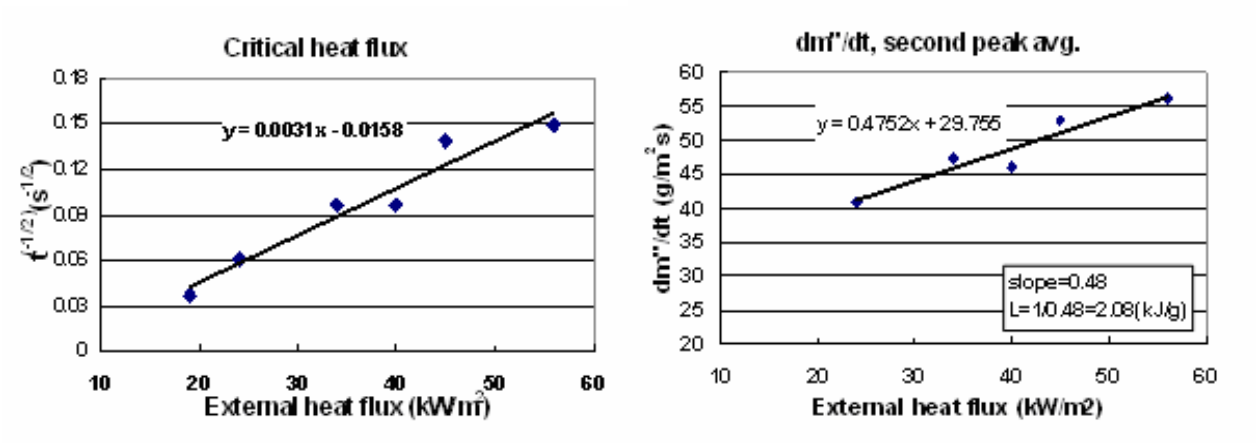

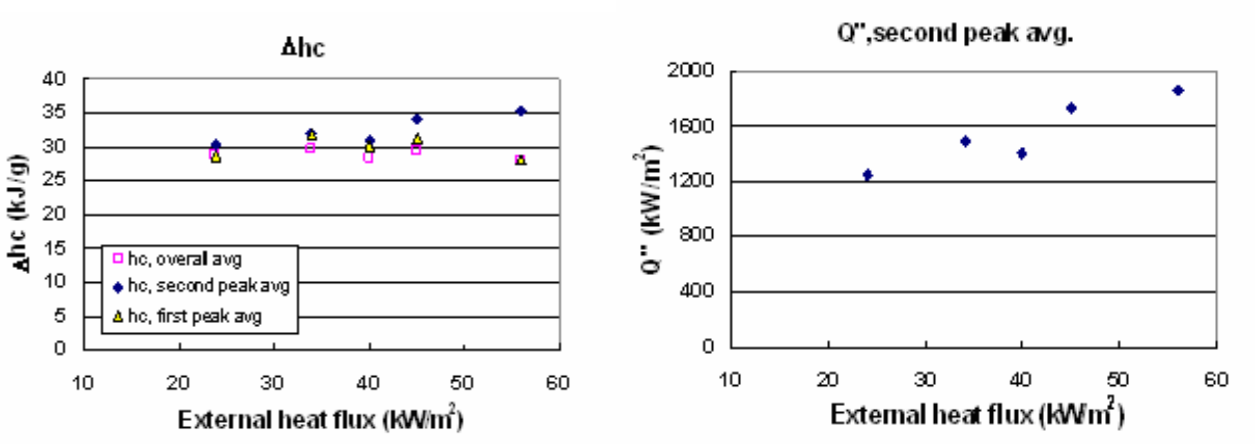

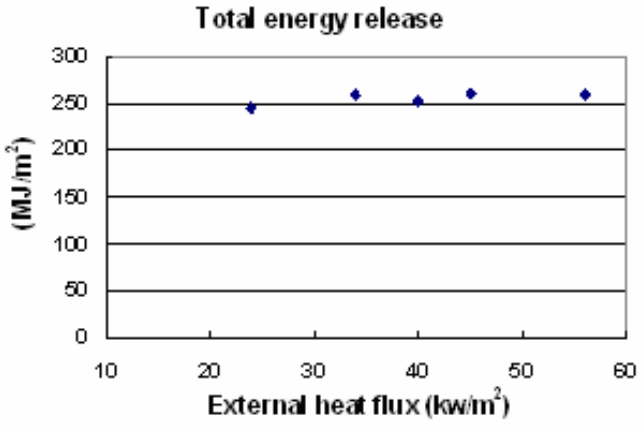

Heat Flux (kW/m^2)	Ignition Time (s)	Char/Mass (g)
56	45	0/38.2
45	52	0/38.2
40	108	0/38.2
34	109	0/38.2
24	270	0.1/38
19	744	0.3/38.3
17.7	No ignition	

Figure D-2. Summary of 8-mm Nylon

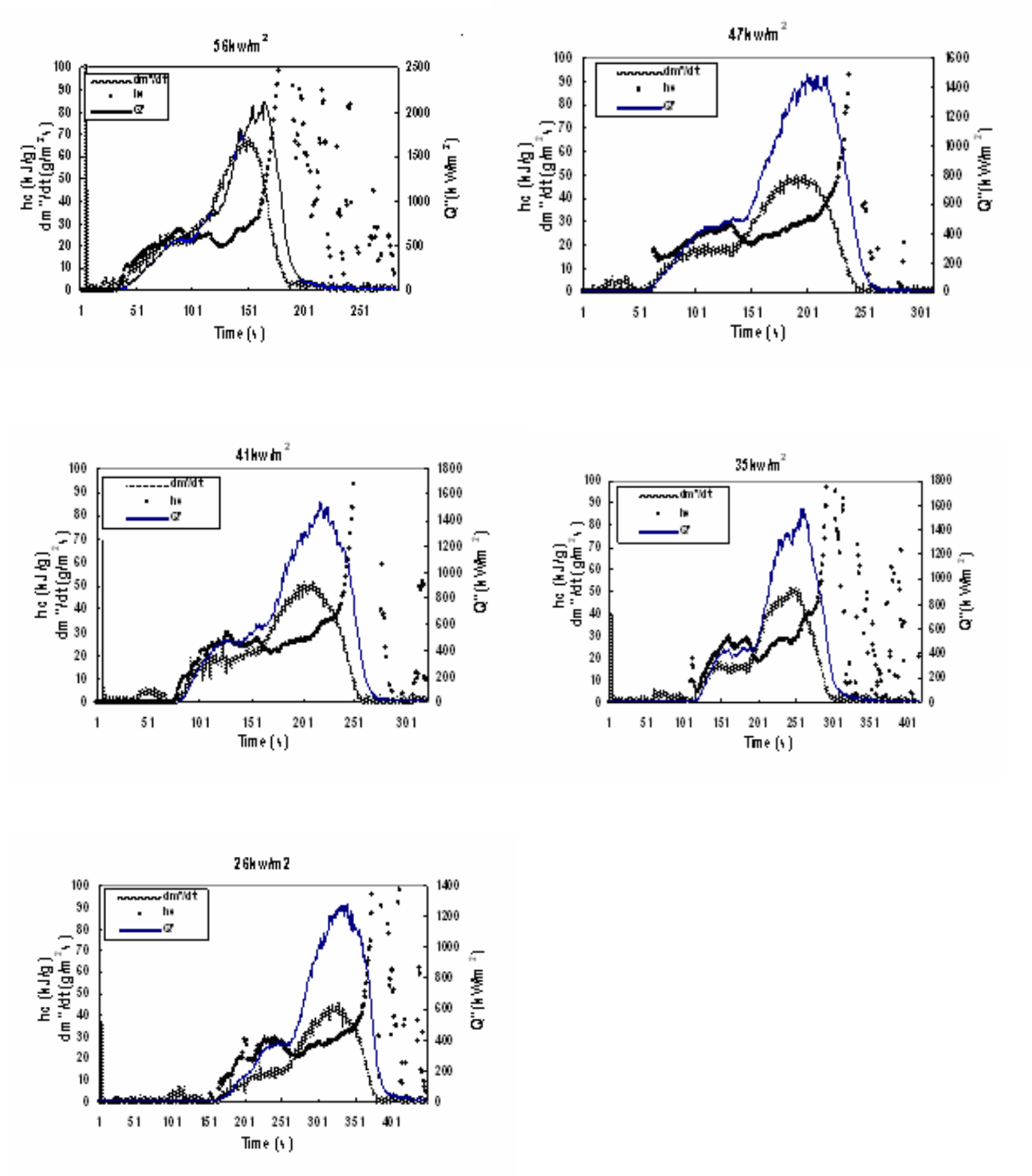

Figure D-3. Nylon Under Different External Heat Flux (Thickness 4 mm, Diameter 74 mm)

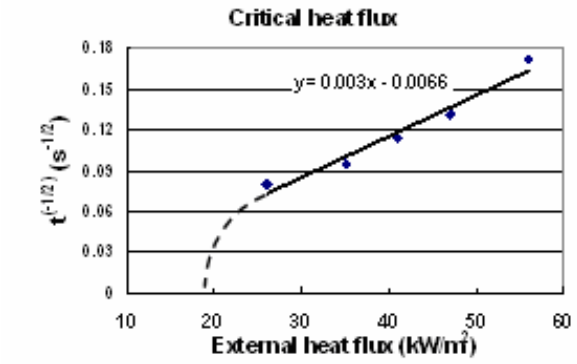

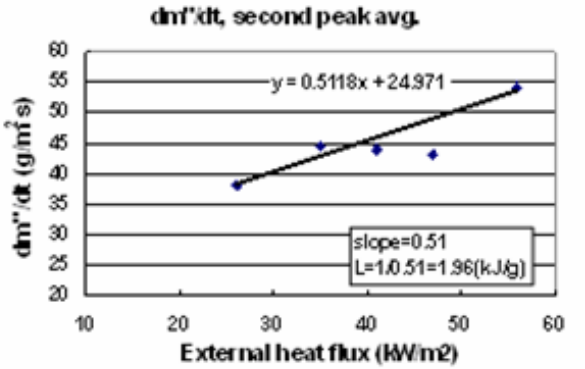

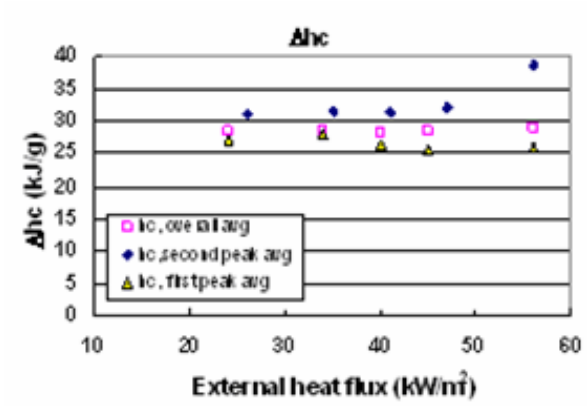

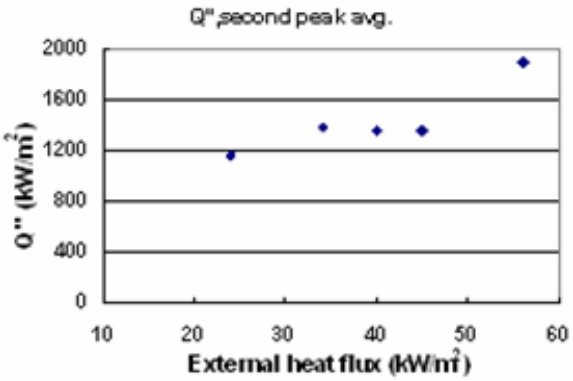

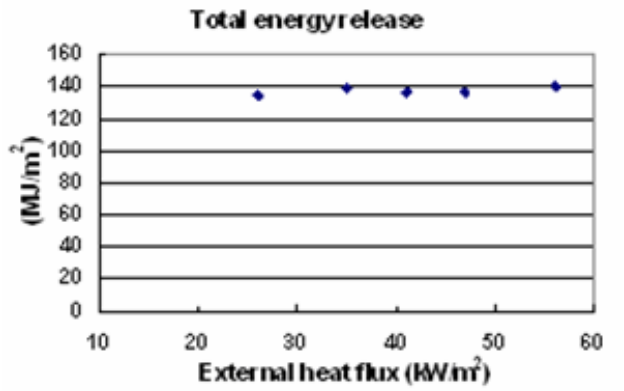

Heat Flux (kW/m^2)	Ignition Time (s)	Char/Mass (g)
56	34	0/20.7
47	58	0/20.6
41	77	0/20.5
35	110	0~0.1/21
26	157	0.1/20.5

Figure D-4. Summary of 4-mm Nylon

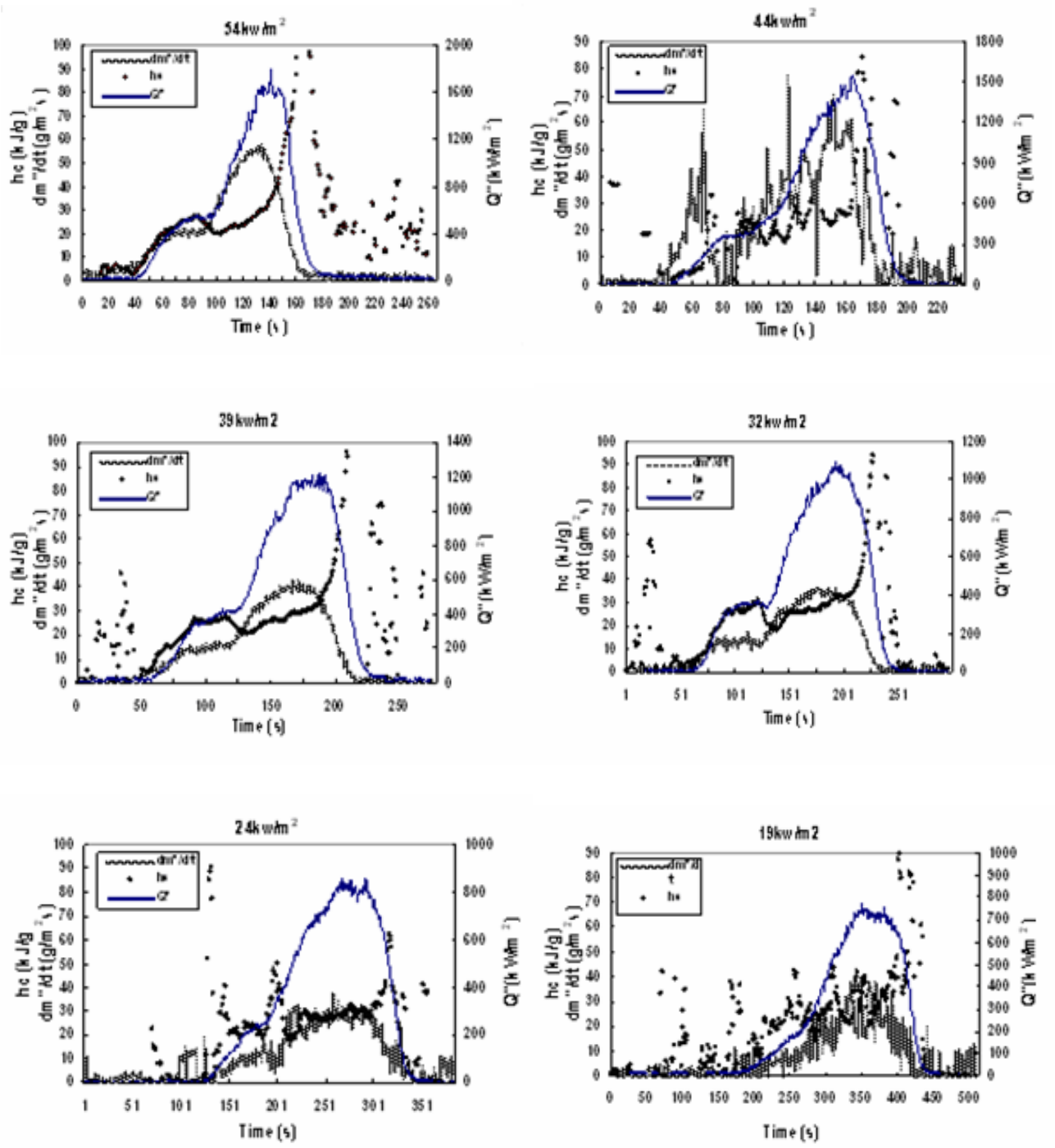

Figure D-5. Nylon Under Different External Heat Flux (Thickness 3.2 mm, Diameter 75 mm)

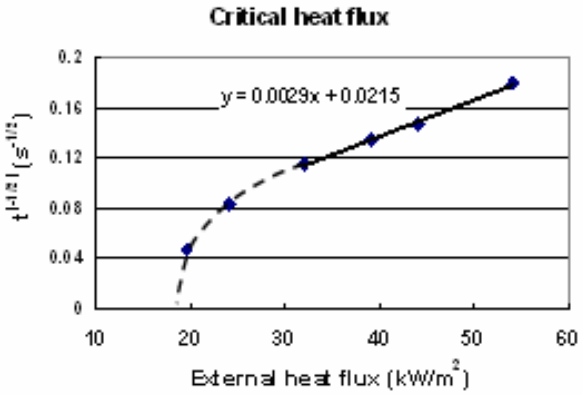

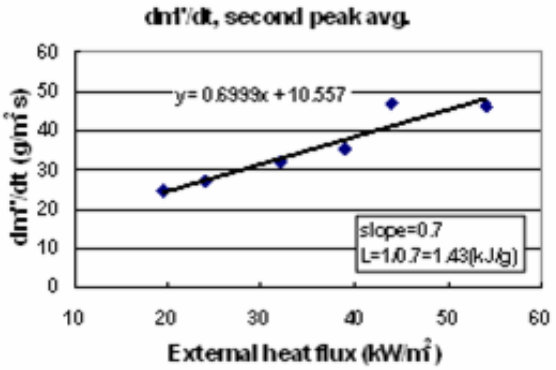

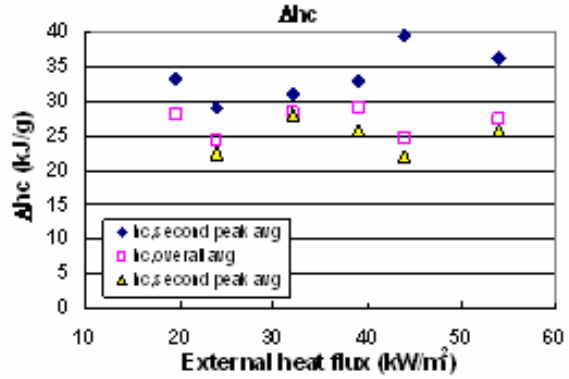

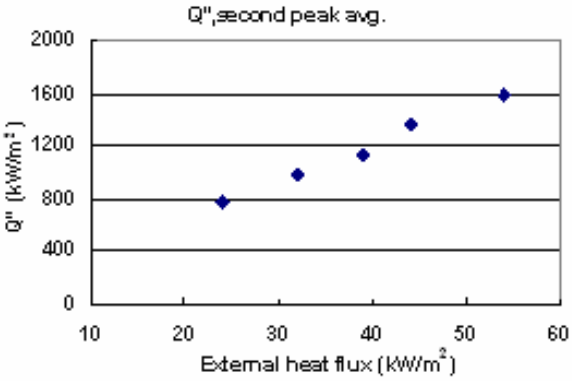

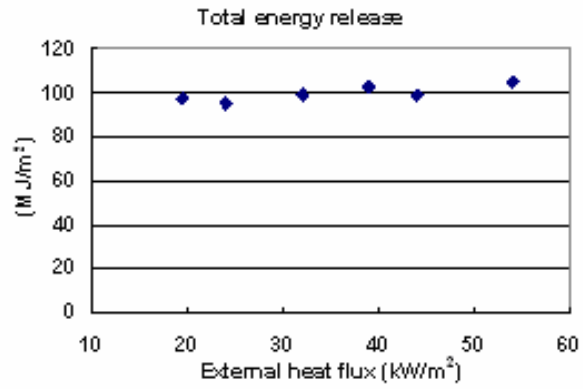

Heat Flux (kW/m^2)	Ignition Time (s)	Char/Mass (g)
54	31	0/15.5
44	47	0/15.4
39	55	0/15.5
32	75	0~0.1/15.5
24	144	0~0.1/15.4
19.5	459	0.2/15.7

Figure D-6. Summary of 3.2-mm Nylon

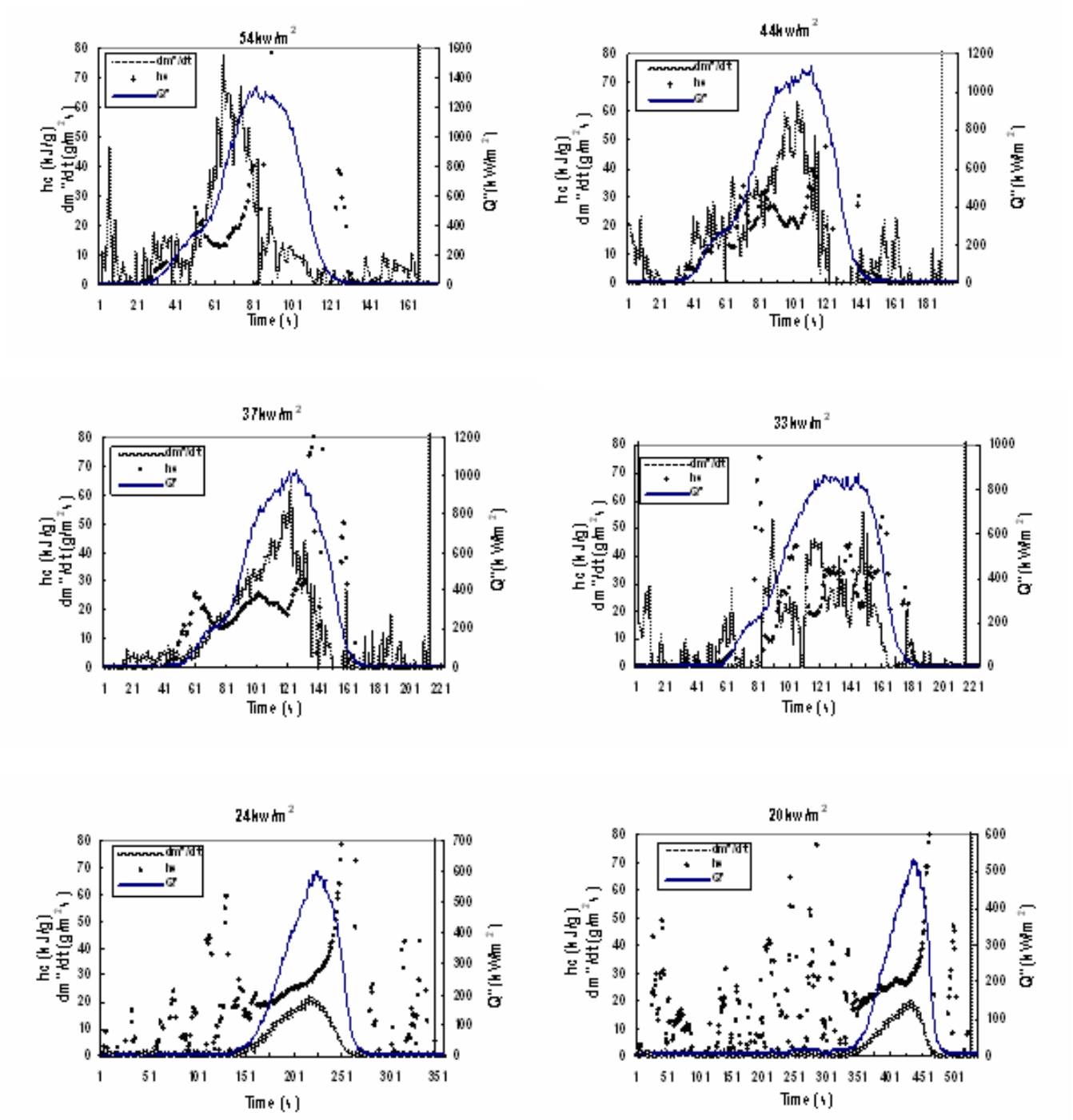

Figure D-7. Nylon Under Different External Heat Flux (Thickness 1.6 mm, Diameter 76 mm)

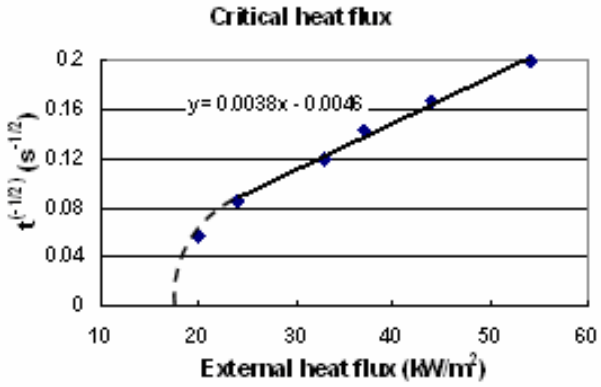

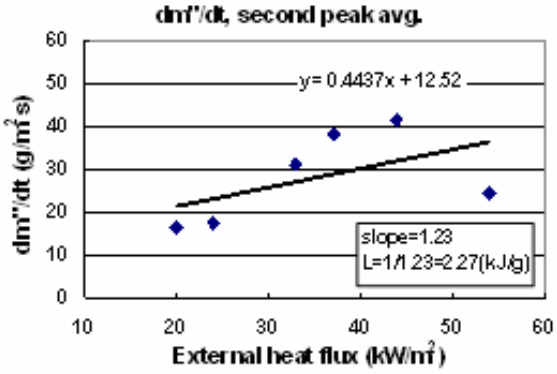

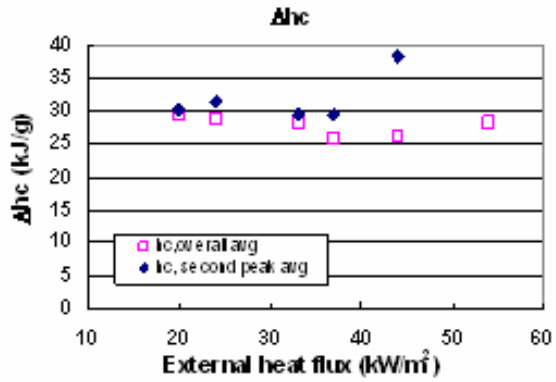

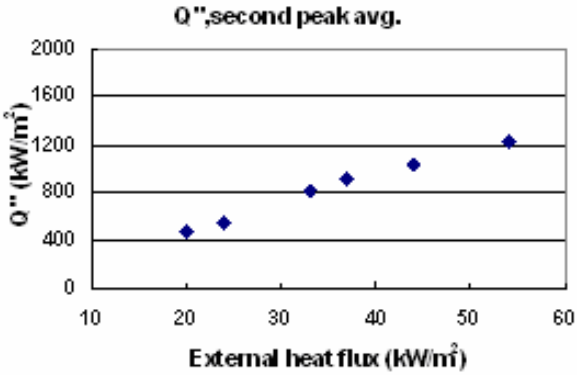

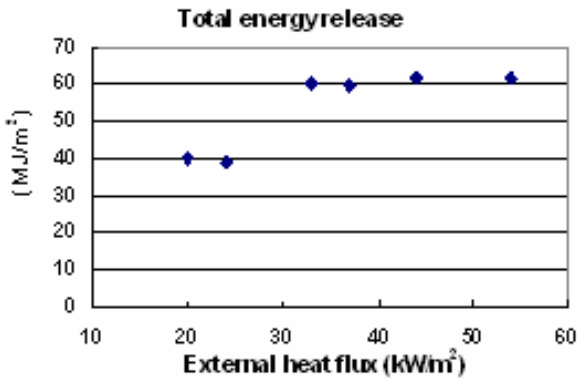

Heat Flux (kW/m^2)	Ignition Time (s)	Char/Mass (g)
54	25	0/9.7
44	36	0/9.9
37	49	0/9.7
33	69	0/9.8
24	137	0.1/9.6
20	314	0.1/9.6
19	465	8.7/9.6

Figure D-8. Summary of 1.6-mm Nylon

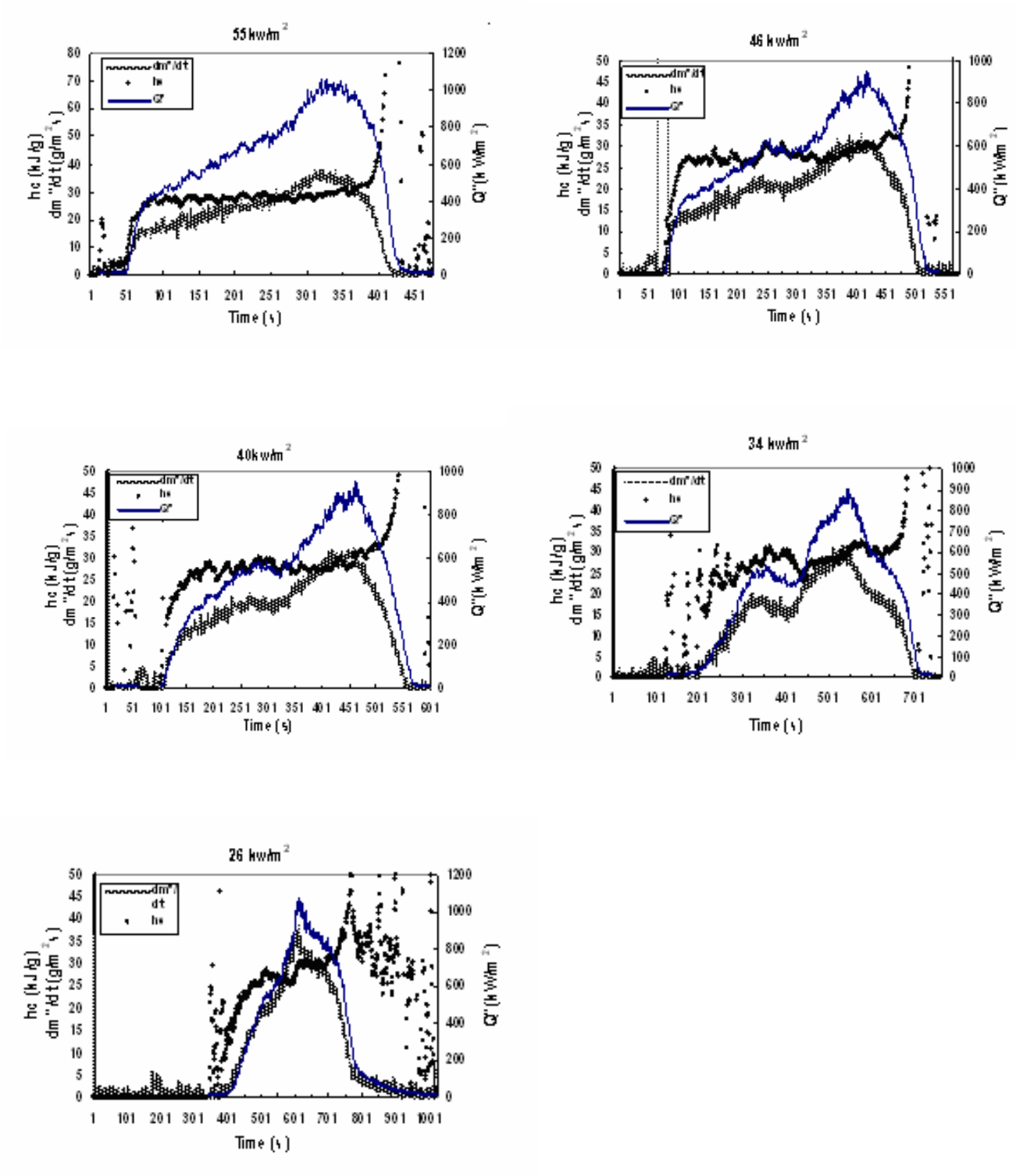

Figure D-9. Nylon +2% Clay Under Different External Heat Flux (Thickness 8 mm, Diameter 75 mm)

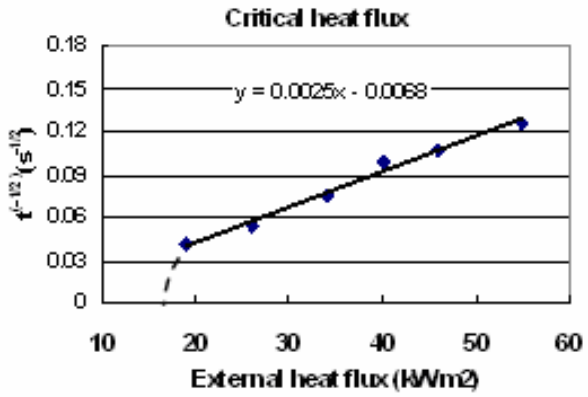

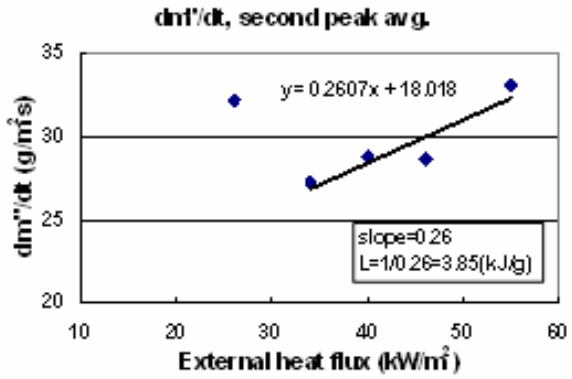

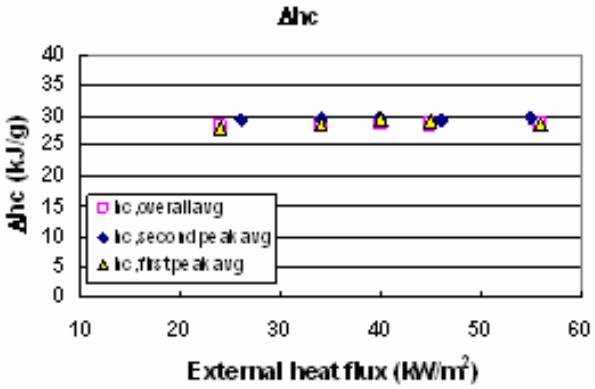

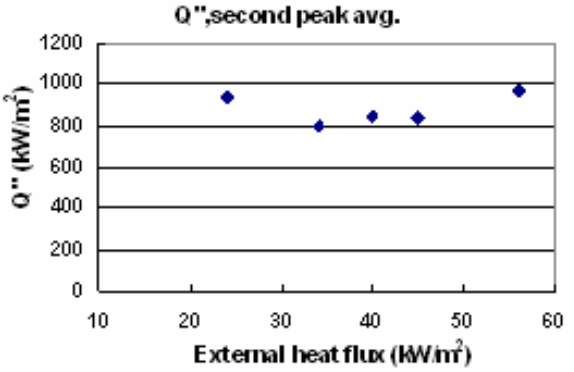

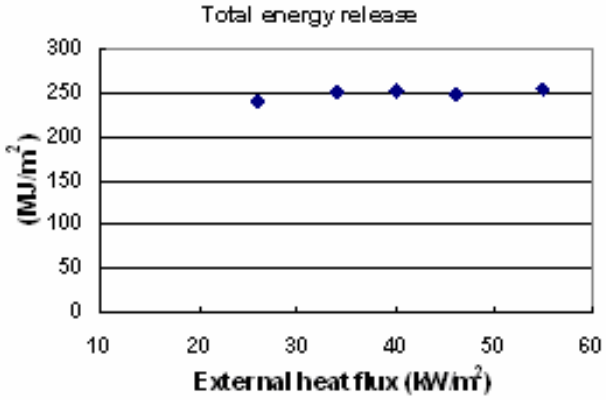

Heat Flux (kW/m^2)	Ignition Time (s)	Char/Mass (g)
55	63	0.8/38.1
46	87	0.7/38.1
40	102	0.7/38.2
34	177	0.8/38.1
26	343	/38.1
19	597	0.7/38.4
17.5	No ignition	

Figure D-10. Summary of 8-mm Nylon +2% Clay

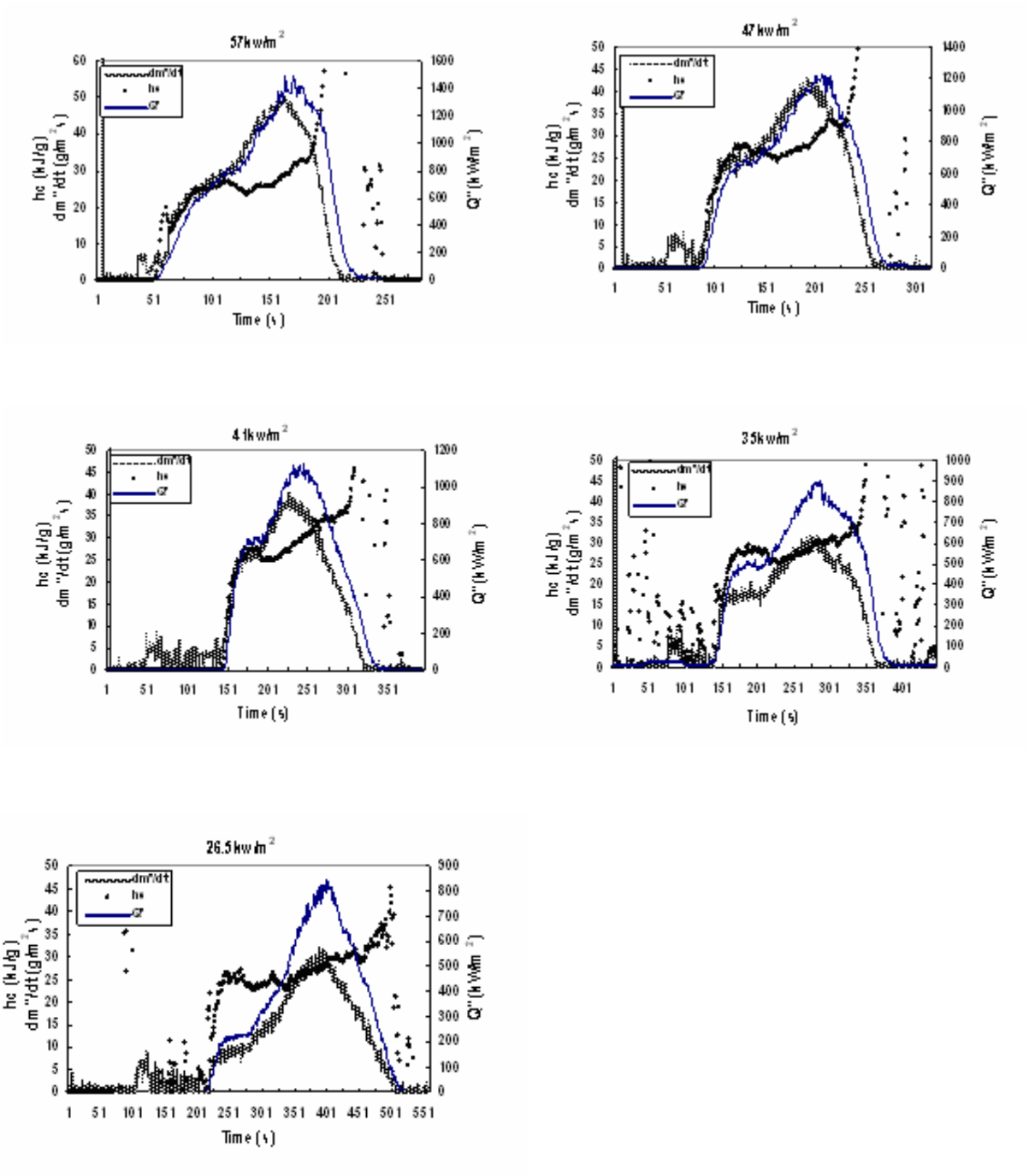

Figure D-11. Nylon +2% Clay Under Different External Heat Flux (Thickness 4 mm, Diameter 75 mm)

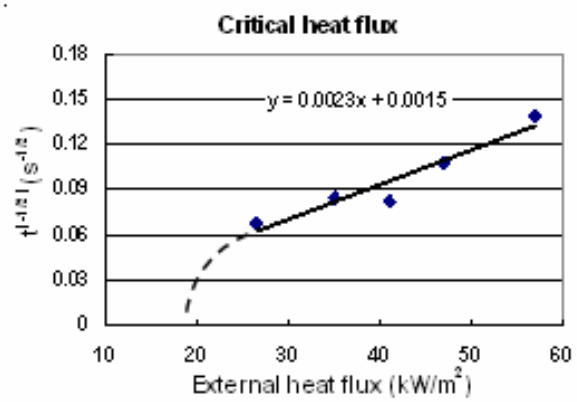

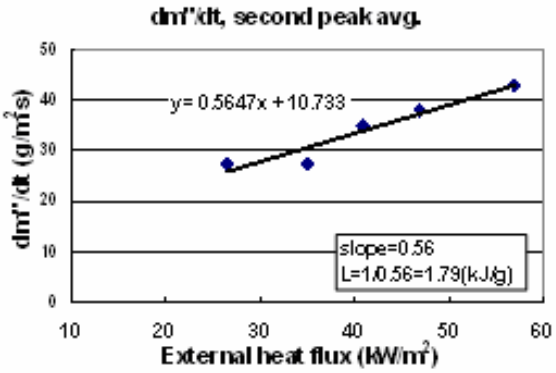

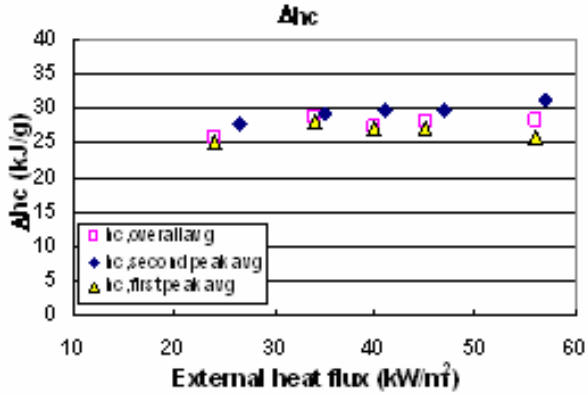

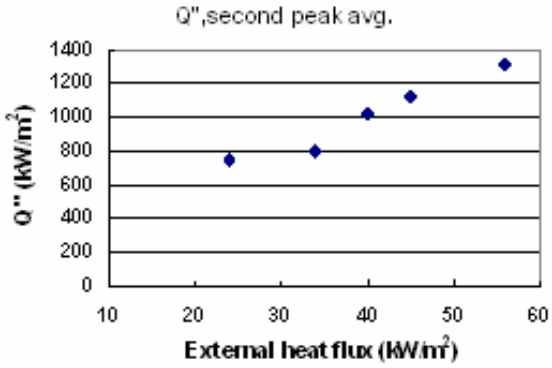

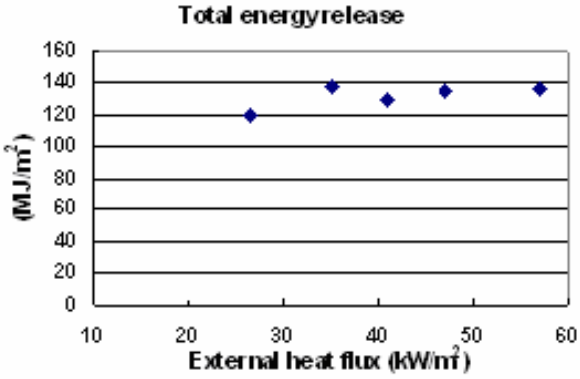

Heat Flux (kW/m^2)	Ignition Time (s)	Char/Mass (g)
57	52	0.3/20.8
47	86	0.4/20.8
41	149	0.4/20.7
35	139	0.3/20.7
26.5	219	0.4/20.9

Figure D-12. Summary of 4-mm Nylon +2% Clay

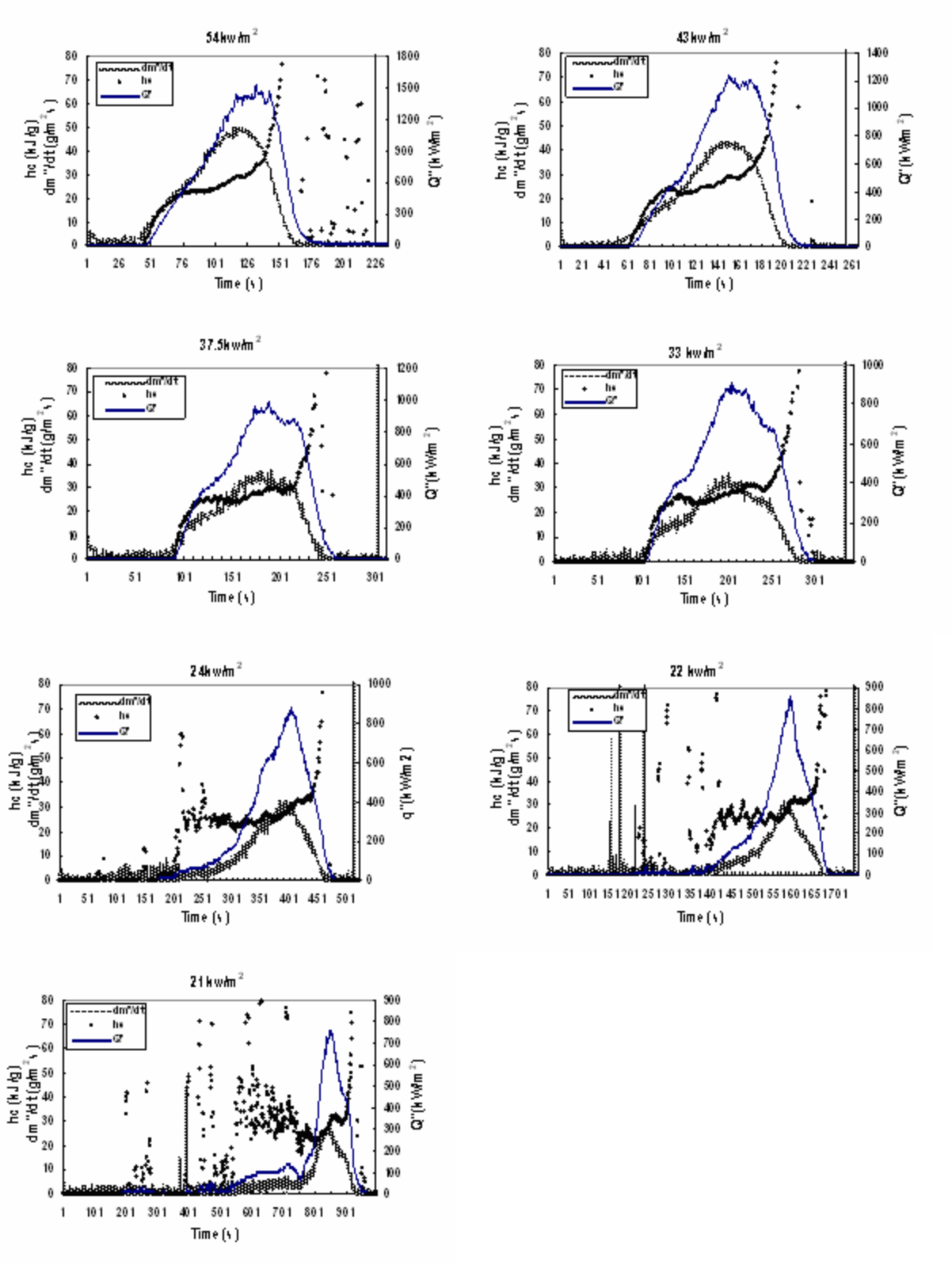

Figure D-13. Nylon +2% Clay Under Different External Heat Flux (Thickness 3.2 mm, Diameter 75 mm)

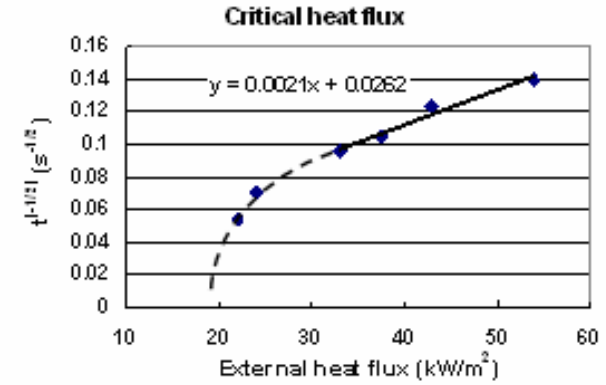

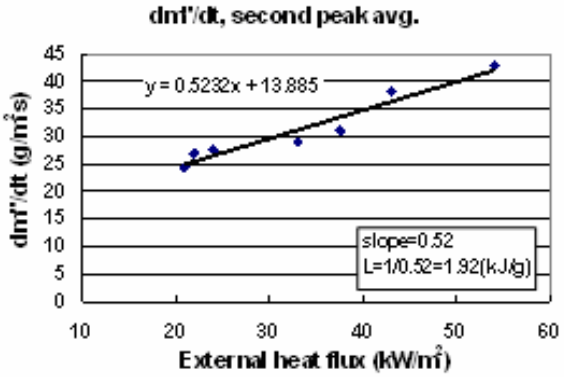

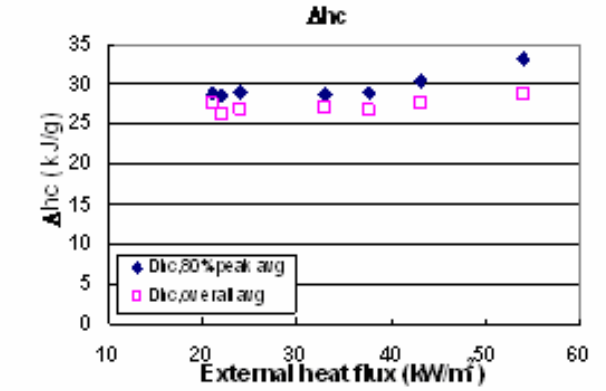

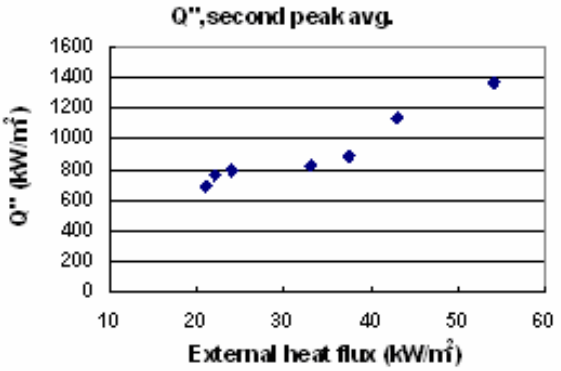

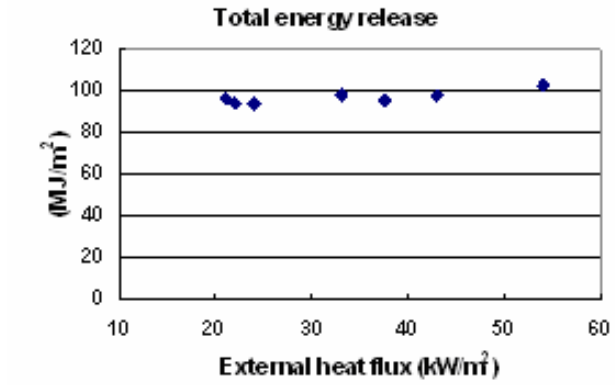

Heat Flux (kW/m^2)	Ignition Time (s)	Char/Mass (g)
54	51	0.1/15.6
43	66	0.3/15.7
37.5	91	0.3/15.5
33	109	0.3/15.9
24	203	0.3/15.4
22	338	0.3/15.7
21	568	0.4/15.5
20	600	0.3/15.6

Figure D-14. Summary of 3.2-mm Nylon +2% Clay

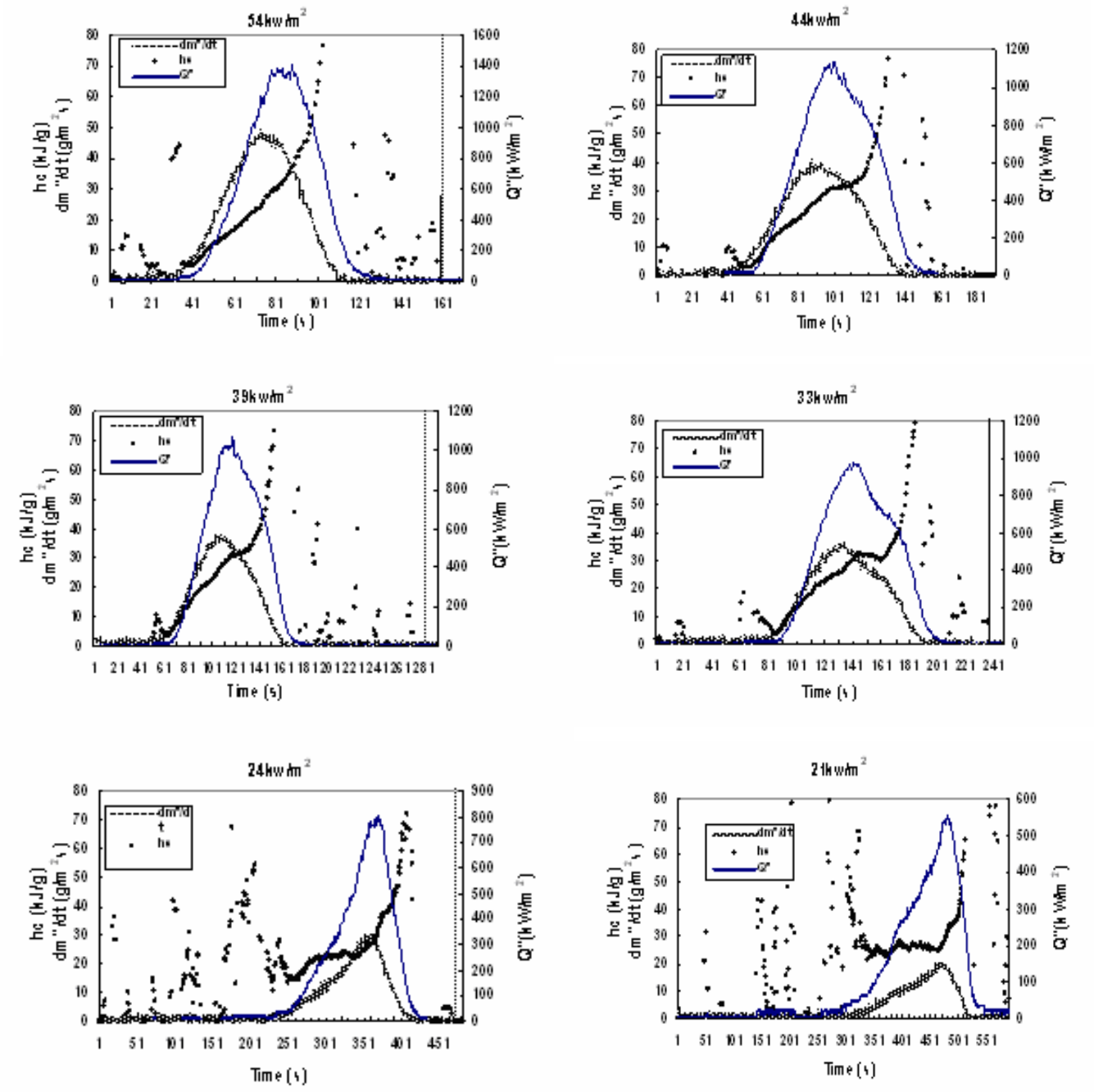

Figure D-15. Nylon +2% Clay Under Different External Heat Flux (Thickness 1.6 mm, Diameter 76 mm)

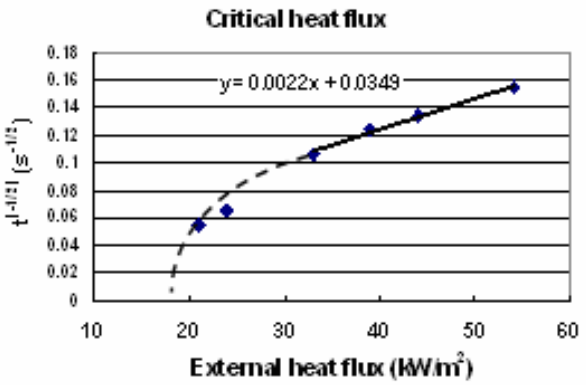

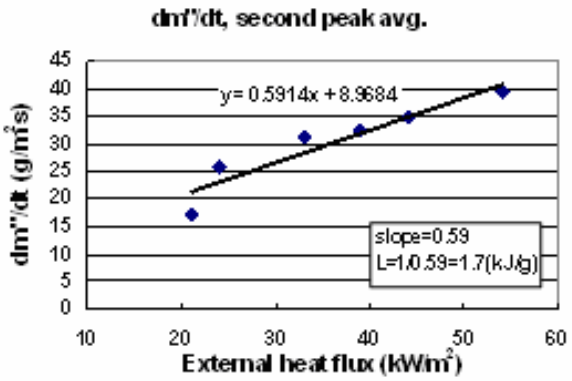

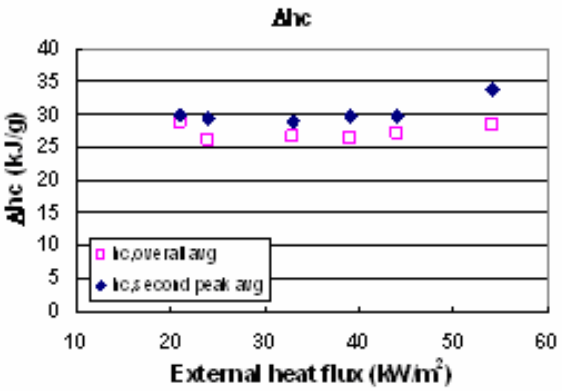

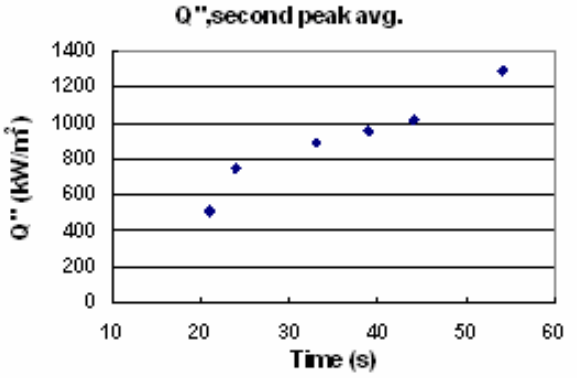

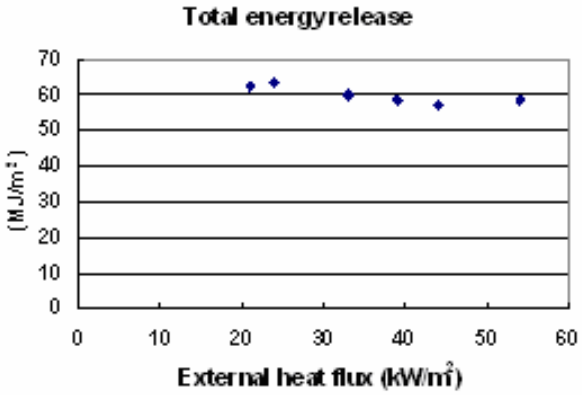

Heat Flux (kW/m^2)	Ignition Time (s)	Char/Mass (g)
54	42	0.1/9.4
44	56	0.1/9.5
39	65	0.1/9.9
33	88	0.1/10.2
24	236	0.3/11.1
21	324	0.3/9.7

Figure D-16. Summary of 1.6-mm Nylon +2% Clay

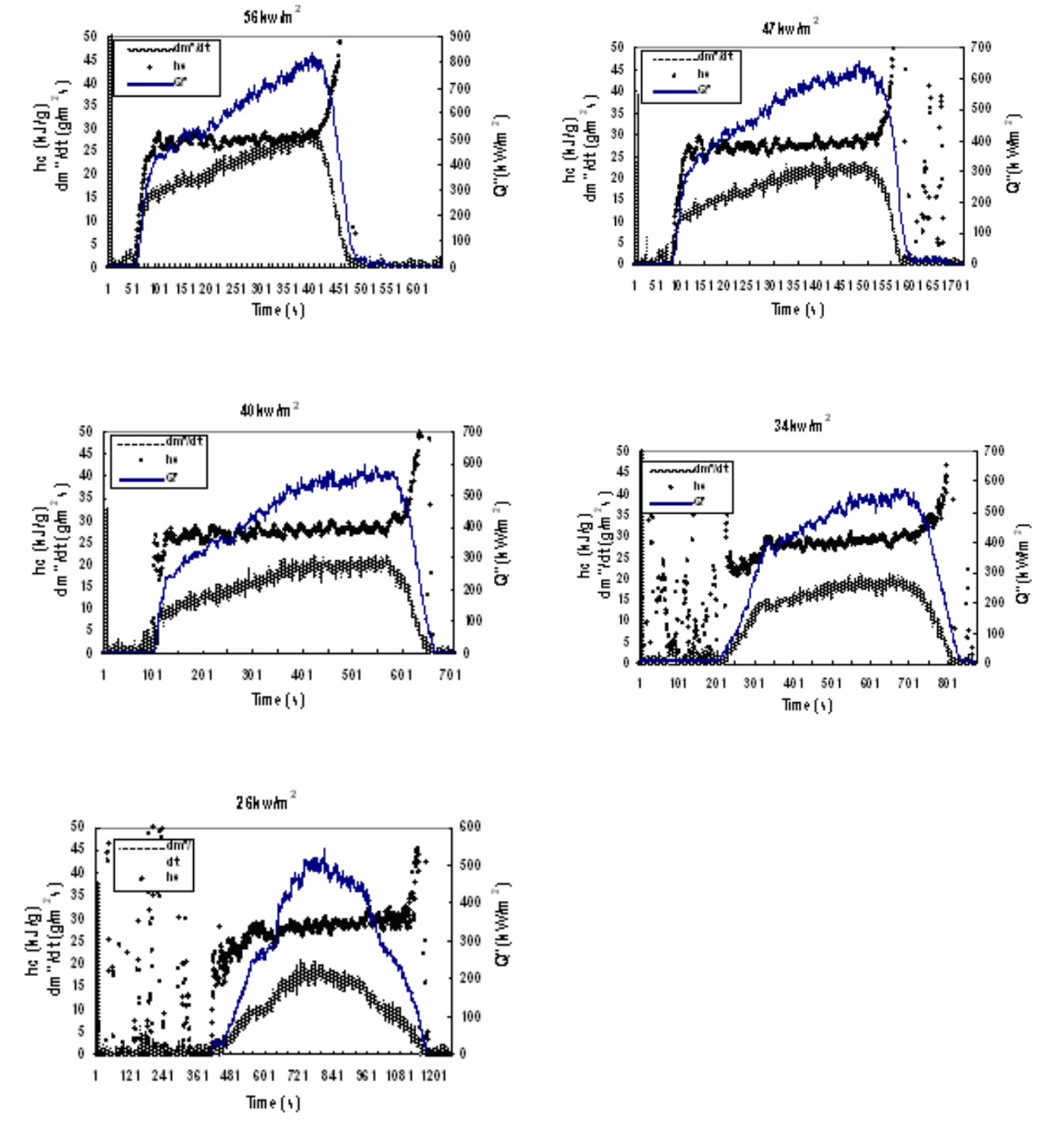

Figure D-17. Nylon +5% Clay Under Different External Heat Flux (Thickness 8 mm, Diameter 74 mm)

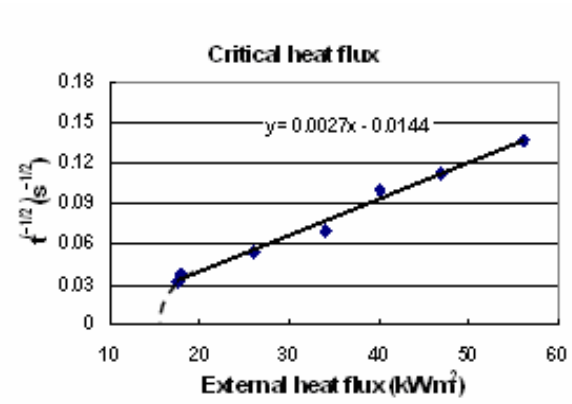

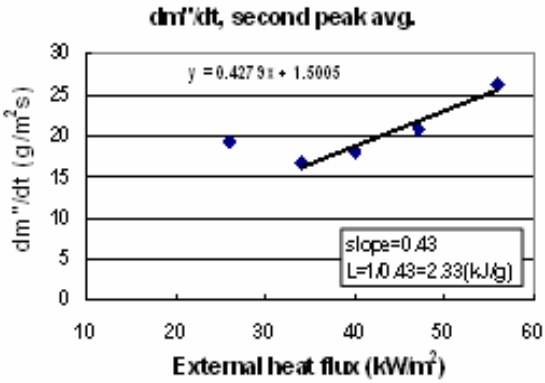

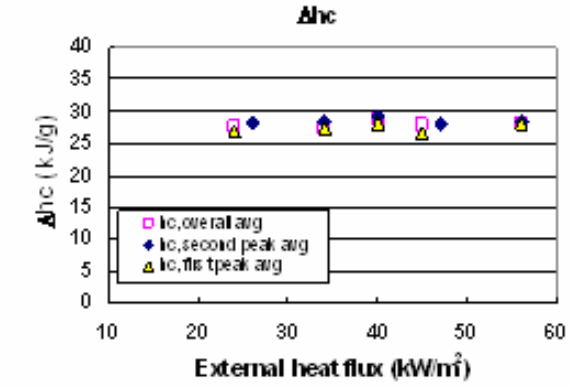

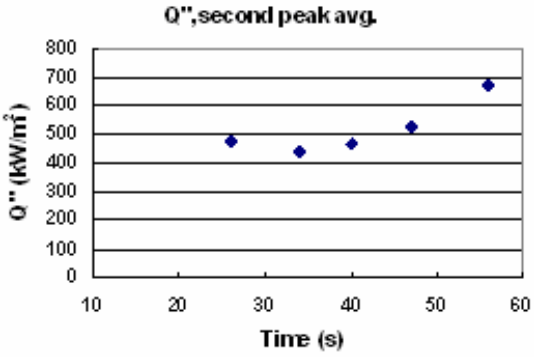

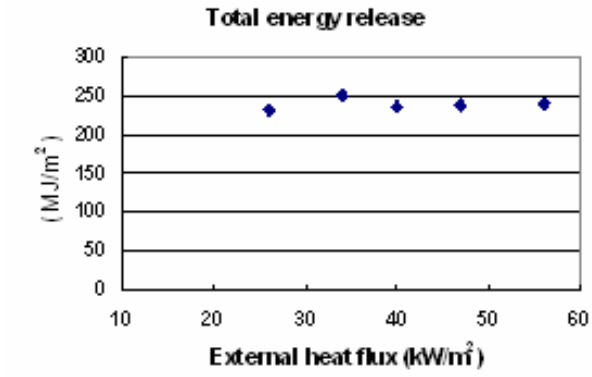

Heat Flux (kW/m^2)	Ignition Time (s)	Char/Mass (g)
56	54	1.6/38.2
47	80	1.7/38.2
40	100	1.7/38.2
34	211	1.9/38.3
26	339	1.8/38
17.8	707	1.9/38.3
17.5	1020	2/38.2

Figure D-18. Summary of 8-mm Nylon +5% Clay

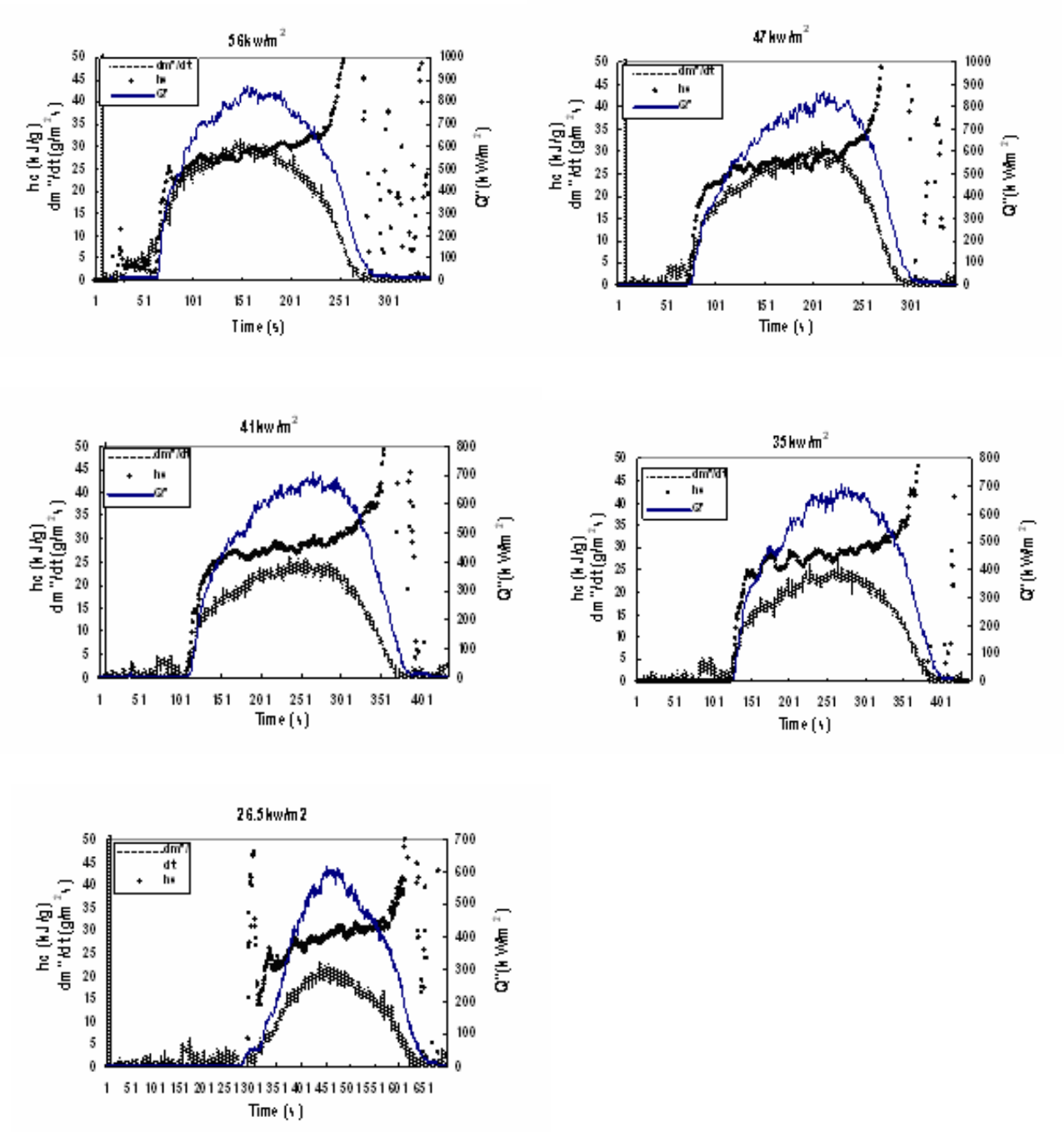

Figure D-19. Nylon +5% Clay Under Different External Heat Flux (Thickness 4 mm, Diameter 74 mm)

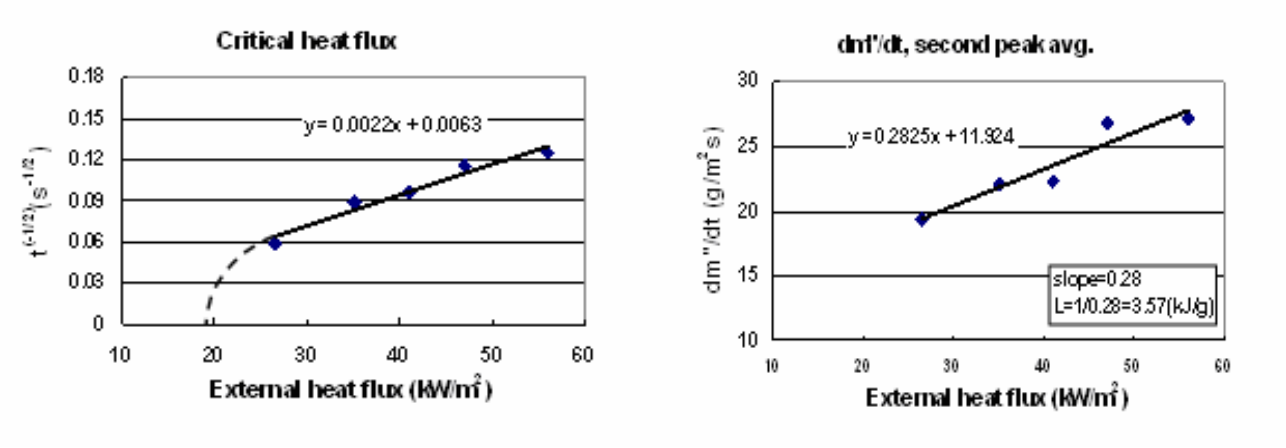

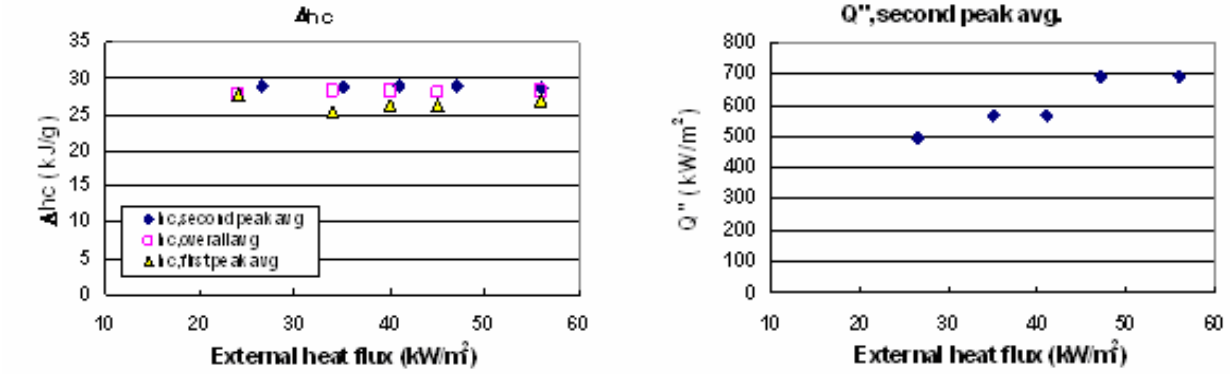

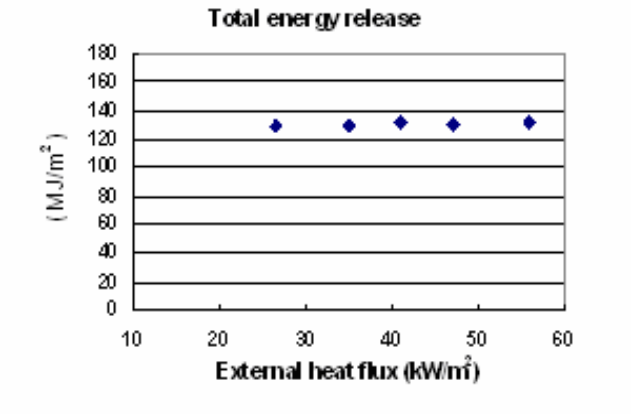

Heat Flux (kW/m^2)	Ignition Time (s)	Char/Mass (g)
56	64	0.8/20.7
47	75	0.9/20.6
41	109	0.9/20.7
35	127	0.9/20.6
26.5	279	1/20.8

Figure D-20. Summary of 4-mm Nylon +5% Clay

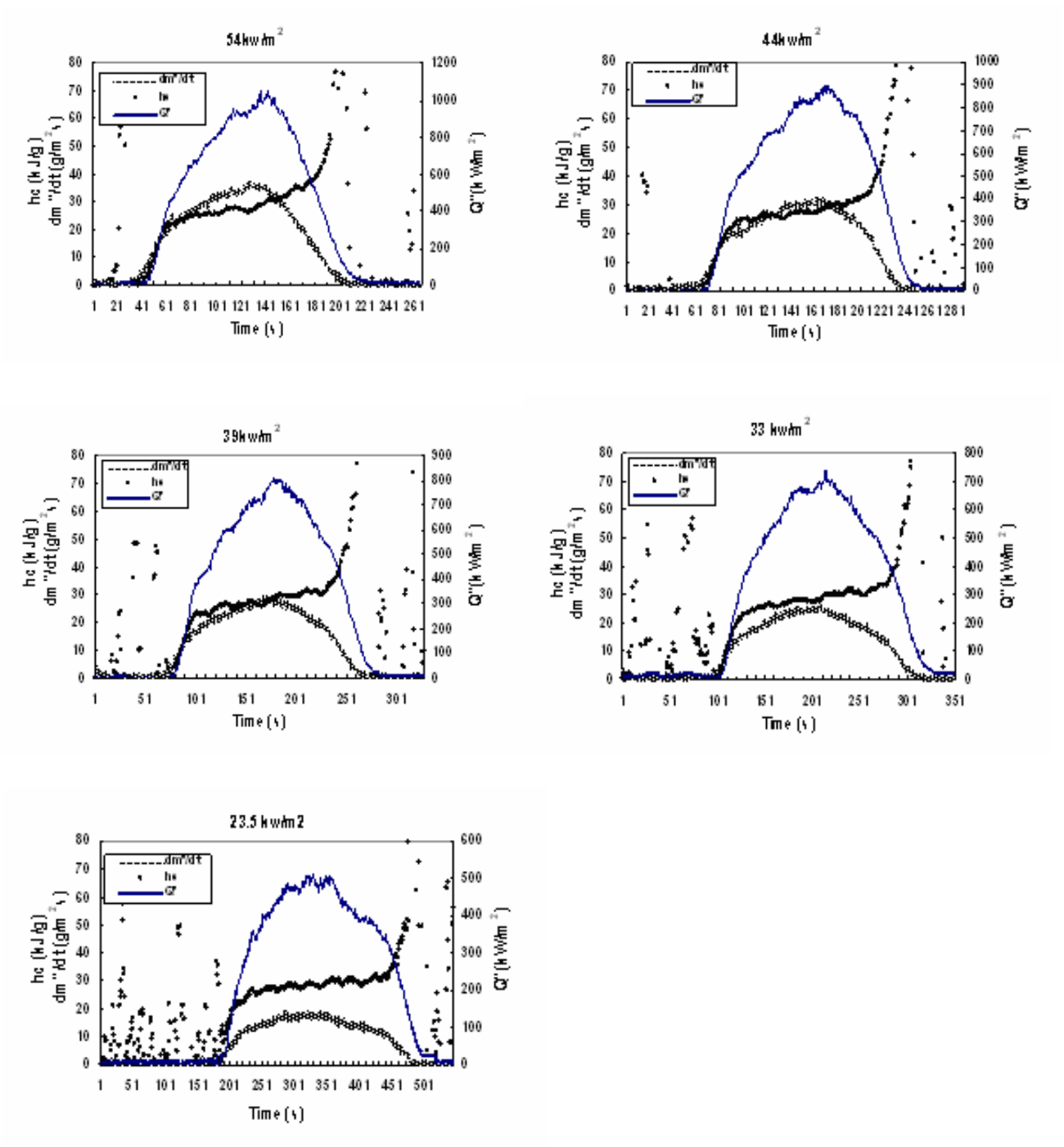

Figure D-21. Nylon +5% Clay Under Different External Heat Flux (Thickness 3.2 mm, Diameter 75 mm)

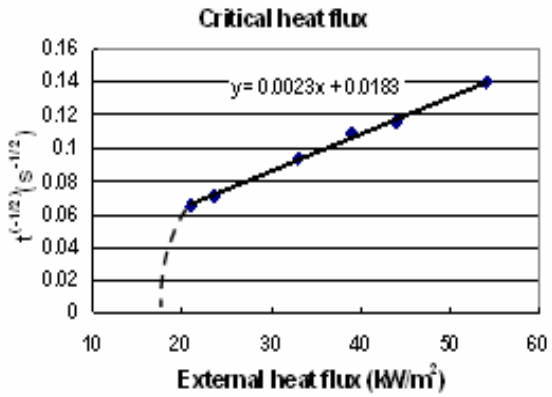

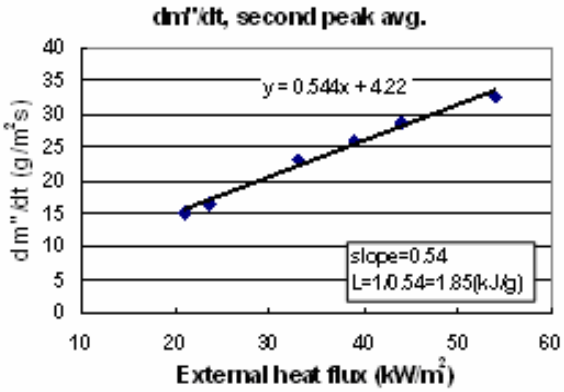

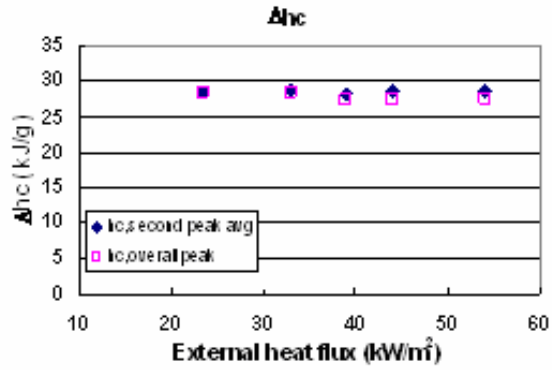

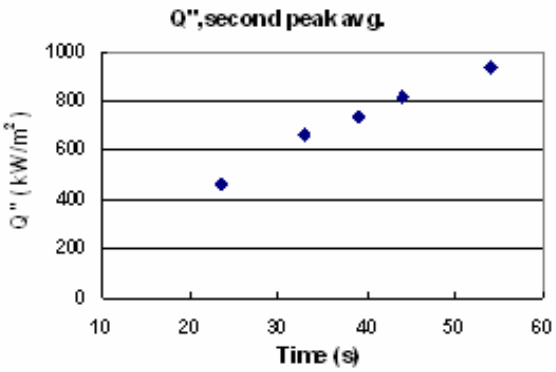

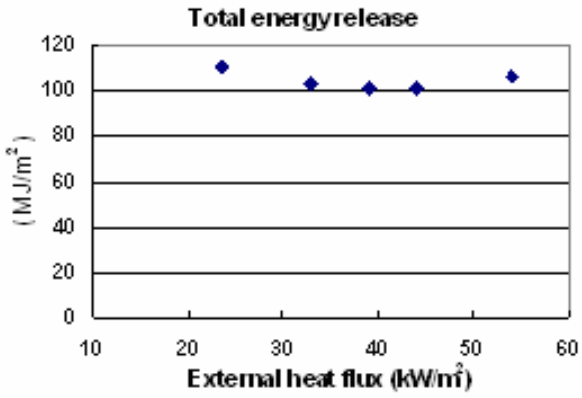

Heat Flux (kW/m^2)	Ignition Time (s)	Char/Mass (g)
54	51	0.7/17.3
44	74	0.8/16.7
39	84	0.8/16.7
33	112	0.7/16.5
23.5	197	0.8/17.7
21	239	0.8/16.5

Figure D-22. Summary of 3.2-mm Nylon +5% Clay

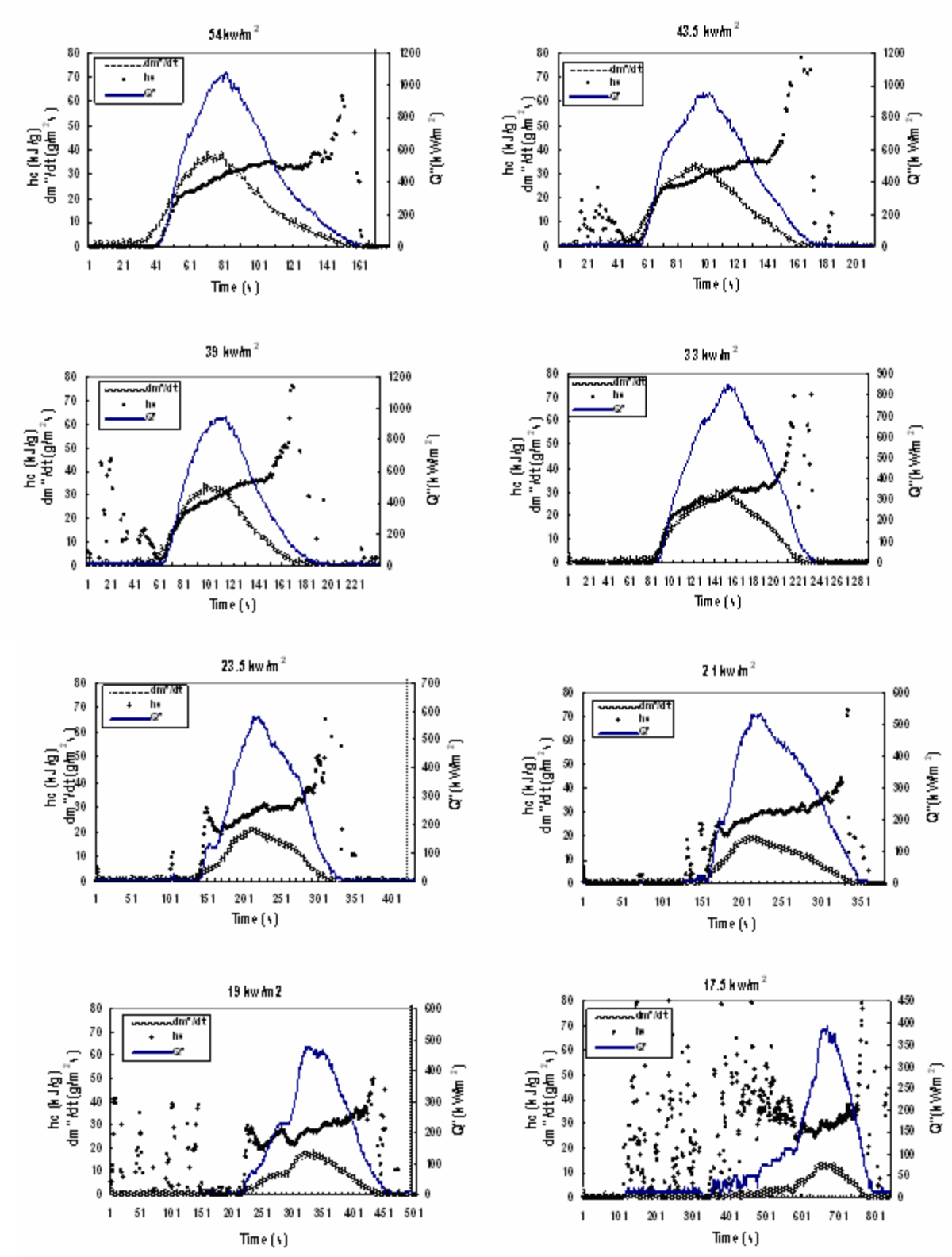

Figure D-23. Nylon +5% Clay Under Different External Heat Flux (Thickness 1.6 mm, Diameter 76 mm)

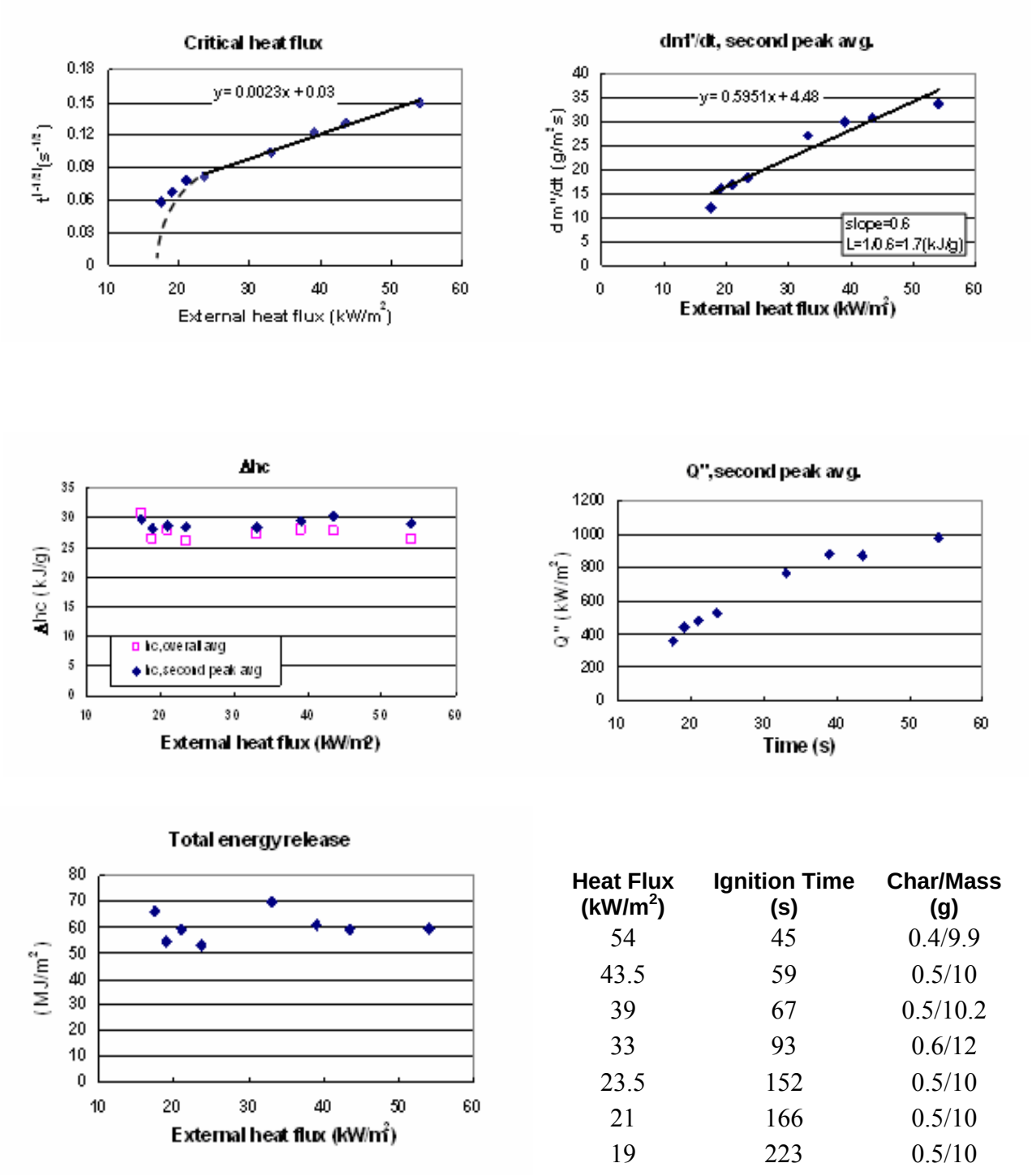

Heat Flux (kW/m^2)	Ignition Time (s)	Char/Mass (g)
54	45	0.4/9.9
43.5	59	0.5/10
39	67	0.5/10.2
33	93	0.6/12
23.5	152	0.5/10
21	166	0.5/10
19	223	0.5/10
17.5	303	0.5/10.1

Figure D-24. Summary of 1.6-mm Nylon +5% Clay

D.1 TWENTY-FOUR mm NYLON UNDER 50 kW/m^2 EXTERNAL HEAT FLUX (DIAMETER 74 mm).

Twenty-four-mm samples were made by three pieces of 8-mm samples, overlapped, with results shown in figures D-25 through D-27 and table D-1. The sample surface was smoothed by sand paper to minimize the gap between the connection of two surfaces. If they were not perfectly contacted, it was still acceptable. During the test, the sample will be melted by the heat. The soft sample can seal the gap itself.

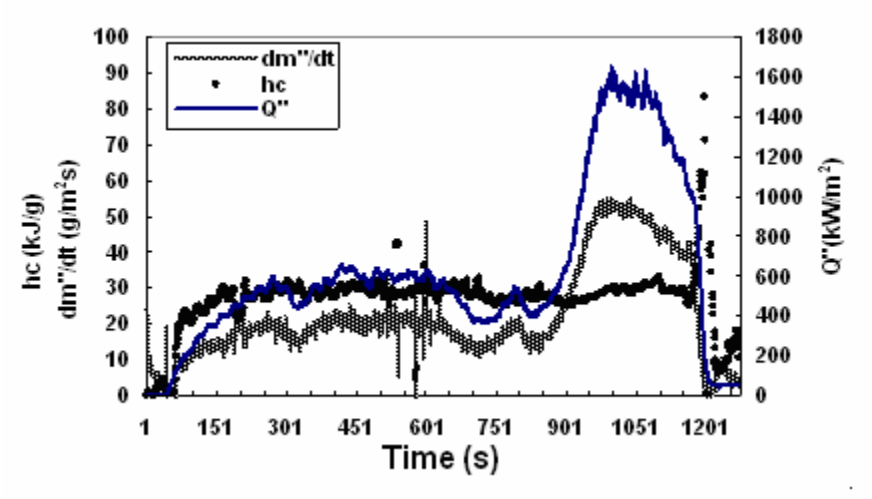

Figure D-25. Twenty-Four-mm Nylon Under 50 kW/m^2 External Heat Flux

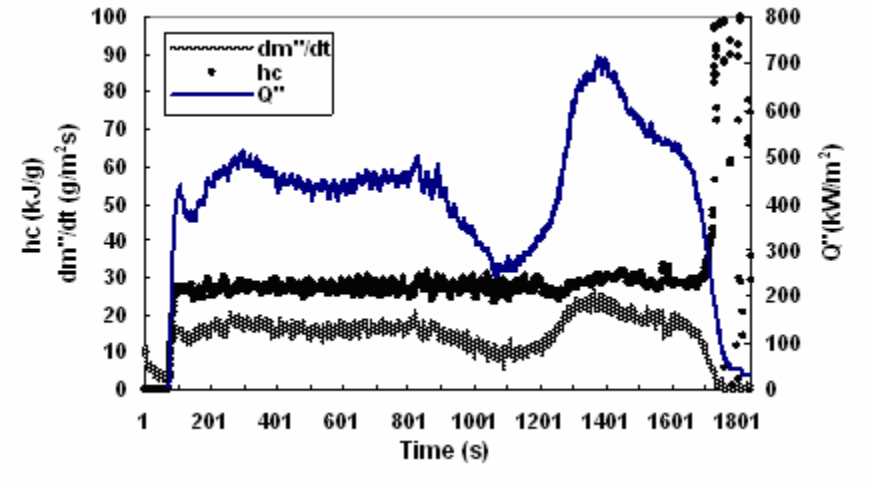

Figure D-26. Twenty-Four-mm Nylon +2% Clay Under 50 kW/m^2 External Heat Flux

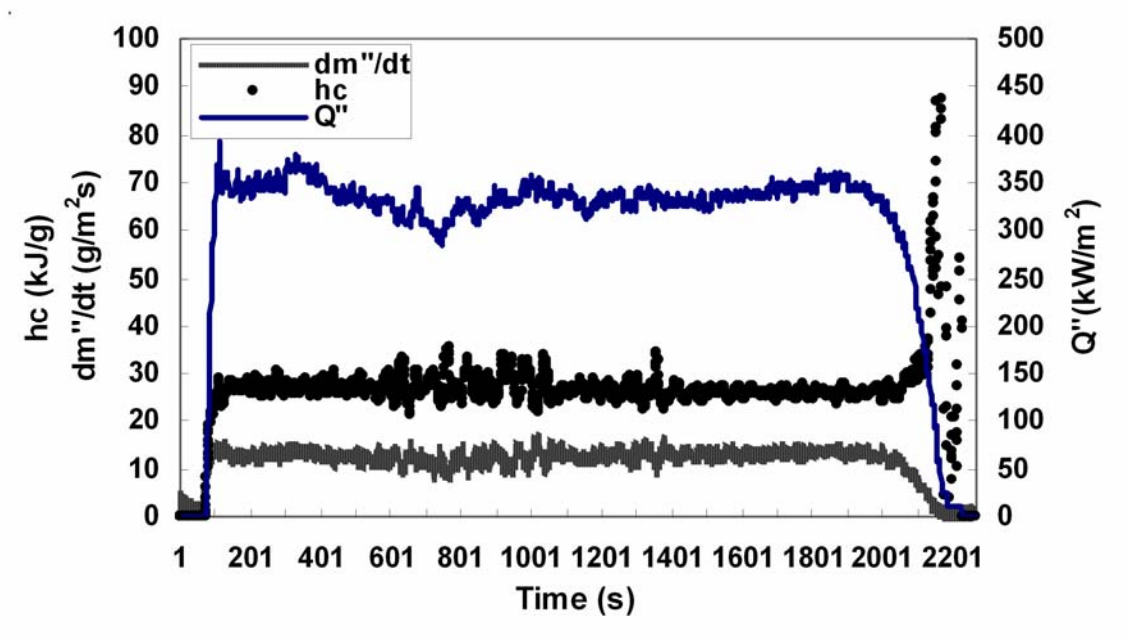

Figure D-27. Twenty-Four-mm Nylon +5% Clay Under 50 kW/m^2 External Heat Flux

Table D-1. Twenty-Four-mm Samples: Ignition Time and Char Yield

Sample	Ignition Time (s)	Char/Mass (g)
Nylon	47	0/113.8
Nylon +2% Clay	57	7/114.4
Nylon +5% Clay	75	8.6/114.4

APPENDIX E—EXPERIMENTAL RESULTS OF CONVECTIVE HEAT TRANSFER COEFFICIENT

Properties:

Air:

$T_S = 500^o\,C \qquad T_o = 25^oC \qquad T = \frac{T_S + T_o}{2} = 263^oC = 536\ K$

So use air properties @ 550 K

$\rho = 0.6329 kg/m^2 \qquad \nu = 45.57 \times 10^{-6} m^2/s$

$\Pr = 0.683 \qquad k = 43.9 \times 10^{-3} w/mK$

Aluminum plate:

Area = $7.7\,cm \times 7.7\,cm$

Mass = $7.4\,g$

c_p = 0.896 *J/g °C*

Kaowool blanket:

Conductivity = 0.15 *W/m°C*

Total thickness = 1/2 inch = 0.0127m

Exhaust duct

Dia. = 0.1106m

Energy conservation: Considering the conductive heat loss from the back side (insulation) of the aluminum plate

$$\dot{m}'' c \frac{dT}{dt} = \alpha \dot{q}''_{ext} - \varepsilon\sigma(T^4 - T_o^4) - h(T - T_\infty) - k_{ins} \frac{T - T_{ins}}{\delta_{ins}}$$

Without conductive heat loss:

$$\dot{m}'' c \frac{dT}{dt} = \alpha \dot{q}''_{ext} - \varepsilon\sigma(T^4 - T_o^4) - h(T - T_\infty)$$

Surface absorptivity α

Energy conservation at initial status:

$$\dot{m}'' c_p \frac{dT}{dt} = \alpha \dot{q}''_{ext}$$

Read the initial slope from temperature-time curve, then calculate α from above equation.

Surface made: Soot was added by a candle flame, and then painted by several layers of high temperature-resistant paint. If the soot was deposited by a burner burning under the plate for 1½ hours, the soot would be thicker and even the absorptivity would be higher.

Figures E-1 through E-3 show the comparison of convective heat transfer coefficient under different exhaust fan speed.

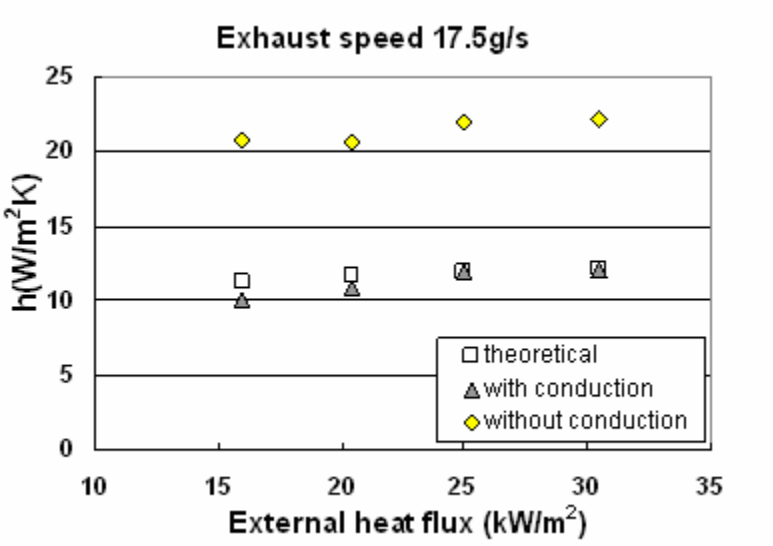

Figure E-1. Heat Transfer Coefficient as a Function of Heat Flux at Air Flow of 17.5 g/s

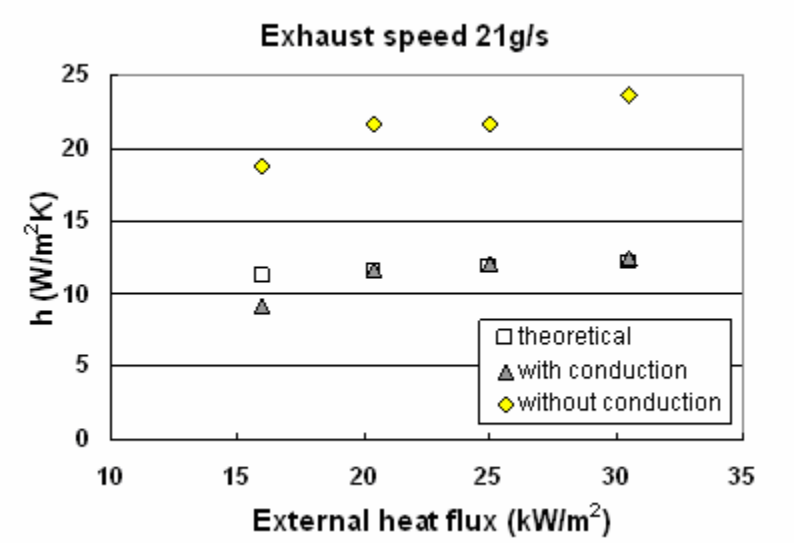

Figure E-2. Heat Transfer Coefficient as a Function of Heat Flux at Air Flow of 21 g/s

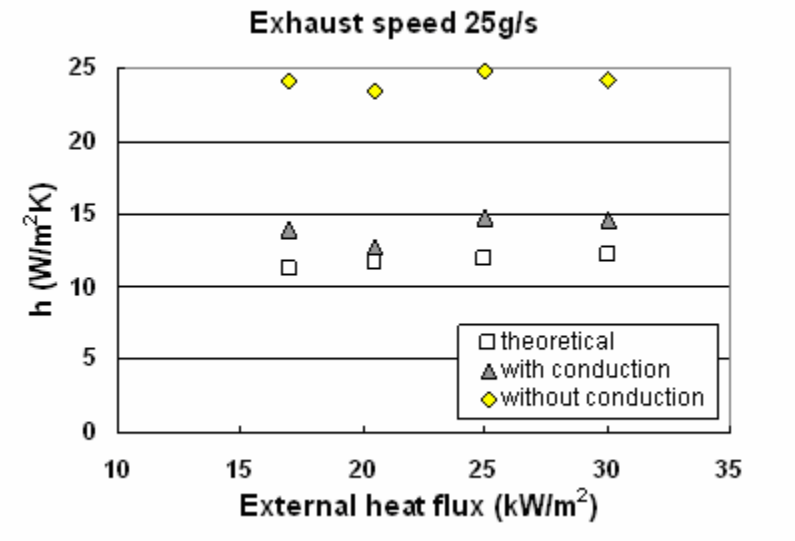

Figure E-3. Heat Transfer Coefficient as a Function of Heat Flux at Air Flow of 25 g/s